



Extraction of Cellulose from Rice Husk, Corn Stem, Corn Tassel and Oil Palm Empty Fruit Bunch Using Alkaline Pretreatment and Bleaching Process

**Chik Jia Ying
J20A0431**

A reported submitted in fulfilment of the requirements for the degree of Bachelor of Applied Science (Bioindustrial Technology) with Honours

FACULTY OF BIOENGINEERING AND TECHNOLOGY

UMK

2024

DECLARATION

I declare that this thesis entitled “title of the thesis” is the results of my own research except as cited in the references.

Signature : _____

Student's Name : _____

Date : _____

Verified by:

Signature : _____

Supervisor's Name : _____

Stamp : _____

Date : _____

UNIVERSITI
MALAYSIA
KELANTAN

ACKNOWLEDGEMENT

First, I express my highest appreciation to the Faculty of Bioengineering and Technology at the University Malaysia Kelantan Jeli Campus for granting me the invaluable chance to acquire knowledge and employ the laboratory facilities and instruments, enabling the successful completion of my research. I want to express my gratitude to the Faculty of Rubber at Prince of Songkla University Surat Thani Campus for their invaluable support and assistance throughout my student exchange programme in Thailand, which significantly contributed to the successful completion of my research project.

Additionally, I would like to extend my sincere appreciation and gratitude to my supervisor at UMK, Dr. Wan Suriyani Faliq Adeeba Wan Ibrahim, as well as my supervisor at PSU, Assistant Professor Dr. Sunisa Suchat, for their invaluable assistance and advice during my academic journey. They dedicated a significant amount of their time to guiding my research. I thank the individuals for their valuable insights and recommendations during the laboratory work.

Furthermore, I would like to express my heartfelt gratitude to the laboratory technicians at UMK Jeli Campus and PSU Surat Thani Campus for their collaboration and support in assisting me with the analysis of the samples. Lastly, I express my sincere gratitude to all my lecturers and friends for their support and encouragement throughout my research and laboratory work.

**Pengekstrakan Selulosa daripada Sekam Padi, Batang Jagung, Rumbai Jagung
dan Tandan Buah Kosong Kelapa Sawit Menggunakan Proses Prarawatan
Beralkali dan Pemutihan**

ABSTRAK

Tujuan penyelidikan ini adalah untuk mengekstrak selulosa daripada pelbagai sisa pertanian, termasuk sekam padi (RH), batang jagung (CS), jumbai jagung (CT), dan tandan kosong kelapa sawit (OPEFB), menggunakan kaedah pengekstrakan alkali untuk menangani isu penghasilan manik mikro yang tidak terbiodegradasi. Delignifikasi dilakukan dengan menggunakan natrium hidroksida untuk sekam padi dan campuran toluena-etanol untuk batang jagung, jumbai jagung, dan tandan kosong kelapa sawit. Agen pelunturan termasuk natrium hipoklorit (NaOCl) untuk sekam padi dan campuran natrium hidroksida dan asid asetik untuk CS, CT, dan OPEFB. Kumpulan berfungsi, morfologi struktur, kehabluran, dan kestabilan terma selulosa yang diekstrak telah dicirikan menggunakan Spektroskopi Infra-Merah Transformasi Fourier (FTIR), Mikroskop Elektron Pengimbasan (SEM), Pembezaan sinar-X (XRD), dan Analisis Termogravimetrik (TGA) , masing-masing. Keputusan menunjukkan bahawa OPEFB menghasilkan peratusan selulosa tertinggi pada 31.40%, diikuti oleh RH (29.28%), CS (14.30%), dan CT (13.27%). Pencirian sampel menunjukkan bahawa rawatan alkali berkesan meningkatkan kandungan selulosa dengan menghapuskan hemiselulosa, lignin, dan kekotoran lain. Antara sampel, RH yang tertakluk kepada pengekstrakan alkali menunjukkan peratusan kehabluran tertinggi pada 59.42%, dengan CS (54.17%), CT (44.97%), dan OPEFB (42.78%).

Kata kunci: Selulosa, Sekam padi, Batang jagung, Jumbai jagung, Tandan kosong kelapa sawit

Extraction of Cellulose from Rice Husk, Corn Stem, Corn Tassel and Oil Palm empty Fruit Bunch Using Alkaline Pretreatment and Bleaching Process

ABSTRACT

This study aims to extract cellulose from various agricultural residues, including rice husk (RH), corn stem (CS), corn tassel (CT), and oil palm empty fruit bunch (OPEFB), using an alkaline extraction method to address the issue of non-biodegradable microbead production. Delignification was done by employing sodium hydroxide for rice husk and a toluene-ethanol mixture for corn stem, corn tassel, and oil palm empty fruit bunch. Bleaching agents included sodium hypochlorite (NaOCl) for rice husk and a mixture of sodium hydroxide and acetic acid for CS, CT, and OPEFB. The functional groups, structural morphology, crystallinity, and thermal stability of the extracted cellulose were characterized using Fourier Transformed Infra-Red Spectroscopy (FTIR), Scanning Electron Microscopy (SEM), X-ray Diffraction (XRD), and Thermogravimetric Analysis (TGA), respectively. The results reveal that OPEFB yielded the highest cellulose percentage at 31.40%, followed by RH (29.28%), CS (14.30%), and CT (13.27%). Characterization of the samples demonstrated that the alkaline treatment effectively enhanced the cellulose content by eliminating hemicellulose, lignin, and other impurities. Among the samples, RH subjected to alkaline extraction exhibited the highest crystallinity percentage at 59.42%, with CS (54.17%), CT (44.97%), and OPEFB (42.78%).

Keywords: Cellulose, Rice husk, Corn stem, Corn tassel, Oil palm empty fruit bunch

TABLE OF CONTENT

DECLARATION	ii
ACKNOWLEDGEMENT.....	iii
ABSTRAK	iv
ABSTRACT.....	v
TABLE OF CONTENT.....	vi
LIST OF TABLES	xi
LIST OF FIGURES	xii
LIST OF EQUATION	xiv
LIST OF ABBREVIATIONS	xv
LIST OF SYMBOLS	xvi
CHAPTER 1.....	1
INTRODUCTION	1
1.1 Background of Study	1
1.2 Problem Statement.....	3
1.3 Objectives	5
1.4 Scope of Study.....	5
1.5 Significances of Study	5
CHAPTER 2.....	6
LITERATURE REVIEW	6

2.1	Cellulose	6
2.2	Source of Cellulose Fiber	9
2.2.1	Rice Husk.....	10
2.2.2	Corn Straw	12
2.2.3	Oil Palm Empty Fruit Bunch	15
2.3	Extraction	17
2.4	Chemical Extraction Method.....	18
2.4.1	Alkali Treatment.....	18
2.4.2	Bleaching Process	19
2.4.3	Delignification	21
2.5	Quantitative Analysis	23
2.6	Characterization of Cellulose	23
2.6.1	Scanning Electron Microscopy (SEM)	23
2.6.2	Fourier Transform Infrared (FTIR)	25
2.6.3	X-ray Diffraction (XRD)	27
2.6.4	Thermogravimetric Analysis (TGA)	29
CHAPTER 3.....		32
MATERIALS AND METHODS		32
3.1	Materials	32
3.2	Apparatus and Equipment	32
3.3	Chemicals	32
3.4	Preparation of Raw Materials	33

3.4.1	Preparation of Dried Rice Husk (DRH) Powder	33
3.4.2	Preparation of Corn Straw (CS) Powder	33
3.4.3	Preparation of Oil Palm Empty Fruit Bunch Fibres (OPEFB) Powder.....	33
3.5	Chemical Extraction	34
3.5.1	Delignification	34
3.6	Bleaching	34
3.6.1	Alkaline Treatment	34
3.6.2	Bleaching Process for CS, CT and OPEFB	35
3.7	Characterization of Cellulose Fibre	35
3.7.1	Scanning Electron Microscope (SEM) Analysis	35
3.7.2	Fourier Transforms Infrared (FTIR) Spectroscopy	35
3.7.3	X-Ray Diffraction (XRD).....	36
3.7.4	Thermogravimetric Analysis (TGA)	36
CHAPTER 4	37
RESULTS AND DISCUSSION	37
4.1	Physical appearance of cellulose	37
4.1.1	Rice Husk.....	37
4.1.2	Corn Stem	39
4.1.3	Corn Tassel	41
4.1.4	Oil Palm Empty Fruit Bunch	42
4.2	Yield of extracted cellulose from different samples.....	46

4.3	Characteristic of Extracted Cellulose	46
4.3.1	Identification of Functional Groups Using Fourier Transform Infrared (FTIR) Spectroscopy	47
4.3.1(a)	Rice Husk	47
4.3.1(b)	Corn Stem	51
4.3.1(c)	Corn Tassel.....	54
4.3.1(d)	Oil Palm Empty Fruit Bunch.....	57
4.3.2	Morphology Study using Scanning Electron Microscopy (SEM). 60	
4.3.2(b)	Corn Stem.....	63
4.3.2(c)	Corn Tassel.....	65
4.3.2(d)	Oil Palm Empty Fruit Bunch.....	67
4.3.3	Determination of Crystallinity Structure using X-ray Diffraction (XRD).....	69
4.3.3(a)	Rice Husk	69
4.3.3(b)	Corn Stem.....	72
4.3.3(c)	Corn Tassel	74
4.3.3(d)	Oil Palm Empty Fruit Bunch.....	76
4.3.4	Thermal Stability Study using Thermogravimetric Analysis (TGA).....	79
4.3.4(a)	Rice Husk	79
4.3.4(b)	Corn Stem.....	80
4.3.4(c)	Corn Tassel.....	82

4.3.4(d) Oil Palm Empty Fruit Bunch.....	84
CHAPTER 5.....	86
CONCLUSIONS AND RECOMMENDATIONS.....	86
5.1 Conclusions	86
5.2 Recommendations	87
REFERENCES.....	88
APPENDIX A	109

LIST OF TABLES

Table 2. 1: Fibre sources and its cellulose content	9
Table 4. 1: The colour changes of different samples before and after treatment	44
Table 4. 2: Yield percentage of each samples	46
Table 4. 3: Peak positions of the infrared spectra of rice husk	47
Table 4. 4: Peak positions of the infrared spectra of corn stem	53
Table 4. 5: Peak positions of the infrared spectra of corn tassel	56
Table 4. 6: Crystallinity and amorphous percentage of different samples	77

UNIVERSITI
MALAYSIA
KELANTAN

LIST OF FIGURES

Figure 2.2: Oil palm empty fruit bunch	12
Figure 2.1: The anatomy of rice grain	12
Figure 4. 1: The rice husk changes colour from dark brown to light brown after alkaline treatment	37
Figure 4. 2: The corn stem changes colour from brown to dark brown after alkaline treatment with toluene-ethanol mixture	38
Figure 4. 3: The corn stem changes colour from brown to dark brown after alkaline treatment with toluene-ethanol mixture	39
Figure 4. 4: The colour transition from brown and gradual discoloration to pale brown due to bleaching process with mixture of sodium hydroxide and acetic acid	40
Figure 4. 5: The corn tassel changes colour from brown to dark brown after alkaline treatment with toluene-ethanol mixture	41
Figure 4. 6: The colour transition from dark brown and gradual discolouration to pale brown due to the bleaching process with a mixture of sodium hydroxide and acetic acid	42
Figure 4. 7: The oil palm empty fruit bunch changes colour from brown to dark brown after alkaline treatment with toluene-ethanol mixture	42
Figure 4. 8: The colour transition from dark brown and gradual discolouration to brown due to the bleaching process with a mixture of sodium hydroxide and acetic acid	43
Figure 4. 9: FTIR spectra between (a) untreated and (b) treated rice husk	47
Figure 4. 10: FTIR spectra between (a) untreated and (b) treated corn stem	51

Figure 4. 11: FTIR spectra between (a) untreated and (b) treated corn tassel	54
Figure 4. 12: Comparison between (a) untreated (b) treated oil palm empty fruit bunch	57
Figure 4. 13: SEM micrographs of untreated rice husk (a) outer, (b) inner surfaces and (c) treated rice husk	61
Figure 4. 14: SEM micrograph of (a) untreated and (b) treated corn stem.....	63
Figure 4. 15: SEM micrograph of (a) untreated and (b) treated corn tassel	65
Figure 4. 16: SEM micrograph of (a) untreated and (b) treated oil palm empty fruit bunch	67
Figure 4. 17: XRD analysis for treated rice husk cellulose	70
Figure 4. 18: XRD analysis for treated corn stem cellulose	72
Figure 4. 19: XRD analysis for treated corn tassel cellulose.....	74
Figure 4. 20: XRD analysis for treated oil palm empty fruit bunch cellulose	76
Figure 4. 21: TG analysis of alkaline-treated rice husk cellulose.....	79
Figure 4. 22: TG analysis of alkaline treated corn stem cellulose.....	80
Figure 4. 23: TG analysis of alkaline treated corn tassel cellulose.....	82
Figure 4. 24: TG analysis of alkaline treated oil palm empty fruit bunch cellulose.....	84

LIST OF EQUATION

Equation 2.1	23
Equation 3. 1	36



LIST OF ABBREVIATIONS

NaOH	Sodium hydroxides	2
OPEFB	Oil palm empty fruit bunch	4
FTIR	Fourier Transforms Infrared	5
SEM	Scanning Electron Microscopy	5
TGA	Thermal Gravimetric Analysis	5
XRD	X-ray Diffraction	5
CH ₃ COOH	Acetic acid	31
CT	Corn tassel	31
NaOCl	Sodium hypochlorite	31
RH	Rice husk	31
CS	Corn stem	32
DRH	Dried rice husk	32
Cell-CS	Cellulose corn stem	34
Cell-CT	Cellulose corn tassel	34
Cell-OPEFB	Cellulose oil palm empty fruit bunch	34
CrI	Crystallinity index	35
OH	Hydroxyl group	36
EDXA	Energy dispersive X-ray micro-analysis	69
FE-SEM	Field-emission scanning electron microscopy	69

LIST OF SYMBOLS

%	Percentage	8
θ	Theta	26
α	Alpha	29

UNIVERSITI
MALAYSIA
KELANTAN

CHAPTER 1

INTRODUCTION

1.1 Background of Study

Cellulose is a structural polysaccharide that is present in plant cell walls. It is a long linear polysaccharide made up of repeating monomer units of beta glucose and several glucose groups connected by a chain (1-4) -glycosidic bonds (Frassoldati & Ranzi, 2019). Cellulose exists in crystalline form with amorphous regions and exists in four forms: I, II, III, and IV. Cellulose I is a naturally occurring cellulose with parallel chains held together by intra- and inter-chain hydrogen bonding. On the other hand, Cellulose II is an artificial type of cellulose that is structured in an anti-parallel manner, with hydrogen bonding happening mostly between nearby chains. Amorphous Cellulose III is made by treating Cellulose I or Cellulose II with aims, while Cellulose IV is made by heating cellulose after treating it with glycerol (Ilham, 2022).

Researchers have extensively studied the process of isolating highly pure cellulose for many years due to the complicated structure of plant cell walls. Dissolving lignin, hemicellulose, pectin, and ash requires a combination of chemical and mechanical treatments. Several methods are used in cellulose extraction, including chemical, mechanical, and enzymatic. The chemical extraction method uses chemical reagents such as acids, alkalis, and solvents to dissolve or remove non-cellulosic components from the plant material. The fibre microstructure, such as hemicellulose, pectin, and other non-cellulosic components, is removed using this approach (Abral et al., 2020). The use of the chemical extraction method can give a high-purity cellulose product; however, the use of chemicals is not environment-friendly, and high levels of chemicals can lead to the degradation of cellulose. Mechanical extraction involves physically grinding or shredding the plant material to break down the non-cellulosic components and isolate the cellulose fibres. Mechanical cellulose extraction includes crushing, grinding, steam explosion,

ultrasonication, and cryo-crushing, where high-intensity ultrasonication can disrupt the cells.

On the other hand, cryo-crushing involves freezing cellulose and then mechanically breaking it down (Gerull & Chou, 2020). Mechanical cellulose extraction is a relatively low-cost method. However, it can cause fibre damage, affecting its quality and strength. Enzymatic cellulose extraction is a procedure that uses enzymes such as cellulase or hemicellulase to break down non-cellulosic components like lignin and hemicellulose to separate and extract cellulose fibres. Enzymatic cellulose extraction is an environmentally friendly approach, but it takes a long time (Xie et al., 2018).

Based on the above, the researchers have developed alkali treatment and bleaching methods to produce high-quality cellulose. The alkali solution sodium chloride (NaOH) breaks down lignin and hemicellulose while disrupting the hydrogen bonds between the cellulose chain before proceeding to the next extraction step (Sayakulu & Soloi, 2022). In the bleaching process, sodium chlorite (NaClO_2) is used as it is an effective oxidation agent that can remove residual lignin and other impurities from the cellulose fibres (Trilokesh & Uppuluri, 2019). NaClO_2 is preferred over oxidizing agents as it is less harsh and causes less damage to the cellulose fibres.

Cellulose may be derived from wood, agricultural leftovers such as straw, maize stalks, and bagasse, and industrial by-products such as paper sludge and cardboard. Cotton, hemp, and flax are other cellulose sources. In recent years, increasing interest has been shown in isolating cellulose from non-traditional sources such as algae and bacteria.

Synthetic polymers such as polystyrene, polyethene, and polypropylene have traditionally been used to manufacture microbeads. Due to their low cost, durability, and adaptability, these polymers are extensively employed in various applications. On the other hand, the environmental effects of microbeads comprised of synthetic polymers have generated concerns since they may collect in the ecosystem and destroy marine life. Consequently, there has been a trend toward producing microbeads from more sustainable and biodegradable sources, such as natural polymers from plants or algae. Natural polymers such as cellulose, chitin, and alginate have been utilized to make microbeads. These materials are biodegradable, non-toxic, and renewable, which gives them various advantages over traditional synthetic polymers (O'Brien et al., 2017). They can also be made with less energy and fewer chemicals, which has a minor environmental effect. The

benefits of employing cellulose microbeads are that they can be broken down by existing wastewater treatment facilities, thereby preventing the build-up of these particles in aquatic ecosystems (O'Brien et al., 2017b).

According to the International Atomic Energy Agency (IAEA), the amount of microplastic in the region is expected to rise dramatically. Compared to 2008 levels, it is predicted to climb approximately 3.8 times by 2023. By 2050, the amount might almost double, reaching 6.4 times the 2008 levels. If nothing is done, the quantity of plastic in the ocean by 2100 is expected to be ten times more than in 2008. In Malaysia, it is estimated that 0.94 million metric tons of plastic waste are produced daily, all of which is disposed of incorrectly. Around 0.14 million to 0.37 million metric tons of plastic garbage are washed into the oceans, causing considerable harm to the marine environment's ecosystem.

Cellulose microbeads have the potential to be used in cosmetics as a replacement for traditional microbeads, which are often made from non-biodegradable materials like plastic (Varma, 2019). Cellulose is a natural polymer derived from plants, making it a sustainable and environmentally friendly alternative. Cellulose microbeads may be used in cosmetics such as facial scrubs, body washes, and soaps to exfoliate the face, clear pores, and improve skin texture (Momin, Nagori, & Patel, 2016). Moreover, it can also act as a carrier for active ingredients in various products, such as sunscreen and acne treatment, delivering the active ingredient to the skin more effectively.

1.2 Problem Statement

The skin care, personal care, and cosmetics industries extensively use tiny particles known as microbeads. Microbeads are small spheres composed of either polypropylene or polyethylene. In most cases, the diameter of a microbead will fall somewhere in the range of 0.5 to 500 micrometers. Therefore, the problem may arise when these minute particles are difficult to filter out during wastewater treatment, and ultimately, they will wind up in rivers, lakes, or even the ocean. Microbeads are a material that difficult to undergo biodegradation and have a low density; as a result, they may accumulate in drainage systems and even float on the surface of the water. These microscopic particles will eventually find their way into waterways, contaminating rivers,

lakes, and seas. Because of their size, which is comparable to fish eggs, they can fool fish and birds into thinking that the material is food, which ultimately results in the animals consuming it. Also, since they function as absorbents, microbeads may also be poisonous because they concentrate harmful compounds such as polybrominated diphenyl ethers (PBDEs) onto their surface. This makes them more dangerous than they already are. If fish consume microbeads contaminated with harmful chemicals, those toxins may make their way up the food chain and into the bodies of humans and other animals. In extreme cases, the consumption of PBDEs by individuals may lead to fertility issues, a reduction in immunological function, and even neurological problems. In this research study, agricultural waste, specifically maize straw, and oil palm empty fruit bunch (OPEFB), is used as a source for cellulose extraction to replace plastic in manufacturing microbeads.

The problem of pollution caused by microbeads may be solved by using cellulose instead of plastic microbeads as an alternative solution. Since cellulose is biodegradable and can be broken down by naturally occurring microbes, it does not accumulate in streams and posing a threat to the animals that live there. Additionally, using agricultural waste as a source for manufacturing cellulose may give farmers an additional value stream while lowering the quantity of trash generated by the agricultural business. Farmers may profit economically from this, and it may also assist in minimizing environmental contamination caused by waste from agricultural production. Overall, this research project has the potential to provide a sustainable solution to the problem of microbead pollution and contribute to the development of a circular economy by using agricultural waste as a source to produce cellulose. This could be accomplished by using agricultural waste to extract cellulose.

1.3 Objectives

The objectives of this study are:

1. To extract cellulose from rice husk, corn straw and oil palm empty fruit bunch (OPEFB) using alkali treatment and bleaching method
2. To characterize the cellulosic material using Scanning Electron Microscopy (SEM), Fourier Transforms Infrared (FTIR), X-ray Diffraction (XRD), and Thermal Gravimetric Analysis (TGA)

1.4 Scope of Study

The study focused on cellulose extraction from different plants (rice husk, corn stem, corn tassel, and oil palm empty fruit bunch) for use in the production of microbeads. Cellulose extracted from rice husk was used as a control to compare two samples: cellulose from corn stover and oil palm empty fruit bunch (OPEFB). The extraction method used for extracting cellulose from rice husk was delignification and bleaching. In contrast, an alkali treatment and bleaching method were used for the cellulose extraction of corn stover and OPEFB.

Four different methods were used to characterize the extracted cellulose from each plant: SEM, FTIR, XRD, and TGA. The purpose of employing SEM was to study cellulose morphology and surface cracks. The purpose of using FTIR was to identify the molecular structure in these plants and cellulose. XRD was used to identify the crystalline material in cellulose, while TGA was used to determine the thermal stability of cellulose.

1.5 Significances of Study

Cellulose extraction is an important area of research as it has various applications, including the production of microbeads. Cellulose microbeads are generally less harmful to the environment than plastic microbeads, which are difficult to degrade. Using alkali treatment and bleaching method may be helpful for future studies involving cellulose extraction from corn stover and OPEFB. This study is a good starting point for further research.

CHAPTER 2

LITERATURE REVIEW

2.1 Cellulose

Cellulose is the structural component of the cell wall in plants and is widely distributed throughout the plant kingdom. It is crucial as the primary structural component in providing the cell wall with significant mechanical strength (Rongpipi et al., 2019). The direction of growth of the cell wall is highly dependent on the positioning and distribution of cellulose microfibrils, as stated in Jordan and Dumais' research (2010). The arrangement of these microfibrils allows for mechanical anisotropy, enabling the cell to preferentially expand in one direction. Cellulose is the most abundant carbohydrate on Earth and can be used in various industries, such as raw material for the paper and textile industry, construction materials, and as a source of dietary fiber for animals and humans.

Regarding its chemical composition, cellulose is a polymer composed of multiple units of glucose molecules ($C_6H_{12}O_6$) linked by α -1,4-glycosidic bonds in a 180° orientation of glucose molecules adjacent to each other (Festucci-Buselli et al., 2007). This creates cellobiose ($C_{12}H_{22}O_{11}$) residues, and the cellulose chain comprises these repeating cellobiose units. To produce compact microfibrils, cellulose chains are aggregated and stabilized by intra- and intermolecular hydrogen bonds between neighboring oxygen and hydrogen groups because cellulose has a significant attraction for substances containing hydroxyl groups (Khazraji & Robert, 2013). Cellulose consists of lengthy glucose molecule chains interconnected by hydrogen bonds, creating a structured and stable crystalline form. Because of the high energy required to break these hydrogen bonds, it is generally insoluble in most common solvents (Ilham, 2022).

Cellulose has significant importance in many industries; however, at the same time, it could be a challenging material to work with as it poses strong intermolecular forces and insolubility in many solvents. Despite this, advances in biotechnology have made it possible to develop new methods for producing and modifying cellulose-based materials. These new methods include the production of nanocellulose, which possesses exceptional mechanical, optical, and electronic properties that make it a potentially useful material for various applications (Hassan et al., 2010). Cellulose fibers have been widely utilized in various fields, including biomedical fields such as wound healing, tissue engineering, and drug delivery (Hasanin, 2022). Cellulose is a biocompatible material that causes no harm to living cells while absorbing fluids such as blood and other body fluids. Cellulose also acts in controlling the release of drugs in the body. Besides that, cellulose is also a common material in pulp and paper production. About 90% of pulp and paper products are made using wood, a cellulose fiber source (Ningtyas et al., 2022). Cellulose fibers are obtained from various plant-based sources, such as wood chips, which are then processed into pulp. Moreover, cellulose is also used in the cosmetic industry; It is commonly used as a natural and biodegradable alternative to synthetic thickeners, such as carbomer or polyacrylamide (Bianchet et al., 2020).

While extracting cellulose from plants, the residual hemicellulose and lignin can be utilized in various industries. The residual hemicellulose showcases diverse qualities such as biodegradability, hydrophilicity, and affordability, thus rendering it suitable for packaging materials. These packaging materials, which include paper, metal, plastic, chemical fiber, natural fiber, and composites, are employed in packaging a wide array of products (Huang et al., 2021). In addition, the utilization of hemicellulose can further extend to the production of alcohol through fermentation and sorbitol via reduction, which in turn finds significance in several industries such as cosmetics, toothpaste, food, papermaking, and explosives (Gírio et al., 2010). Notably, the pentose component of hemicellulose holds significant value in the production of feed xylose, xylitol, yeast, and furoic acid (Li et al., 2019). Moreover, xylooligosaccharides, a degradation product of hemicellulose, exhibit unique physical and chemical properties with physiological functions, making them widely used in the pharmaceutical and functional food sectors.

The residue of lignin, obtained from cellulose extraction, presents several useful applications. These include the adsorption of heavy metal ions in waste, the synthesis of

nanoparticles, and the production of hydrogel based on lignin. Nevertheless, the potential of lignin for adsorption is limited, and its effective range for certain types of heavy metal ions needs to be clearly defined (Gao et al., 2019). To overcome these limitations, it is possible to prepare adsorbents based on lignin through several techniques, such as copolymerization, condensation, network formation via hydrogen bonding, hybridization, cross-linking, and formulation. Lignin can be readily altered by utilizing the chemical reactivity of the primary phenol hydroxyl groups and the active hydrogen atom in ortho- and para-positions.

Moreover, a copolymerisation approach that involved kraft lignin, organosolv lignin, lignosulfonate, propylene oxide, and multiwall carbon nanotubes was employed for the development of lignin-based hydrogels in biosensor applications. This approach facilitated the preparation of a high-conductivity and stable all-solid-state hydrogel. The biosensor exhibited sensitivity towards Cr(VI) rather than all transition metal cations, alkali earth, and alkalis.

In conclusion, cellulose is a fascinating and versatile material with many applications. Its unique properties make it an essential component of plant cell walls, while its industrial applications have made it a valuable material for various products. The residue obtained from the extraction of cellulose, comprising hemicellulose and lignin, offers a multitude of versatile applications.

2.2 Source of Cellulose Fiber

Cellulose is an abundant polysaccharide found in many sources, including the cell walls of plants and wood, various species of algae and bacteria, and even tunicates, the sole animals known to contain cellulose. Other sources of cellulose fibers include coir, cotton, flax, jute, rice husk, and sisal, as shown in Table 2.1.

Table 2. 1: Fibre sources and its cellulose content

Fiber Source	Origin	% Cellulose
Banana	Leaf	60,0 – 65,0
Coir	Fruit	32,0 – 43,0
Coir bark	Leaf	12,0 – 25,0
Corn cob	Stalk	33,7 – 41,2
Cotton	Seed	82,7 – 95,0
Curaua	Leaf	63,4 – 73,6
Flax	Stem	64,0 – 84,0
Hardwood	Stem	39,0 – 50,0
Hemp	Stem	67,0 – 78,0
Jute	Bast	51,0 – 78,0
Kenaf	Bast	44,0 – 72,0
Maize Straw	Straw	28,0 – 44,0
Nettle	Bast	53,0 – 86,0
Ramie	Bast	67,0 – 99,0
Rice Husk	Straw	25,0 – 35,0
Softwood	Stem	42,0 – 50,0
Sugar cane bagasse	Stem	32,9 – 50,0
Sisal	Leaf	60,0 – 73,0
Wheat Straw	Stalk	30,0 – 35,0

Source: (Hernandez & Rosa, 2016)

2.2.1 Rice Husk

Rice is the primary dietary staple in over 75 nations globally, whereas rice husk is a by-product derived from dehusking rice at mills. Rice husks as shown in Figure 2.1 refer to the hard-protective coverings that enclose rice grains and are extracted from the grains as part of the milling procedure. According to Acharya et al. (2018), the annual production of rice husk amounts to around 80 million tons, representing approximately one-fifth of the global annual rice yield. Malaysia generates a yearly output of approximately 400,000 tons of rice husk. The rice milling industry produces a significant amount of rice husks by separating the husks from the raw grain to obtain whole brown rice, which is then further milled to eliminate the bran layer and get white rice. In the milling process of paddy, it is seen that around 78% of the total weight comprises bran, rice, and broken rice, while the remaining 22% of the weight consists of husk. It is worth noting that the husk component contains a considerably large amount of organic carbon, ranging from 30% to 50%. The conventional method of rice husk disposal involves the combustion of rice husk, resulting in the emission of hazardous pollutants and solid particles into the surrounding environment.

Consequently, the use of rice husk for industrial purposes emerged as a viable alternative for managing rice husk waste, primarily due to its abundant availability and cost-effectiveness. An additional advantageous application of rice husk disposal is the extraction of its constituent elements, namely cellulose comprising 50%, hemicellulose comprising 25%, lignin comprising 25% to 30%, silica comprising 15%, and moisture comprising 10% to 15% (Singh, 2018). Given that cellulose is the predominant constituent of rice husk, the utilization of rice husk as a potential source of cellulose to produce cellulose fiber holds considerable promise. Conversely, using rice husk in industrial applications would incentivize rice farmers to trade the husk rather than resorting to its combustion, fostering environmental sustainability.

According to the study conducted by Satbaev et al. (2021), rice husk can be classified as an organo-mineral substance. Rice production waste, in the form of massive tonnages, is a significant environmental pollution challenge on a big scale. The production of rice on a global scale result in the generation of a substantial amount of waste, which has the potential to create considerable environmental pollution. This pollution is mainly attributed to silicon dioxide in the waste, as it hinders the humification process (Satbaev et al., 2021). In the meantime, the

coexistence of carbon and silicon dioxide within its composition has extensive potential for its utilization as a valuable primary resource. Typically, the combustion of rice husk in an oxygen-rich environment results in rice husk ash, primarily composed of silica with trace impurities. Heavy metals in rice husk ash have been identified as a potential source of environmental and health risks to both ecosystems and human populations (Ogbuefi et al., 2020). The characteristics of rice husk ash are influenced by the combustion process used in burning the rice husk and the environmental factors associated with its source. Each year, a remarkable 7.4 million tonnes of rice husk ash is generated, presenting a significant environmental hazard since it adversely impacts the surrounding area and land upon its disposal. While burning rice husk into ash, the ignition cycle effectively removes organic components, resulting in the development of residue abundant in silica (Zaid et al., 2021). Inhalation of silica particles poses a significant health risk since it can result in the development of silicosis, a potentially fatal lung disease. Silica possesses inherent hazards due to its finely particulate nature, which enables it to infiltrate the respiratory system and have detrimental effects readily.

However, there has been growing interest in using rice husk due to its abundance and potential as a valuable resource. Rice husk has several important uses, including energy production. Rice husk burning generates refined heat and power for many applications. Indian scientists and engineers developed a nomograph to calculate the husk needed for grinding, parboiling, and drying. Rice husk's high calorific value, low sulphur, and low ash content make it a good biomass fuel. It is 50% as calorific as coal (Singh, 2018). India parboils 50% of processed paddy. Parboiling and grinding need thermal and mechanical energy, whereas drying uses solar energy (Goyal, 2014).

Moreover, due to the characteristic of rice husk from cellulose, it has the application of microbead production. Cellulose extracted from rice husks has high strength and durability. Cellulose is a solid and durable material, making it ideal for microbeads that must withstand the wear and tear of use. Besides, cellulose is a biocompatible material that is safe to contact with the skin and body. Most importantly, it is a biodegradable material that will eventually break down naturally in an environment that does not cause pollution.

In summary, rice husk, a by-product generated during rice milling, is a substantial waste substance produced on a global scale of approximately 80 million tonnes per year. The

conventional practice of incineration as a means of disposal has been found to have adverse effects on the environment, leading to contamination. Nevertheless, there has been increasing scholarly attention towards using rice husk owing to its abundant availability and promising prospects. The high calorific value of this substance renders it a feasible biomass fuel option, enabling its utilization in energy generation applications. Moreover, the recovery of constituents such as cellulose from rice husk presents diverse potential applications, such as the production of microbeads, owing to its robustness and capacity to decompose naturally. Using rice husks in various industries yields economic advantages and adds to environmental sustainability by mitigating the detrimental practice of husk combustion.

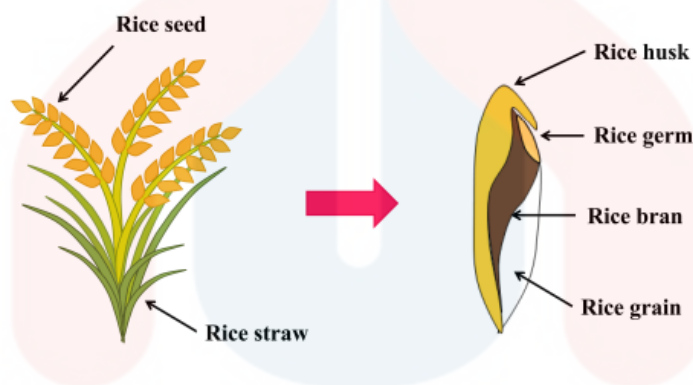


Figure 2.2: The anatomy of rice grain

(Peanparkdee & Iwamoto, 2019)

2.2.2 Corn Straw

Corn straw, also known as corn stover, remains the leftover material after the corn grains have been harvested. It comprises the stalks, leaves, and other plant components of the corn plant, which is grown worldwide for its grains and used as animal feed. According to Ruan et al. (2019), corn straw typically contains about 35% cellulose, 20% hemicellulose, and 12% lignin by weight. Corn straw has been used for various purposes throughout history, including fuel, thatching material for roofs, and animal bedding. According to the September 2021 World Agricultural

Supply and Demand Estimates (WASDE) report from the United States Department of Agriculture (USDA), the projected global production of corn for the 2021/2022 marketing year is 1.194 billion metric tons, representing a 3% increase from the previous year. The United States, China, Brazil, Argentina, and Ukraine are the largest corn producers in the world.

Instead of being direct burn, the waste corn straw will eventually lead to environmental problems, corn; nowadays, corn straw is increasingly recognized for its potential as a source of renewable resources as the starch content is from 20% to 80% of dry mass (Muffler et al., 2011). The cellulose extraction from corn straw offers a promising pathway to produce sustainable and renewable materials, which can be used in various industrial applications. Generally, corn straw can be used as a renewable source of fertilizer as it contains valuable nutrients such as nitrogen (0.6%), phosphorus (0.27%), and potassium (2.28%) as well as organic matter (15%) (Zhonglan Gao et al., 2013). Thus, corn straw as a natural fertilizer can be returned to the soil to improve soil fertility while improving the physical and chemical properties of the soil. Moreover, corn straw is a nutrient-rich resource that can produce protein feed through straw production technology. This approach can effectively reduce costs and improve economic benefits in aquaculture. At the same time, promoting grain-saving and resource-oriented animal husbandry. Nazli and colleagues (2018) found that corn straw had the most favourable nutritive composition compared to other feed sources, with lower levels of highly indigestible fibre and higher concentrations of organic matter and energy.

The maize tassel is generally considered a waste biomaterial derived from maize plantations, primarily due to the limited applications of its tassels. The maize tassel as shown in Figure 2.2, also known as the male flower, is the reproductive structure of the maize plant that emerges from the apical meristem. The maize tassels exhibit a range of purple, yellow, and green shades, which begin to emerge at the plant's apex after its primary growth phase. According to Duangpapeng et al. (2018), wind plays a crucial role in the pollination process of maize. Specifically, the study highlights that the pollen generated on the apex of the maize tassel is dispersed by wind to fertilize the silk, representing the plant's female flowers. The typical tassel can generate approximately 25 million pollen grains. The viability of pollen grains lasts for 60 to 240 minutes following their shedding, during which they can travel distances exceeding 300 metres. A single ear of maize generally yields a minimum of 1,000 fully developed kernels.

Consequently, each tassel of maize produces an abundance of pollen to ensure successful ear pollination. Once the process of maize fertilization has concluded and the crops have been harvested, the maize tassels typically become agricultural waste. They are discarded in significant quantities, as are the remaining parts of the corn plant. However, due to their composition as a carbohydrate-rich fibrous component of plants, maize tassels are expected to comprise large amounts of polysaccharides. The cellulose surface of these tassels is known to contain hydroxy groups and residual aromatic compounds, which contribute to the release of a distinct scent throughout the vegetative phase. Maepa et al. (2015) have reported that carbonyl, hydroxyl, and amine functional groups and conjugated bonds on the surface of maize tassels offer potential binding sites for metal oxoanions and cations.

In contrast, the maize stalk, classified as a gramineous plant, exhibits toughness and thickness, measuring around 0.8 m to 3 m in height and 2 cm to 4.5 cm in width. Distinct nodes and internodes characterise it. The primary components of maize stalks are predominantly leaves and stems, with the stems including both cortex and pith. One of the distinguishing features of maize stalks is the presence of a significant amount of pith within the branch. The proportion of cortex, leaf, and pith in the overall weight of stalks is 40%, 35%, and 15%, respectively. The composition of maize stalk typically consists of cellulose ranging from 35% to 50%, lignin ranging from 5% to 34%, and petosan ranging from 20% to 41%, while Huang et al. (2017) reported that the cellulose content in maize stalk is around 32.73%. The intermolecular bonding of cellulose, hemicellulose, and lignin in maize stalks leads to the emergence of specific characteristics in the plant, including flexibility, mechanical strength, and resistance to enzymatic digestion (Terrett & Dupree, 2019). Hence, to enhance the efficient utilization of maize stalk and optimize its value, completely dismantle, or partially modify the condensed structure by pretreatment. This will enable the effective utilization of the primary constituents and the conversion of other components, improving the high-value utilization of maize stalk.

Although corn straw has several benefits for different purposes like energy or feed, it has potential environmental drawbacks. Removing corn straw from fields can decrease soil organic matter and increase the risk of erosion, negatively affecting soil quality and water resources. Moreover, using corn straw for energy may increase greenhouse gas emissions if not managed appropriately. The burning of corn straw releases carbon dioxide, methane, and other gases that

contribute to climate change. Therefore, it is essential to consider the environmental implications of using corn straws for various purposes and prioritize sustainable practices that minimize negative impacts on ecosystems and the climate.

In conclusion, corn straw remains after harvesting maize grains and can be used for various purposes such as fuel, animal bedding, and roof thatching. With its high cellulose, hemicellulose, and lignin content, it also has the potential to be a promising renewable resource for industrial use.

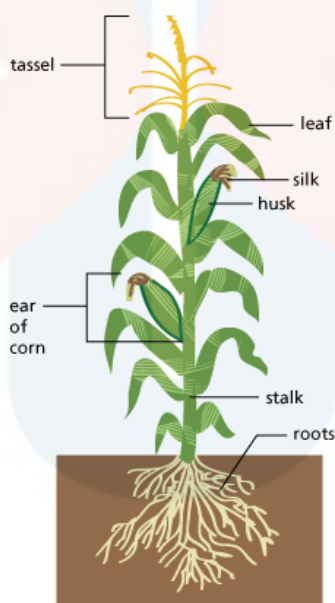


Figure 2.2: Corn plant parts

Source: (learning-fields, 2020)

2.2.3 Oil Palm Empty Fruit Bunch

Oil palm empty fruit bunches (OPEFB) as shown in Figure 2.3 refer to the leftover fruit after the oil extraction from the *Elaeis guineensis* tree (Noah, 2022). OPEFB is among the most abundant agricultural waste worldwide, mostly generated in Indonesia and Malaysia, the leading palm oil producers globally. According to the Malaysian Palm Oil Board (2022), the palm oil industry experienced a slight increase in crude palm oil (CPO) production in 2022 compared to

2021, and the total exportation of palm oil and its by-products reached 24.72 million tonnes. The empty fruit bunches from oil palm comprise cellulose, hemicellulose, and lignin, which constitute the fundamental elements of lignocellulosic biomass. Biomass waste that includes lignocellulosic components typically consists of 37.1% cellulose, 39.9% hemicellulose, 18.6% lignin, and 3.1% extractives, which can have practical applications in producing valuable chemicals (Megashah et al., 2018).

Oil palm empty fruit bunches (OPEFB) were once considered waste and burned, leading to environmental pollution and greenhouse gas emissions. However, OPEFB's unique characteristics, such as thermal properties, low density, specific strength, lightweight structure, biodegradability, and affordability, have made it an attractive resource for various applications, including bioenergy, paper and pulp, and high-value biochemical and biomaterial production (Arya et al., 2015). Nonetheless, the palm oil industry faces a challenge managing its solid and liquid waste, which includes organic waste from the harvest process, such as empty fruit bunches, fresh fruit bunches, oil palm trunks, palm fronds, palm oil mill effluent, palm oil mill sludge, and carbon dioxide emissions. OPEFB accounts for 9% of this waste, and its efficient management is crucial to mitigate the environmental impact of the palm oil industry. (Gabriel et al., 2020).

OPEFB have the potential to be a valuable resource in sustainable and environmentally friendly applications. However, further research is necessary to fully explore the range of benefits that can be derived from this waste material while also addressing potential environmental concerns related to its use.



Source: (Dullah, 2018)

Figure 2.3: Oil palm empty fruit bunch

2.3 Extraction

According to Zhang et al. (2018), extraction is the first step in obtaining natural products from raw materials, which involves separating the desired components. On the other hand, cellulose extraction is the process of isolating cellulose from plant cell walls using different methods, such as mechanical, chemical, and bio-extraction methods. In mechanical cellulose extraction, several techniques are used, including steam explosion, grinding, crushing, and high-pressurized homogenization (Omran et al., 2021). Steam explosion involves heating plant material with steam, followed by rapid depressurization to disrupt the cell wall structure and release the cellulose. Grinding and crushing physically break down the plant material into smaller pieces to expose the cellulose fibres. At the same time, high-pressurized homogenization involves forcing the material through a narrow gap under high pressure to achieve similar effects. Although mechanical cellulose extraction is a simple, eco-friendly, and cost-effective method that does not require harsh chemicals or solvents, it has some disadvantages. One of the main challenges is that it is an energy-intensive process that requires specialized equipment for the mechanical disintegration of plant fibres into cellulose (Lee et al., 2014).

Chemical methods for cellulose extraction typically involve using degumming processes, acid or alkali treatments, chemical retting, and chemical-assisted natural methods to remove lignin from plant fibres while also affecting other components of the fibre microstructure such as hemicellulose, pectin, and other non-cellulosic materials (Abral et al., 2020). Chemical extraction is achieved by heating, cleaning, and soaking the fibre in an acid or alkali solution that causes minimal damage to the fibre while improving its properties. Degumming removes gummy and pectin content while maintaining the shape of ramie fibres. Chemical retting, on the other hand, reduces water and lignin content in fibres. Although chemical cellulose extraction can effectively remove lignin and other impurities from plant fibres, chemical materials may produce toxic waste by-products, so proper handling methods are necessary.

Bio-extraction methods for cellulose involve using microorganisms such as fungi and bacteria to break down plant materials' hemicellulose and lignin components to extract the cellulose (Behera et al., 2017). Enzymatic hydrolysis is one technique that involves using enzymes like hemicellulase and lignin-degrading enzymes to break down the hemicellulose and lignin

components of plant material, resulting in cellulose fibres. Another technique is microbial fermentation, which uses microorganisms such as bacteria and fungi to break down the lignocellulosic material and extract the cellulose. Bio-extraction has potential advantages over mechanical and chemical methods due to lower energy consumption and fewer environmental impacts. However, further optimization of this method through additional research is necessary.

2.4 Chemical Extraction Method

The alkaline treatment method is commonly used for cellulose extraction from various plant-based materials. It involves the use of alkaline solutions such as alkali treatment, delignification, and bleaching process to remove non-cellulosic components such as lignin, hemicellulose, and pectin from the raw material, leaving behind a purified cellulose product.

2.4.1 Alkali Treatment

The alkaline treatment or mercerization process involves immersing natural fibers in an aqueous sodium hydroxide solution of a specific concentration for a designated duration and temperature. This treatment effectively removes substances such as hemicellulose, lignin, wax, and oils from the outer surface of natural fibers, thereby altering their surface. For example, the pectin in hemp fibers may be removed using an alkaline treatment, which does not leave any residue behind. However, the amount left behind of lignin depends on the quantity of NaOH that was employed. Removing less dense components such as hemicellulose and lignin enhances the interaction between the fiber and matrix, thereby ensuring strong adhesion between them. The procedure of alkaline treatment applied to hemp fibers has been found to effectively eliminate pectin without leaving any residual matter. However, the quantity of lignin remaining in the fibers depends on the NaOH concentration utilized during treatment. Fibers' density can be enhanced by an alkaline treatment, which removes lower-density elements like hemicellulose and lignin. During treatment, lignin degradation and transformation result in fibers exhibiting a progressively more yellowish appearance.

The fibers separate during the alkaline treatment, increasing the accessible surface area for resin wetting. In addition, the treatment causes variations in the crystallinity of the fibers, as well as changes in the structure of the unit cells and the orientation of the fibers. Recent research by Jakob et al. (2021) has revealed that cellulose fibers exhibit greater strength and stiffness with a specific orientation. Consequently, the alkaline treatment promotes an increase in the proportion of crystalline cellulose, thereby enhancing the mechanical properties of the composite through improved charge transfer between the matrix and the fibers. Notably, after washing the fibers with distilled water, acetic acid is utilized to neutralize the fibers, thereby halting any ongoing reaction and eliminating residual hydroxyl groups.

The surface of natural fibers can be modified by applying alkali treatment, a technique that enhances the interaction between the fibers and polymer matrix. Removing certain substances such as hemicellulose, lignin, wax, and pectin is the primary benefit of alkali treatment on natural fibers, as these substances typically cover the surface of the fibers. This is achieved through the breaking of lignin bonds and the hydrolyzing of glycosidic bonds. The previously smooth surface of natural fibers becomes rough because of the alkali treatment, leading to improved mechanical bonding. Additionally, the bonding between natural fibers and the matrix is enhanced through alkali treatment. The composite interface's strength depends on mechanical interlocking and bonding mechanisms, and alkali treatment of natural fibers has been shown to optimize the bonding between the fibers and the matrix, resulting in stronger composites compared to untreated natural fibers. Studies have demonstrated that alkali treatment can effectively remove lignin and hemicellulose from empty fruit bunch fibers, rice husks, and oil palm empty fruit bunches, thereby enhancing cellulose accessibility and reducing the lignin and hemicellulose content in these materials.

2.4.2 Bleaching Process

Bleaching is a chemical procedure that eliminates hemicellulose and any remaining lignin that may not have been removed during pretreatment, all while preserving the pulp fiber's yield, integrity, and strength (Tarchoun et al., 2019). Since lignin consists of diverse connections, the bleaching process for chemical pulp or lignin removal involves multiple stages using chlorine or

oxygen compounds. These compounds are employed to break down the different bonds present in lignin.

Bleaching agents, such as sodium hypochlorite (NaOCl) and sodium chlorite (NaClO_2), are commonly utilized as oxidizing chemicals to facilitate the process of bleaching (Marzoug et al., 2010). The bleaching process typically involves the disintegration of water-insoluble lignin via specific bond cleavages, including β -O-4 bonds, carbon-carbon bonds, or aryl ether bonds, which results in the creation of water-soluble products such as carboxylic acids and aromatic aldehydes (Dai et al., 2016). The decomposition of NaClO_2 gives rise to chlorine dioxide, known for its potent oxidizing properties. Moreover, the rate of sodium chlorite decomposition escalates with a reduction in pH and an elevation in bleaching bath temperature. In alkaline conditions, aqueous sodium chlorite remains highly stable; however, to activate and enhance its bleaching properties, the medium necessitates acidification by introducing acetic acid (Abdel-Halim, 2014). Using concentrated acids for activation produces toxic and corrosive chlorine dioxide gas, which mandates regulating its evolution rate.

The primary objective of the bleaching process of cellulose-based materials is to eradicate non-cellulosic impurities that cause cellulose discoloration or alter them to facilitate their removal later. When dealing with woody cellulose material, it is customary to subject it to chlorine treatment, which results in the oxidation of a substantial portion of the non-cellulosic substances. This is subsequently accompanied by washing and bleaching procedures to reduce the color of the cellulose. Hypochlorite, chlorine dioxide, and hydrogen peroxide are conventionally utilized in the subsequent stages to achieve bleached cellulose. The selection of specific steps in a bleaching sequence primarily depends on the sort of cellulose-based materials involved.

The various stages involved in bleaching hemicellulose can be appropriately classified into two categories, which include acidic and alkaline treatments. The alkaline treatments can be further subcategorized into cold caustic extraction (CCE) and hot caustic extraction (HCE). The former is performed at temperatures that oscillate between $25\text{--}45^\circ\text{C}$, while the latter is typically conducted at temperatures between $70\text{--}120^\circ\text{C}$ (Li et al., 2017). However, it is noteworthy that with an increase in temperature, the treatments become less specific and can lead to various reactions, such as the degradation of cellulose through either acidic or alkaline processes. It has been reported that strong

alkaline degradation of cellulose, which includes hydrolysis, only transpires at temperatures that exceed 140°C (Friebel et al., 2019).

Determining the concentration of ions dissociating in water from the bleaching agent depends on the pH level, which plays a pivotal role in cellulose bleaching. These ions subsequently interact with cellulose fibers, leading to the bleaching and decolorization of cellulose. The pH level also significantly impacts the fibers' characteristics, such as their softness and tensile strength. It is worth noting that lower pH levels can instigate the degradation of fibers, which may culminate in a reduction in their tensile strength. Achieving fully brightened cellulose typically necessitates several consecutive bleaching stages, which range from three to seven, as reported by Pinto and colleagues (2022).

2.4.3 Delignification

Delignification is breaking down the lignocellulosic material into its fibrous constituents. This process entails the separation of lignin from plant sources through diverse techniques, as stated by Kucharska et al. (2018). Delignification is typically categorized into two main types which are chemical and solvent processes. The most used methods in industrial settings are alkaline and sulfite pulping, which fall under chemical pulping processes. These processes represent the two extremes of the pH scale. Alkaline or kraft pulping leads to the production of thio-lignin or alkali-, while the acidic sulfite process produces liginosulfonate, also known as lignin sulphonic acid.

Lignin, a type of phenolic compounds found within the secondary cell wall of plants, plays a vital role in maintaining structural strength and connecting cellulose carbohydrates essential for paper fibre production., as highlighted by Liu et al. (2018). This intricate arrangement creates a hydrophobic matrix that repels water and enables plants to transport water throughout their system. According to Mariana et al. (2021), lignin greatly increases the strength of cell walls. It decreases their digestibility, both by animals and during the chemical delignification process, resulting in a higher level of integrity and reduced susceptibility to decomposition. Furthermore, this polymer decreases plants' vulnerability to attacks from insects and plant pathogens. As plants decompose,

lignin remains one of the last compounds, accumulating in the soil as a humus. Overall, the delignification process is a critical step in producing paper and other products, as it allows for the extraction of lignin and the separation of fibrous components, thereby enabling the utilization of cellulose for various applications.

Alkaline delignification, as a pretreatment method, is highly effective due to its strong efficiency and straightforward process. The technique utilizes different alkaline substances, including sodium carbonate (Na_2CO_3), calcium hydroxide ($\text{Ca}(\text{OH})_2$), sodium hydroxide (NaOH), and ammonia (HN_3), for the elimination of lignin from the biomass. The alkalis break down the structure of lignin and separate it from carbohydrates, thereby enhancing the accessibility of carbohydrates in the biomass for enzymatic degradation. Furthermore, the alkali treatment causes the biomass to swell, increasing its porosity and internal surface area while reducing the degree of polymerization and cellulose crystallinity (Bajpai, 2016). Unlike other pretreatment methods, alkaline delignification requires lower temperatures and pressures, making it less energy intensive (Jørgensen et al., 2007). However, it is important to mention that while alkaline delignification can be conducted at ambient temperature, extended pretreatment durations, typically lasting hours, or days rather than minutes or seconds, may be required to attain comparable digestibility levels. (Balat et al., 2008).

When comparing acid pretreatment with alkaline delignification, the latter causes less sugar degradation. Nevertheless, a drawback is that some of the alkalis are converted into salts that cannot be recovered or incorporated into the biomass as salts during the pretreatment. It should also be mentioned that in alkaline systems, the cleavage of β -aryl ether bonds can occur in phenolic and nonphenolic aryl propane units. Overall, the advantages of alkaline delignification, including its low energy requirements and mild reaction conditions, make it a promising pretreatment method for lignocellulosic biomass.

2.5 Quantitative Analysis

After extracting of cellulose, the dried cellulose was weight and the yield was calculated using Equation 2.1.

Analysis of cellulose yield:

$$\frac{\text{final weight of extracted cellulose (g)}}{\text{initial weeight of sample (g)}} \times 100\% \quad \text{Equation 2.1}$$

2.6 Characterization of Cellulose

Cellulose can be assessed using various analytical methods, including scanning electron microscopy (SEM), Fourier transform infrared spectroscopy (FT-IR), X-ray diffraction (XRD), and thermogravimetric analysis (TGA). These techniques enable the examination of surface structure, chemical groups, crystalline structure, and thermal characteristics of cellulose, respectively.

2.6.1 Scanning Electron Microscopy (SEM)

SEM is a method that enables the analysis of particle size, shape, and texture using small quantities of material (Amidon et al., 2009). It is a highly effective and non-destructive technique that provides detailed information on the composition, structure, and composition of the sample. The first scanning electron microscope was invented in 1942. It was demonstrated at that time that a positive bias on the collector, rather than the sample itself, produced topographic contrast through Secondary Electrons (SE). The crucial elements of SEM consist of an electron emitter, electromagnetic lenses to concentrate electrons, detectors for electron detection, chambers for sample placement, computers, and a display for visualizing images (Figure 2.4). Electrons produced at the upper part of the column are propelled downwards, traversing a sequence of lenses and openings to form an accurate electron beam. This beam subsequently engages with the surface of the specimen (Figure 2.5), which is situated on a mobile platform within a vacuum environment. (Pallares-Rusiñol et al., 2023). The electron-beam coils are manipulated to scan the surface of the

sample, enabling the gathering of data pertaining to a particular region of the sample. Upon interaction with the sample, the electron beam produces diverse signals that are detectable using suitable detectors.

In Scanning Electron Microscopy (SEM), two categories of electrons are detected which are secondary electrons (SE) and backscattered electrons (BSE) (Vac Coat, 2023). BSEs, or backscattered electrons, are electrons that undergo redirection after elastically colliding with the sample. In contrast, secondary electrons are generated from the sample's atoms and are produced because of inelastic collisions between the electron beam and the sample. Secondary electrons has generally lower energy content when compared to backscattered electrons. When the electron beam undergoes inelastic collision with the surface of the sample, the energy carried by the electrons in the beam is transferred to the conduction band electrons and occasionally to the valence band of the sample. This transfer separates these electrons from the sample atoms, leading to the formation of secondary electrons. BSEs, on the other hand, are reflected back from deeper places within the sample, and the atomic number of the material has an effect on how intensely they are reflected. A higher atomic number of the material produces a brighter image.

SEM offers numerous benefits, such as its ability to generate detailed three-dimensional (3D) topographic images and obtain versatile information through various detectors. It possesses advantages like high resolution, a wide depth of field, powerful magnification, and effective stereoscopic vision (Wen et al., 2021). Operating the microscope is straightforward, and the associated software is user-friendly. However, SEM has drawbacks related to its size and cost. Operating SEM can be expensive, and sample preparation may result in artifacts. Moreover, a notable constraint of SEM lies in its capability to only analyses solid, inorganic samples that are suitable for insertion into a vacuum chamber equipped to withstand moderate vacuum pressure. (Singh, 2016).

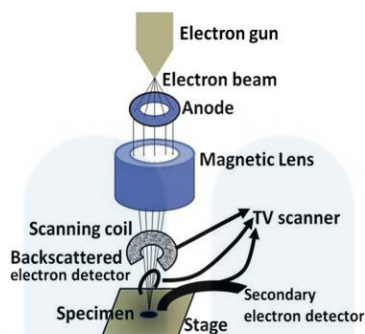


Figure 2.4: Components of scanning electron microscopy (SEM)

Source: (Singh, 2016)

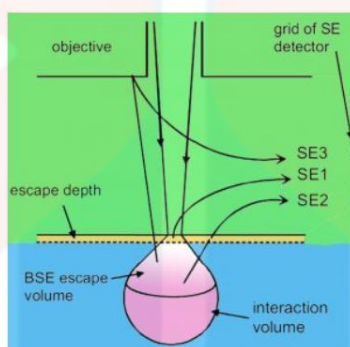


Figure 2.5: Electron interactions with the specimen

Source: (Singh, 2016)

2.6.2 Fourier Transform Infrared (FTIR)

The Fourier transform infrared spectrometer, commonly called FTIR, is a highly advanced infrared spectrometer offering numerous advantages over traditional dispersive spectrometers. Notably, it offers unparalleled speed, precision, accuracy, increased sensitivity, ease of use, and non-destructive sampling capabilities. Undavalli et al. (2021) reported that infrared spectroscopy technology is founded on the atomic vibrations of molecules that selectively absorb specific frequencies and energy of infrared light. By analyzing the unique infrared spectra of molecules, FTIR spectrometers can accurately identify and classify them.

The FTIR spectrometer uses an interferometer to determine the heat being sent to the sample. The resulting spectrum is produced by applying a Fourier transformation to the coherent signal captured in the time domain (Siemens, 2018). The interferometer detects infrared radiation

emitted by a dark body and encodes the signals spectrally. The resultant interferogram signal then either travels through or reflects off the sample's surface, where certain energy wavelengths are absorbed. Finally, the beam reaches the detector, which is further processed by a computer to perform Fourier transformation on the energy signals (Figure 2.6).

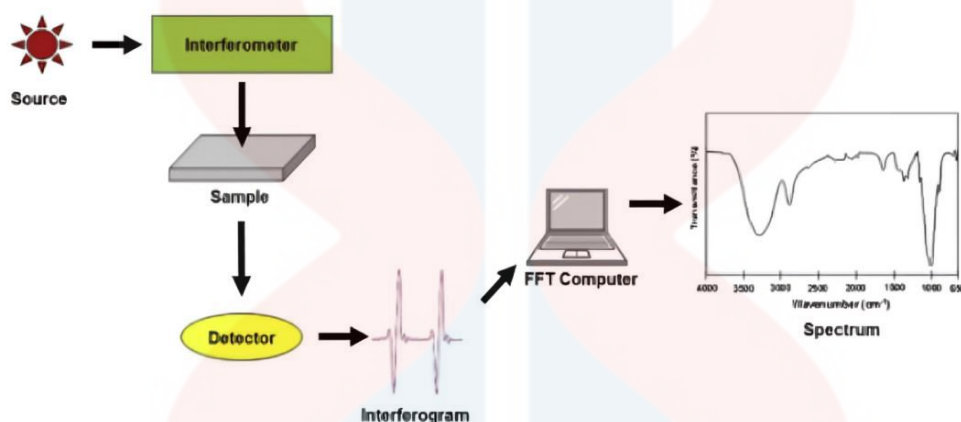


Figure 2.6: Fourier transform infrared processing

Source: (Undavalli et al., 2021)

When a certain amount of light energy is sent through a given sample, there is a possibility that it will be absorbed by atom clusters contained inside the material. This happens when the frequency of the entering light coincides with the frequency of vibrations inside the bonds connecting the atoms (Torres-Rivero et al., 2021). The energy associated with these vibrations depends on various elements, including the masses and chemical environments of the atoms involved and the type of vibration itself. It is possible to identify the functional groups on the sample's surface by scanning through a range of wavelengths (400-4000 cm⁻¹) and measuring the quantity of light transmitted at each wavelength (Pednekar et al., 2017).

Fourier Transform Infrared (FTIR) spectroscopy is a quick and non-destructive method for determining biomass's qualitative and quantitative composition in the mid-infrared range. Identifying molecular fragments and determining the presence or absence of certain functional groups are two of the most important contributions that FTIR spectroscopy makes to understanding the structure of fibers (Hospodarova et al., 2018). Furthermore, it enables identifying and quantifying essential functional groups such as carbonyl groups (C=O), hydroxyl groups (-OH),

and glycosidic connections, all of which are critical for cellulose's distinctive chemical composition. In addition to chemical characterization, FTIR spectroscopy allows for a full structural investigation of cellulose.

Fourier Transform Infrared (FTIR) spectroscopy, according to Rani et al. (2015), provides necessary information about the level of crystallinity. This critical parameter determines the mechanical strength and physical properties of cellulose materials. FTIR spectroscopy also allows for analyzing cellulose interactions with other components or additions. The impact of various treatments or alterations on cellulose may be examined by monitoring the shifts or changes in absorption bands.

2.6.3 X-ray Diffraction (XRD)

According to Raja et al. (2022) X-ray diffraction (XRD) is a non-destructive analytical method that provides an in-depth examination of the crystallographic structure, physical characteristics, and chemical composition of materials. Notably, XRD is also highly advantageous for stress measurement and texture analysis. It should be emphasized that XRD requires crystalline samples, although it can also determine the degree of crystallinity in polymers (Nasrazadani & Hassani, 2016). The fundamental principle of XRD is based on Bragg's equation, $n(\lambda) = 2d \sin \theta$, which describes the reflection of a collimated X-ray beam on a specific crystal plane of the sample under examination (Figure 2.8). X-ray diffraction (XRD), a technique that follows Bragg's law, is fundamentally concerned with the phenomenon in which reflected X-rays originating from crystal layers exhibiting long-range order encounter constructive interference. (Gu & Burgess, 2014).

The presence of intense peaks in the spectrum is a manifestation of this particular phenomenon. X-ray diffraction (XRD) is reliant on the scattering of X-rays at wide angles and is frequently utilized in the analysis of well-organized materials, particularly those with a high degree of crystalline order. However, it is not the most favored approach to investigate disordered materials. In the XRD technique, a sample is subjected to a beam of X-rays, leading to the scattering or diffraction of atoms in the path of the X-rays. Through the application of Bragg's law and the use of a suitably positioned detector, the interference derived from the X-ray scattering is

observed, thereby enabling the determination of the crystalline structure characteristics of the sample (Raval et al., 2019).

X-ray diffraction (XRD) technique are founded on the concept of elastic scattering of X-rays from materials that possess a significant level of structural uniformity, thereby allowing for the determination of important structural properties of the material under examination. The capacity of crystals to diffract X-rays stems from the similarity in wavelength between X-rays and the inter-atomic distances inherent within the crystal lattice. When the X-ray beam encounters the well-ordered three-dimensional atomic arrangements within the crystal, a significant proportion of the X-rays will experience destructive interference, resulting in their attenuation. It is the amplified diffracted X-rays that engender the distinctive diffraction pattern that is subsequently harnessed for the determination of the crystal's structural properties (Figure 2.7).

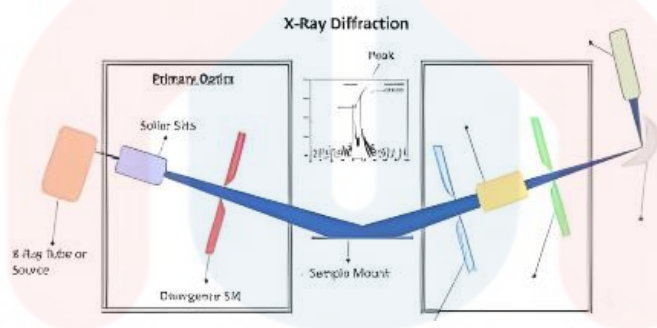


Figure 2.7: X-ray diffraction analysis

Source: (FerroThinfilms Lab, 2018)

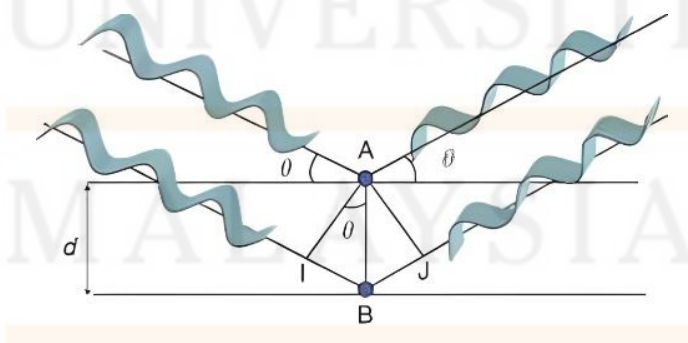


Figure 2.8: Bragg's law

(Pevelen, 2010)

However, the challenges associated with X-ray diffraction (XRD), which may include lengthy processing times and the need for significant sample quantities, the technique is widely used for the precise determination of atomic-level structures in samples (Ginder-Vogel & Sparks, 2010). However, one of the limitations of XRD is its inability to analyze crystal growth in real-time, which restricts the technique to providing information solely on a single conformation or binding state. Moreover, XRD exhibits lower intensity of diffracted X-rays, particularly for materials with low atomic numbers, compared to electron diffraction. Nonetheless, ongoing advancements in the application of femtosecond pulses generated by a hard X-ray free electron laser are currently enhancing XRD analysis. This approach facilitates the structural determination of macromolecules that cannot be adequately accomplished with conventional radiation sources due to the requirement for larger crystal sizes (Chapman, 2019).

2.6.4 Thermogravimetric Analysis (TGA)

Thermogravimetric analysis (TGA) is an efficient method, as stated by Ebnesajjad (2006), to assess the thermal stability of different materials, including polymers. As defined by Nurazzi et al. (2021), the essential principle of thermal analysis involves adjusting temperature as an experimental variable to scientifically or technologically characterize materials. TGA entails subjecting a sample to temperature increments within a controlled environment while measuring the weight changes of the sample (Dwivedi et al., 2017). Usually, the sample, weighing 10 to 50 mg, is positioned in a pan, then inserted into the TGA equipment comprising a furnace and an accurate balance (Mauer & Bradley, 2017). The TGA system involves a highly sensitive scale for weight alteration measurement and a programmable furnace for sample heating regulation.

The precision balance is positioned above the furnace and is thermally insulated to prevent heat transfer. A fine hang-down wire of remarkable precision is suspended from the balance and extends into the furnace (Figure 2.9). The sample pan is located at the tip of the wire, and its placement must be consistent to ensure accurate measurements. To improve precision, sensitivity, and weight accuracy, the balance is protected from thermal influences, often using a thermostatic chamber. Additionally, combining an infrared spectrometer with TGA allows for examining and identifying gases generated during the sample's degradation process (Figure 2.10).

The TGA instrument is equipped with a micro-furnace that allows for rapid cooling. The heating element is made of dependable platinum, which can tolerate temperatures up to 1000 °C. An external furnace with an alloy heating element consisting of 30% rhodium and platinum can be utilized to increase the temperature range, allowing for temperatures up to 1500 °C. Contemporary TGA apparatuses incorporate a computer to compute the weight-loss fraction or percentage accurately. According to Menczel and Prime (2009), commercial TGA systems possess remarkable capabilities, which include temperature capabilities that exceed 1000 °C, balance sensitivity as low as 0.1 µg, and adjustable controlled heat-up rates in the presence of air or other gases. The heat-up rate of the TGA may vary from 0.1 °C to 200 °C per minute.

Thermogravimetric analysis (TGA) has emerged as a feasible alternative for evaluating the constitution of lignocellulosic biomass, offering rapidity, cost-effectiveness, and user-friendliness. As per the findings of Gomes et al. (2018), TGA enables a more precise determination of the content of α -cellulose and hemicellulose compared to conventional wet chemical techniques. TGA has been effectively utilized in scrutinizing biochemical components such as cellulose, hemicellulose, and lignin in alkaline lignin and pretreated corn stover, which has augmented the precision of compositional analysis.

Cellulose is a crucial component of natural fibers and has a significant impact on their physical properties as well as their thermal degradation. Despite its importance, cellulose exhibits poor thermal resistance and is prone to decomposition at lower temperatures. This process is catalyzed by naturally occurring inorganic ions and may increase char production. While thermogravimetric analysis is a valuable tool for assessing polymers like lignin, it is a destructive method that can lead to changes in the analytes due to temperature ramping.

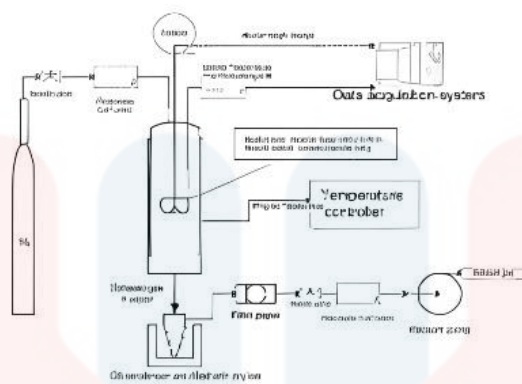


Figure 2.9: Schematic diagram of thermogravimetric analysis (TGA)

Source: (Unapumnuk et al., 2006)

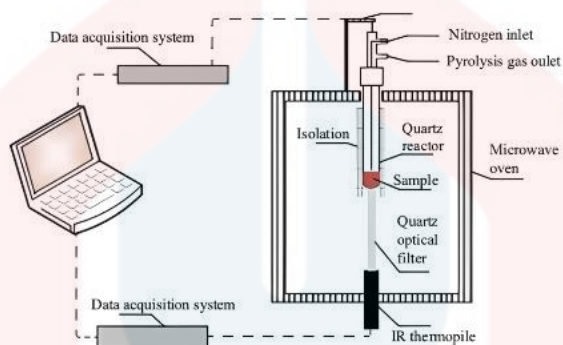


Figure 2.10: Schematic of microwave TGA apparatus

Source: (Saadatkhan et al., 2019)

UNIVERSITI
MALAYSIA
KELANTAN

CHAPTER 3

MATERIALS AND METHODS

3.1 Materials

In this study, sample of rice husk (RH) was collected at Sekinchan Paddy Field, Selangor. The corn straw (CS) and corn tassel (CT) was collected from Kampung Paloh, Bukit Panau, Tanah Merah, Kelantan, whereas the oil palm empty fruit bunch (OPEFB) was obtained from Ladang Kelapa Sawit Kampung, Kemahang, Kelantan.

3.2 Apparatus and Equipment

The apparatus that was used in this study are beaker (1000mL and 500mL), round bottom flask, measuring cylinder (100mL), stirrer, pH meter, filter paper and glass rod, sieve, hammer mill, magnetic stirrer, centrifuge, knife and chopping board.

Equipment that used in this study is Scanning Electron Microscope (SEM), Fourier-Transform Infrared Spectroscopy (FTIR), X-ray diffraction (XRD), Thermogravimetric Analysis (TGA), weighing balance, hot plate, heating mantle, oven, water bath, and thermometer.

3.3 Chemicals

Chemicals that were used in this study are sodium hydroxide (NaOH), sodium hypochlorite (NaOCl), toluene, ethanol, acetic acid (CH_3COOH), distilled water, dish detergent.

3.4 Preparation of Raw Materials

3.4.1 Preparation of Dried Rice Husk (DRH) Powder

Dried rice husk (DRH) was collected from Sekinchan Paddy Field, Selangor, and used as the raw material for control and cellulose source for this experiment. The rice husk, weighing 10 g, was washed and sun-dried for one week. The dried rice husks were then ground into smaller particles using a heavy blender and sifted through a 500-mesh sieve to obtain a finer powder. Finally, the dried rice husk powder was subjected to delignification and bleaching to extract cellulose.

3.4.2 Preparation of Corn Straw (CS) Powder

The harvested corn straw was collected Kampung Paloh, Bukit Panau, Tanah Merah, Kelantan. 100 g of corn stem (CS) and corn tassel (CT) was respectively rinsed with distilled water and dried under sun for one week. Then, they were ground using blender and sieved with 500-mesh to form a fine powder and stored in a zipper bag for further use.

3.4.3 Preparation of Oil Palm Empty Fruit Bunch Fibres (OPEFB) Powder

The study utilized dried oil palm empty fruit bunch (OPEFB) from Ladang Kelapa Sawit Kampung, Kemahang, Kelantan. The raw OPEFB was washed with 1% dish detergent to remove any impurities and visible dirt on its surface. It was then washed with distilled water until it turned from dark brown to colorless, before being sun-dried for one week. The dried sample was cut into small pieces using small knife and ground into powder. The powder was then sieved with 500-mesh to form a fine powder and stored in a zipper bag for further use.

3.5 Chemical Extraction

The powder sample of rice husk undergoes delignification and bleaching. In contrast, corn stem, corn tassel and oil palm empty fruit bunch undergo an alkaline treatment and bleaching process to extract cellulose for microbead production.

3.5.1 Delignification

10 grams of rice husk powder was placed into a 250 mL beaker, followed by 100 mL of 12% NaOH. The mixture was heated to 80°C for 3 hours and stirred with a magnetic stirrer. After that, the mixture was filtered, and the residue was washed with distilled water until a neutral pH was reached.

3.6 Bleaching

The process involved taking the delignification residue of the rice husk and placing it in a 250 mL beaker. Then, 100 mL of a 2.5% NaOCl solution was added, and the mixture was heated to 80°C and stirred for one hour. The resulting precipitate was filtered and washed with distilled water until a neutral pH was achieved. After allowing the sediment to sit for one hour, a cellulose extract was obtained from the rice husk.

3.6.1 Alkaline Treatment

10 grams of CS, CT, and OPEFB were respectively immersed in a 2:1 toluene-ethanol mixture and stirred continuously for 6 hours. The mixture was then filtered to remove the CS, CT and OPEFB, and the samples were dried overnight (16 hours) at 80°C. The CS, CT and OPEFB fibres were treated with a 0.1 M sodium hydroxide (NaOH) solution and swirled continuously at 80°C for 4 hours. To ensure the full elimination of NaOH residue, the sample was rinsed with distilled water until it achieved a neutral pH.

3.6.2 Bleaching Process for CS, CT and OPEFB

CS, CT and OPEFB were bleached using a combination of sodium hydroxide (NaOH) and acetic acid (CH_3COOH) in a 1.3:10 (v/v) ratio for 4 hours at 80°C . Following that, and the fibre was sufficiently washed with 0.1 M NaOH followed by distilled water till the pH of the fibre became neutral. The treated fibre was dried overnight (16 hours) at 80°C , yielding Cell-CS, Cell-CT, and Cell-OPEFB respectively.

3.7 Characterization of Cellulose Fibre

The maximum yield of a cellulose fibre derived from rice husk, corn stem, corn tassel, and oil palm empty fruit bunch is subjected to various tests such as SEM, FTIR, XRD, and TGA to analyse its physical and chemical properties. The purpose of these tests is to examine the characteristics of the cellulose in detail.

3.7.1 Scanning Electron Microscope (SEM) Analysis

The morphology of the obtained cellulose for rice husk, corn stem, corn tassel, and oil palm empty fruit bunch determined through the scanning electron microscope (SEM) with the brand JEOL JSM IT100. The electron beam scans across the surface of the sample, producing high-resolution images of the morphology of the extracted cellulose. The images can be magnified and viewed in real-time on a computer screen to get detail information of cellulose obtained.

3.7.2 Fourier Transforms Infrared (FTIR) Spectroscopy

FTIR spectroscopy is used to study the molecular fragments and identify the functional group of extracted cellulose after the treatment. A beam of infrared radiation is passed through the cellulose and the transmitted light is measured as a function of wavelength. The FTIR is performed using a Thermo Scientific™ Nicolet iZ10 FTIR spectrophotometer in the range of $400\text{--}4000\text{ cm}^{-1}$ with the resolution of 4 cm^{-1} .

3.7.3 X-Ray Diffraction (XRD)

The crystallinity of cellulose fibres in rice husk, corn straw, and oil palm empty fruit bunch is investigated after undergoing complete treatment. X-ray diffraction (XRD) analysis is employed to examine the crystalline structure. The XRD measurements are carried out using a Bruker D2 Phaser model X-ray diffractometer, which operated at 30 kV and 10 mA with Cu K α radiation. The scanning range for the measurements is set between 10° and 90° in the 2 θ scale. To assess the degree of crystallinity, the crystallinity index (CrI) is determined using the amorphous subtraction method. The CrI value is calculated utilizing Equation (3.1):

$$\text{CrI (\%)} = \frac{(I_{002} - I_{\text{am}})}{I_{002}} \times 100\% \quad \text{Equation 3. 1}$$

The symbol I_{002} represents the highest intensity observed in the diffraction peak corresponding to the (002) lattice plane, while I_{am} represents the intensity of the scattering caused by the amorphous portion of the samples. The diffraction peak associated with the (002) plane is situated at an angle of approximately $2\theta = 22^\circ$, while the intensity resulting from the scattering by the amorphous section is found around $2\theta = 18^\circ$.

3.7.4 Thermogravimetric Analysis (TGA)

The thermal stability of the samples is assessed using a Mettler Toledo TGA/DSC 2 HT thermogravimetric analyser. Approximately 7 mg of each sample is utilized for the measurements. The analyses are conducted under a nitrogen atmosphere, with a constant gas flow rate of 10 mL min⁻¹. The samples are heated from room temperature to 700°C at a controlled heating rate of 10°C min⁻¹.

CHAPTER 4

RESULTS AND DISCUSSION

4.1 Physical appearance of cellulose

4.1.1 Rice Husk

The initial color of untreated rice husk is dark brown. The color changed to light brown as a result of alkali treatment by using 2.5% sodium hydroxide in Figure 4.1. Sodium hydroxide is used to break down the hydroxyl (OH) groups, and the densely arranged crystalline structure into a new form amorphous network structure. Additionally, it eliminates certain compositions of fiber lignin, waxes, oils, and hemicelluloses that contribute to increased roughness of the fiber's surface (Selvakumar & Meenakshisundaram, 2022).

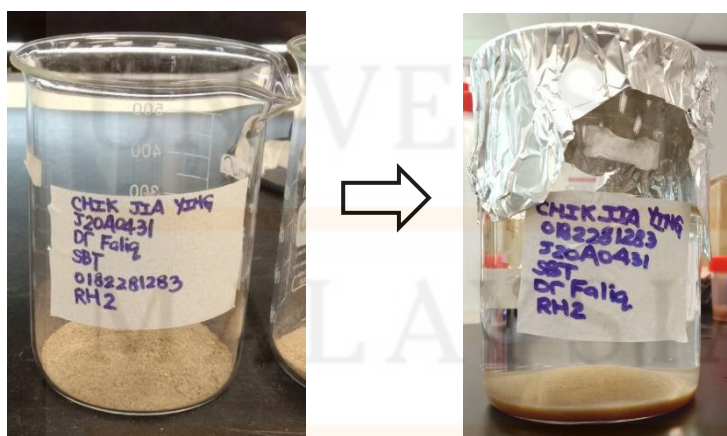


Figure 4. 1: The rice husk changes colour from dark brown to light brown after alkaline treatment

The delignification process of rice husk with 12% NaOH causes the color of the rice husk to become darker due to the alkaline, as shown in Figure 4.2. During cellulose extraction using NaOH during the delignification process, the darkening of biomass can be attributed to the

formation of lignin degradation products and lignin solubilization. When rice husk is treated with NaOH, it leads to the breakdown of lignin, releasing lignin degradation products such as phenolic compounds. These compounds can contribute to the dark coloration of the delignified rice husk (Geng et al., 2018). After the delignification process, the color of the rice husk changed from dark brown to light brown during bleaching with sodium hypochlorite (NaOCl). This can be attributed to the oxidation of chromophores and lignin in the rice husk. NaOCl is an oxidizing agent that can break down chromophores, which are responsible for the color of rice husks, resulting in a lighter appearance (Wang & Zhao, 2021). Additionally, NaOCl is capable of oxidizing lignin, leading to the formation of water-soluble products such as carboxylic acids and aromatic aldehydes, which can contribute to the removal of color from the rice bleached rice husk (Aridi et al., 2021).

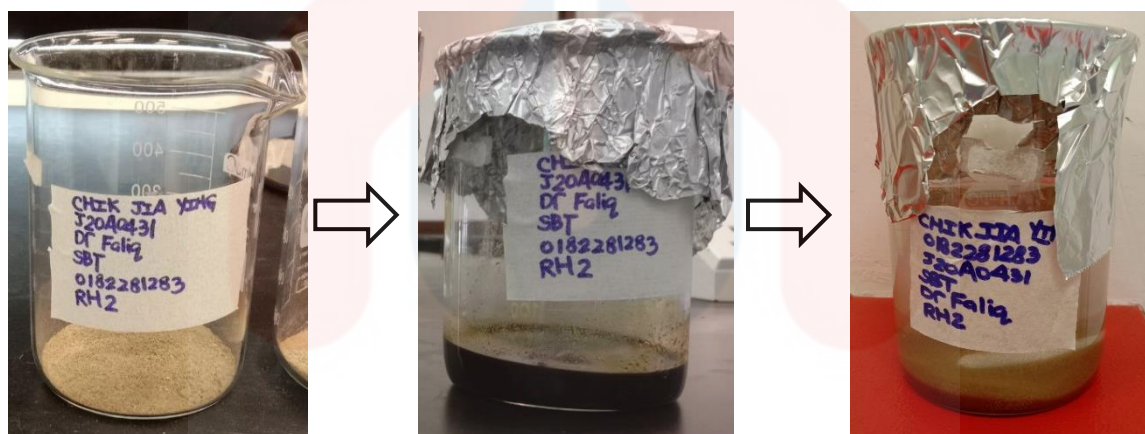


Figure 4. 2: The corn stem changes colour from brown to dark brown after alkaline treatment with toluene-ethanol mixture

4.1.2 Corn Stem

The initial color of the untreated corn stem is brown, and the color changed to dark brown due to alkali treatment by using a 2:1 toluene-ethanol mixture and washed with 0.1M NaOH, as shown in Figure 4.3. The corn stems delignification with a toluene-ethanol mixture plays a role in the cellulose extraction by serving as a solvent for dewaxing the corn stem fiber samples. This mixture helps remove impurities, waxes, and lipid substances from the fibers, which are later removed by filtering (Da Silva Vallejo et al., 2021). The dewaxing process is important as it helps to clean the external surface of fiber cell walls and remove impurities, making the fibers more suitable for following bleaching steps (Ng et al., 2015). The corn stem fiber undergoes a process involving the use of sodium hydroxide (NaOH) to facilitate the removal of lignin, pectin, waxes, and hemicellulose resulting in a textured surface (Wirawan et al., 2022). Among these components, lignin is the most challenging to degrade due to its intricate structure, strong insolubility, and high molecular weight. Lignin forms a complex three-dimensional network by connecting through carbon-carbon and ether bonds, associating with the hemicellulose polysaccharides within the cell wall (Misson et al., 2009). In addition, the alkaline treatment causes the fiber bundles to break down into smaller fibers, decreasing their diameter and increasing their aspect ratio (Patel & Parsania, 2018). This modification increases the total surface area of contact with the matrix material. Alkaline treatment disrupts the hydrogen bonds influenced by alkaline conditions within the fibers, resulting in the creation of new, active hydrogen bonds between cellulose molecules. As a result, certain water-attracting hydroxyl groups are partially eliminated, resulting in increased resilience against moisture.



Figure 4. 3: The corn stem changes colour from brown to dark brown after alkaline treatment with toluene-ethanol mixture

The corn stem fiber was bleached using a mixture of sodium hydroxide and acetic acid (CH_3COOH) with a ratio of 1.3:10 (v/v) and then washed with 0.1 M NaOH to remove the non-cellulosic component further. The color of the delignified rice husk fiber was dark brown and gradually changed to pale brown of bleached corn stem cellulose, as shown in Figure 4.4. Acetic acid acts as a solvent that aids in dissolving cellulose from the corn stem matrix. This dissolution process allows for separating cellulose fibers from other components of the corn stem, such as hemicellulose and lignin (Sato et al., 2003). The mixture of sodium hydroxide and acetic acid in the bleaching process can help improve the bleaching process's efficiency and reduce the amount of chemicals required. The corn stem fiber was washed with NaOH to remove any residue impurities or chemicals present after bleaching. NaOH is a strong base that can effectively neutralize and remove any acidic residues that may be present on the surface of corn stem cellulose (He et al., 2022). The washing step is important to ensure the purity and quality of the final extracted corn stem cellulose and to prevent any potential adverse effects on the properties and performance of the cellulose.

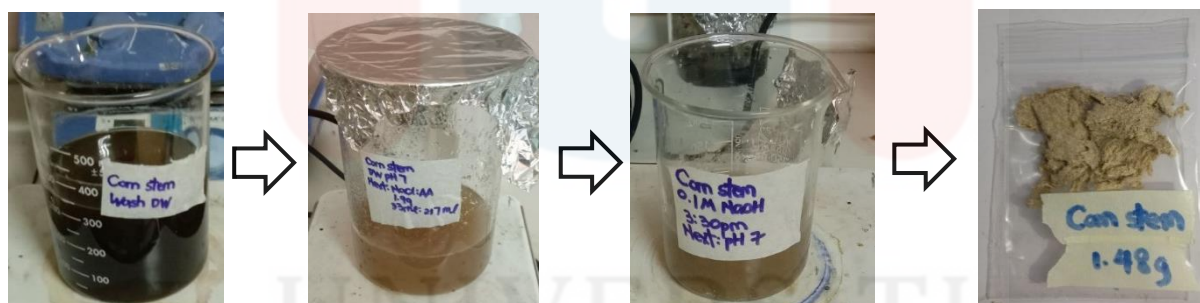


Figure 4. 4: The colour transition from brown and gradual discoloration to pale brown due to bleaching process with mixture of sodium hydroxide and acetic acid

4.1.3 Corn Tassel

The initial colour of the untreated corn tassel is brown, and the colour changed to dark brown due to alkali treatment by using a 2:1 toluene-ethanol mixture and washed with 0.1M NaOH, as shown in Figure 4.5. The toluene-ethanol mixture is used as a dewaxing agent in the delignification process. Dewaxing removes waxes and similar compounds from the raw corn tassel (Pham et al., 2022). This can contribute to the purification of corn tassel cellulose yield. Meanwhile, the corn tassel fibre is treated with 0.1 M NaOH, which serves the function of solubilizing and removing lignin from the corn tassel. The 0.1 M NaOH solution dissolves the lignin from the corn tassel matrix, allowing for a subsequent bleaching process. NaOH is a strong base that can disrupt the association of lignin with other components, such as carbohydrates, and facilitate its dissolution (Kangas et al., 2014).



Figure 4. 5: The corn tassel changes colour from brown to dark brown after alkaline treatment with toluene-ethanol mixture

The corn tassel fiber was bleached using a mixture of sodium hydroxide and acetic acid (CH_3COOH) with a ratio of 1.3:10 (v/v) and then washed with 0.1 M NaOH to remove the non-cellulosic component further. The color of the delignified corn tassel fiber was dark brown and gradually changed to the pale brown of bleached corn tassel cellulose, as shown in Figure 4.6. The bleaching process removes lignin and hemicellulose from the cellulosic fibers that were not removed during pretreatment while maintaining the yield and integrity of corn tassel cellulose. Meanwhile, acetic acid is used in the bleaching process as a pH adjuster or buffer to control the bleaching solution's acidity (Pinto et al., 2022).

Fi

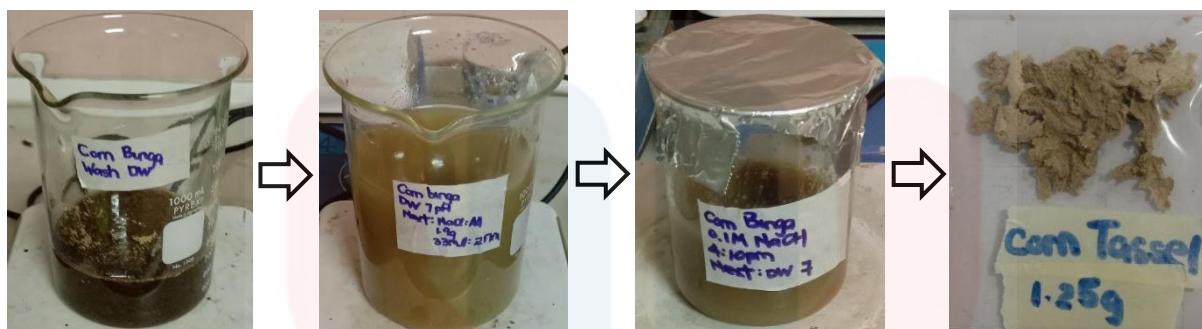


Figure 4. 6: The colour transition from dark brown and gradual discolouration to pale brown due to the bleaching process with a mixture of sodium hydroxide and acetic acid

4.1.4 Oil Palm Empty Fruit Bunch

The untreated oil palm empty fruit bunch initially exhibits a brown colouration. However, a significant change in its colour is observed after subjecting it to an alkali treatment process. This treatment involves using a toluene-ethanol mixture in a ratio of 2:1, which effectively alters the material's colour. Specifically, the brown oil palm empty fruit bunch fibre transforms into a darker shade of brown. Following this toluene-ethanol treatment, the OPEFB fibre is further processed through a washing step utilizing a 0.1 M NaOH solution. This washing process plays a crucial role in the treatment sequence. It not only aids in removing impurities but also contributes to the alteration in colouration. As a result of the alkali wash, the colour of the oil palm empty fruit bunch becomes even darker, as shown in Figure 4.7.



Figure 4. 7: The oil palm empty fruit bunch changes colour from brown to dark brown after alkaline treatment with toluene-ethanol mixture

The oil palm empty fruit fiber was bleached using a mixture of sodium hydroxide and acetic acid (CH_3COOH) with a ratio of 1.3:10 (v/v) and then washed with 0.1 M NaOH to remove the non-cellulosic component further. The color of the delignified oil palm empty fruit bunch fiber was dark brown and gradually changed to the brown of bleached oil palm open fruit cellulose, as shown in Figure 4.8. Similarly, the bleaching process removes lignin and hemicellulose from the cellulosic fibers that were not removed during pretreatment. At the same time, the acetic acid is used in the bleaching process as a pH adjuster or buffer to control the bleaching solution's acidity.

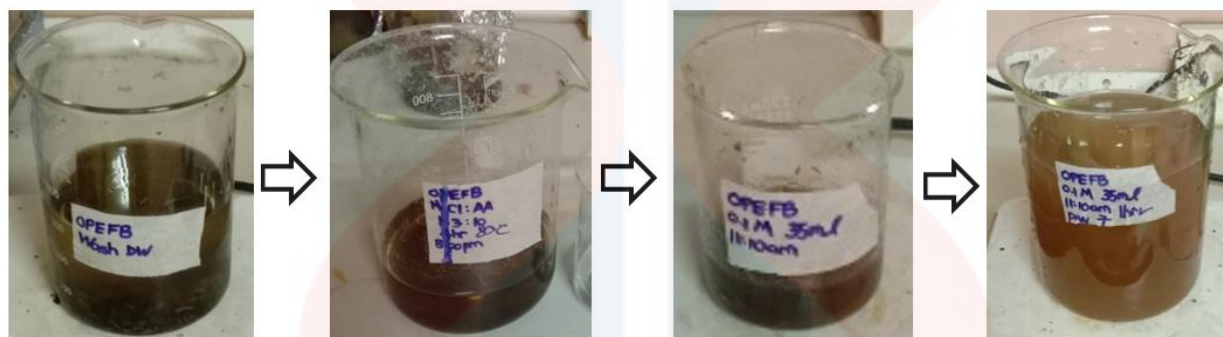


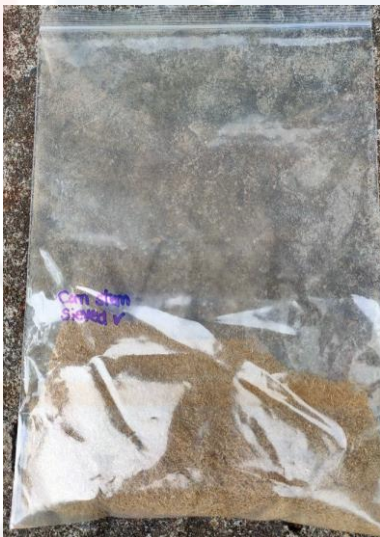
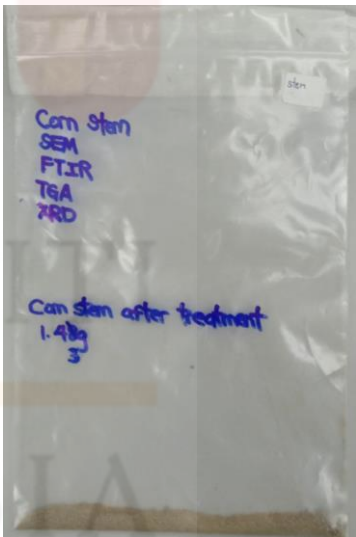

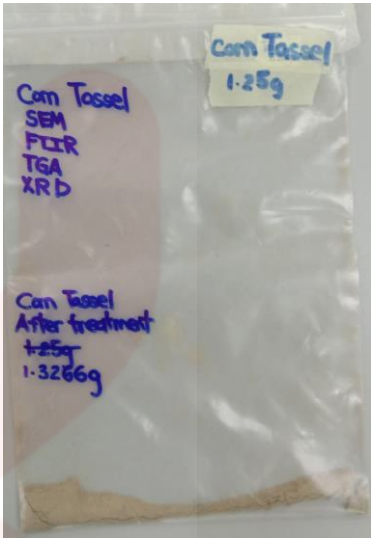

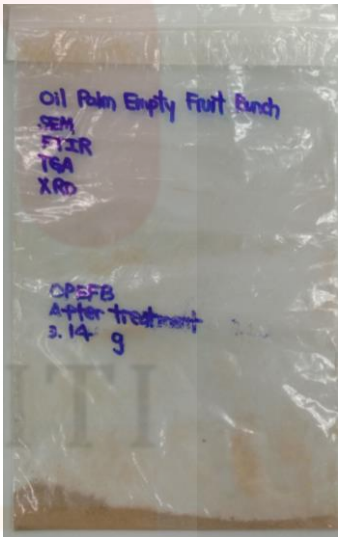


Figure 4. 8: The colour transition from dark brown and gradual discolouration to brown due to the bleaching process with a mixture of sodium hydroxide and acetic acid

Table 4. 1: The colour changes of different samples before and after treatment

Samples	Before Treatment	After Treatment
Rice Husk		
Corn Stem		

<p>Corn Tassel</p>	 A clear plastic bag containing a brown, granular sample of corn tassel. The bag has a purple label at the bottom left that reads "Corn Bunch Sieved ✓".	 A clear plastic bag containing a brown, granular sample of corn tassel. The bag has a yellow label at the top right that reads "Corn Tassel 1.25g". It also has a purple label on the left side that lists the analysis methods: "Corn Tassel", "SEM", "FTIR", "TGA", and "XRD". Below this, it says "Corn Tassel After treatment 1.25g 1.3266g".
<p>Oil Palm Empty Fruit Bunch</p>	 A clear plastic bag containing a brown, granular sample of oil palm empty fruit bunch. The bag has a purple label at the bottom left that reads "Oil Palm Empty Fruit Bunch Sieved ✓".	 A clear plastic bag containing a brown, granular sample of oil palm empty fruit bunch. The bag has a purple label on the left side that lists the analysis methods: "Oil Palm Empty Fruit Bunch", "SEM", "FTIR", "TGA", and "XRD". Below this, it says "OPFEB After treatment 3.14 g".

4.2 Yield of extracted cellulose from different samples

Table 4. 2: Yield percentage of each samples

Samples	Yield, %
Rice husk	29.28
Corn stem	14.30
Corn tassel	13.27
Oil palm empty fruit bunch	31.40

Table 4.2 describes the percentage of cellulose yield after being chemically treated. The oil palm has a higher yield of cellulose, which is 31.4%, followed by rice husk (29.28%), corn stem (14.30%) and corn tassel (13.27%). OPEFB have a high cellulose content, ranging from 40% to 65%, while the rice husk has a lesser cellulose content, typically between 35% and 45%. Corn stem has a significantly lower cellulose content, usually around 20% to 30%, while corn tassel has a relatively low cellulose content, ranging from 15% to 25%. The lower cellulose content in raw materials will give a lower cellulose yield after alkaline treatment for cellulose extraction. As expected, removing non-cellulosic materials from OPEFB indicates that the alkaline treatment and bleaching process efficiently removed the hemicellulose and lignin and produced a higher yield of cellulose.

4.3 Characteristic of Extracted Cellulose

The non-invasive method of Fourier-transform infrared (FTIR) spectroscopy was used to study the physical and chemical properties of cellulose. This method utilizes a range of wavenumbers spanning from 400 to 4000 cm^{-1} to determine the chemical structure of cellulose. The infrared spectra of rice husk (RH), corn stem (CS), corn tassel (CT), and oil palm empty fruit bunch (OPEFB) were analyzed both in their untreated state and treated or after undergoing alkaline treatment. In this study, the goal of using FTIR is to find out hemicellulose and lignin are removed when chemicals are used to extract cellulose.

4.3.1 Identification of Functional Groups Using Fourier Transform Infrared (FTIR) Spectroscopy

4.3.1(a) Rice Husk

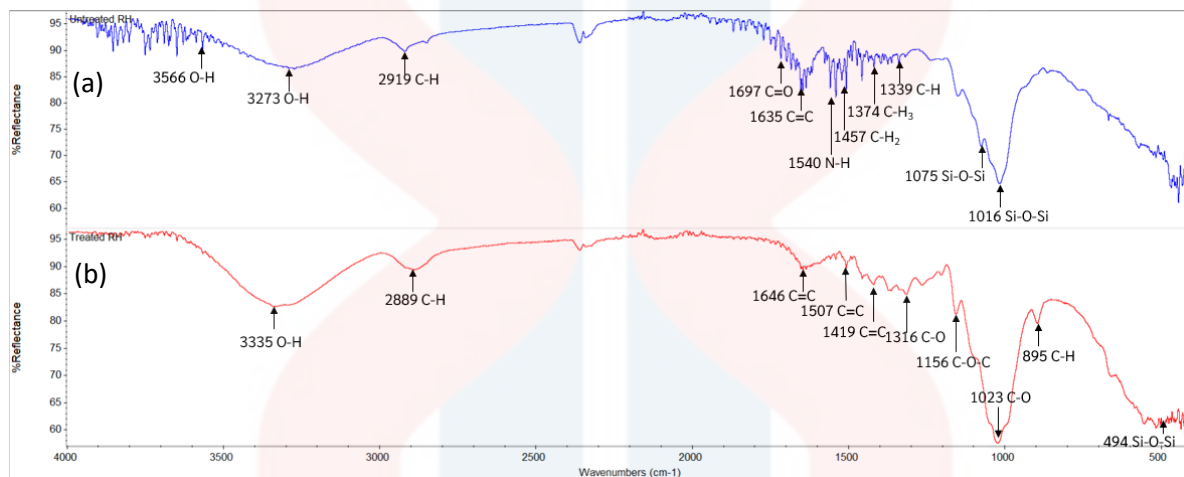


Figure 4. 9: FTIR spectra between (a) untreated and (b) treated rice husk

Figure 4.9 shows a comparative analysis of FTIR spectra obtained from untreated and treated rice husks. The FTIR spectra of untreated rice husk exhibited a more significant number of detected peaks in comparison to the FTIR spectra of treated rice husk. The N-H bending vibration was detected in untreated rice husk with the wavenumber of 1540 cm^{-1} , while the observed peaks at 1457 cm^{-1} can be attributed to the C-H₂ bend. The observed peaks at 1374 cm^{-1} and 1339 cm^{-1} can be attributed to the C-H₃ bend and C-H stretch, respectively. Si-O-Si stretch has been observed in the last few peaks at 1075 cm^{-1} and 1016 cm^{-1} .

In contrast, the O-H stretching vibration is likewise detected in alkaline treated rice husks, exhibiting a peak value of 3335 cm^{-1} indicating the presence of alcohols or phenols. This observation aligns with the findings of Royan et al. (2018), who also reported the presence of free-OH groups at a wavenumber of 3333 cm^{-1} . However, the C-H stretching vibration appears at a peak value of 2889 cm^{-1} . The observed peak at 1419 cm^{-1} , 1507 cm^{-1} and 1646 cm^{-1} can be attributed to the C=C stretching vibration, while a peak indicates C-O stretch at 1316 cm^{-1} . The C-O-C stretching vibration was detected at a wavenumber of 1156 cm^{-1} , whereas the C-O stretching

vibration was once again discovered at a wavenumber of 1023 cm^{-1} . The peak at 895 cm^{-1} indicates the presence of a C-H bend. Last but not least, a lesser number of Si-O-Si peaks was observed, suggesting the presence of Si-O-Si bonds associated with silica impurities. The observed peaks were identified at 494 cm^{-1} , 455 cm^{-1} , 436 cm^{-1} , 425 cm^{-1} , and 417 cm^{-1} .

Based on the graph presented in Figure 4.9(b), it is evident that the alkaline treated rice husk exhibited a reduced number of peaks, which can be attributed to the removal of hemicellulose and lignin. Additionally, the presence of identical functional groups was observed in the treated sample. Nevertheless, comparable functional groups were present, including the O-H stretch, C-H stretch, C=C stretch, and Si-O-Si stretch. The similarity in functional groups between untreated and treated rice husk indicates cellulose is present in the sample. The O-H functional group can indicate the presence of alcohols and carboxylic acids. Hydrogen bonding between cellulose molecules is mainly attributed to the presence of hydrogen atoms in cellulose, hence facilitating strong intermolecular interactions. Etale et al. (2023) have reported that cellulose exhibits favorable interactions with water due to many hydroxyl groups along its molecular chain.

Moreover, the findings were further supported by Daffalla et al. (2020), whose research also demonstrated that the FTIR spectra of raw rice husk exhibited a distinct peak at approximately 3403.3 cm^{-1} , corresponding to the presence of O-H groups. Additionally, the presence of the C-H group in both untreated and treated rice husk samples is consistent with their observation, highlighting the prevalence of organic compounds containing hydrocarbons, which are fundamental constituents of organic materials.

According to Korotkova et al. (2016), rice husk comprises around 28-30% inorganic compounds and 70-72% organic compounds. The inorganic components of rice husk consist of silica and other minerals, while organic components include cellulose, hemicellulose, and lignin. The constituents of these components consist of atoms of carbon, hydrogen, and oxygen. Furthermore, identifying the C=C functional group in both the untreated and treated rice husk suggests the presence of alkenes and alkynes, which are fundamental to cellulose and contribute to its strength and rigidity. The observed shift in the peak of the C=C stretch, from 1635 cm^{-1} , in treated rice husk cellulose can potentially be explained by the elimination of hemicellulose and lignin from the rice husk due to the chemical treatment process. When the peak shifts towards the higher wavenumber side, which is at 1646 cm^{-1} , it indicates a reduction in the molecule's weight.

The relationship between the frequency of vibration and the mass of a vibrating molecule is inversely proportional. Consequently, molecules with lower mass exhibit greater vibration frequencies, resulting in higher wave numbers.

Daffalla et al. (2020) also propose that the C=C functional group is observed within the spectral range of $1546.8 - 1652.9 \text{ cm}^{-1}$ in untreated rice husk, hence identified the existence of this functional group at a wavenumber of 1635 cm^{-1} in raw rice husk. Furthermore, the presence of the Si-O-Si functional group is observed in both the untreated and treated rice husks, indicating the presence of silica in the sample. According to the findings of Battegazzore et al. (2014), the primary constituents of rice husk were identified as 38.3% of cellulose, 31.6% of hemicellulose, 11.8% of lignin, and 18.3% of silica. The intensity of the silica functional group (Si-O-Si) in the rice husk treated with alkali was observed to be lower compared to the untreated or raw rice husk. This can be attributed to the elimination of inorganic substances from the surface of the rice husk by the alkaline treatment, as reported by Asadi et al. (2008). However, completely removing silica from rice husks via chemical treatment methods is a significant challenge, as highlighted by Liu et al. (2015).

However, only two functional groups, C-O and C-O-C, were observed in the treated rice husk. The presence of these two functional groups can be explained by the alkaline treatment process, which has resulted in increased exposure of the existing C=O and C-O-C bonds in the cellulose. This situation may occur if the alkaline treatment procedure effectively eliminates hemicellulose and lignin constituents from the rice husk. Hemicellulose and lignin possess the ability to mask the C=O and C-O-C bonds within cellulose, hence reducing their detectability in the FTIR spectrum. The removal of hemicellulose and lignin leads to an increased visibility of the C=O and C-O-C bonds within cellulose in the FTIR spectrum. In the untreated rice husk, four distinct functional groups were observed, namely the C=O stretching, N-H bending, C-H₂ bending, and C-H₃ bending groups. The observed C=O stretch can be attributed to the existence of hemicellulose and lignin, which are both classified as carbohydrates. The N-H bend is observed in the amine bond, a functional group typically found in proteins, including those in rice husks. The C-H₂ bending peak in the FTIR spectrum of rice husk indicates the presence of alkanes and alkenes, which are hydrocarbons that make up the bulk of rice husk components. Methyl groups,

which are constituents of alkanes, alkenes, and esters, all of which are found in rice husks, are responsible for the observed C-H₃ bending peak in the FTIR spectrum.

Table 4. 3: Peak positions of the infrared spectra of rice husk

Assignment	Untreated Rice Husk (wavelength, cm⁻¹)	Alkaline Treated Rice Husk (wavelength, cm⁻¹)
Hydroxyl group and bonded OH stretching	3566, 3273	3335
C-H stretching, O-H stretch – Alkanes (CH; CH₂; CH₃), carboxylic acids	2919, 1339	2889
C=O stretching (carboxylic acids and esters)	1697	-
C-H bending – Alkanes (hemicellulose and pectin)	1457, 1374	895
C-O stretching, C-O-C stretching – Alcohol (cellulose; hemicellulose; lignin), Carboxylic Acids, Esters, Ethers	-	1316, 1156, 1023
C=C stretching	1635	1646, 1507, 1419
N-H bending	1540	-
Si-O-Si asymmetric	1075, 1016	494

4.3.1(b) Corn Stem

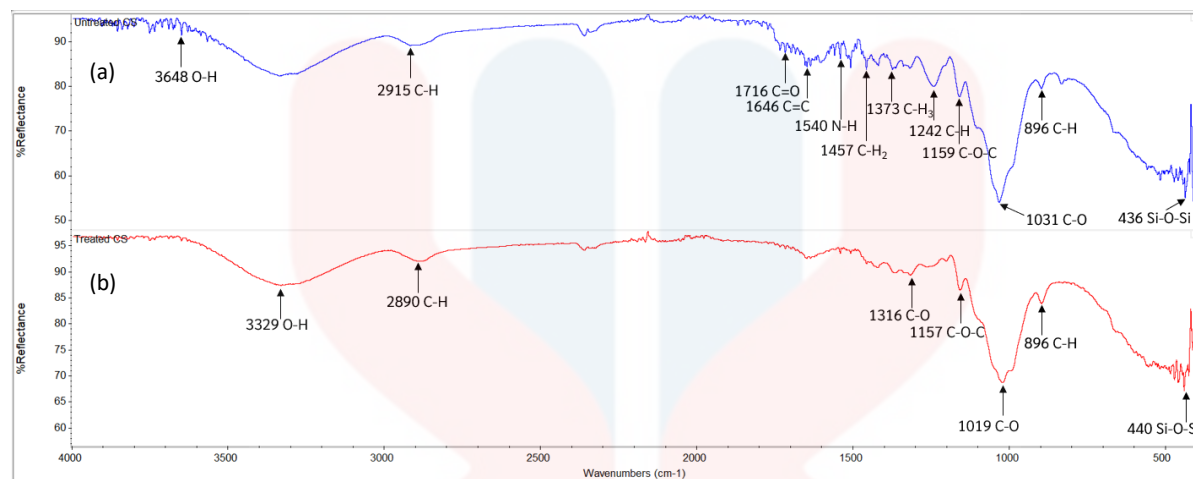


Figure 4. 10: FTIR spectra between (a) untreated and (b) treated corn stem

From Figure 4.10, the O-H stretch shifted from 3648 cm^{-1} in untreated corn stem to 3329 cm^{-1} of alkaline treated corn stem, likely due to the removal of hemicellulose and lignin during the alkaline treatment. Hemicellulose and lignin contain hydroxyl groups, contributing to the O-H stretch peak in untreated corn stems. When these components are removed, the O-H stretch peak shifts to a lower frequency due to the weaker hydrogen bonding interaction between the remaining hydrogen bonding. According to the study of Youssefian et al. (2017), removing hemicellulose disrupts the hydrogen bond network in the plant's cell wall. It weakens the hydrogen bonds between the remaining cellulose and lignin fibres and the surrounding water molecules. Next, the C-H stretch shifted from 2915 cm^{-1} to 2890 cm^{-1} in alkaline-treated corn stem, which is likely due to the increased crystallinity of cellulose. Crystalline cellulose has a more ordered structure than amorphous cellulose, which leads to a stronger hydrogen bonding interaction between the cellulose molecules. Bian et al. (2021) also cited the presence of cellulose-II at bands at 2891 cm^{-1} representing -CH stretching.

Moreover, the C=O stretch shifted from 1716 cm^{-1} to 1647 cm^{-1} in alkaline-treated corn stem, which is likely due to the formation of carboxylate anions. Carboxylate anions are formed when the alkaline solution deprotonates the carboxylic acid groups in cellulose. Carboxylate anions have a weaker C=O bond than the carboxylic acid group, which leads to a shift in the C=O stretch peak to a lower frequency. Meanwhile, the shift of C-O-C stretch from 1159 cm^{-1} to 1157

cm^{-1} is likely due to the formation of cellulose nanocrystals, which are small, highly crystalline cellulose particles. The C-O-C bonds in cellulose nanocrystals are stronger than C-O-C bonds in amorphous cellulose, which leads to a shift in the C-O-C stretch peak to a lower frequency. Javier-Astete et al. (2021) also found that the C-O-C asymmetric stretching vibration at 1157 cm^{-1} is present in cellulose. Next, the C-O stretch shifted from 1031 cm^{-1} to 1019 cm^{-1} , likely due to the removal of hemicellulose and lignin from the corn stem sample. Hemicellulose and lignin contain ether groups, which contribute to the C-O stretch peak in untreated corn stems. When these components are removed, the C-O stretch peak shifts to a lower frequency due to the weaker hydrogen bonding interactions between the remaining ether group. Not only that, the peak 1316 cm^{-1} corresponds to the C-O stretch also being observed in the treated corn stem sample. According to Mahmood et al. (2014), the spectral range of $1335\text{-}1316 \text{ cm}^{-1}$ is attributed to the cellulose component of the fibre and is indicative of the crystallinity and amorphous nature of cellulose. The result shows an increase in the degree of crystallinity. The 896 cm^{-1} peak indicates C-H deformation vibrations localized to the cellulose present in both untreated and treated corn stem. According to Zhao et al. (2013), the peaks ranging from 898 to 899 cm^{-1} are attributed to the out-of-plane C-H stretching of the aromatic ring, varying with corn stalk particle sizes from $300 \mu\text{m}$ to $15 \mu\text{m}$. This is further supported by the presence of glycosidic linkages in cellulose, as confirmed by the C-H bend at 896 cm^{-1} , which represents the rocking vibration of C-H in cellulose I. This finding is consistent with the research of both Huang et al. (2017) and Peng et al. (2021).

Moreover, the observed shift of the Si-O-Si bending peak from 436 cm^{-1} to 440 cm^{-1} may be attributed to the elimination of hemicellulose and lignin because of the alkaline treatment. Hemicellulose and lignin contain silica, contributing to the Si-O-Si bend peak in untreated corn stems. When these components are removed, the Si-O-Si bend peak shifts to a higher frequency due to the stronger hydrogen bonding interactions between the remaining silica molecules.

Furthermore, it has been shown that untreated maize stem exhibits a limited number of peaks, including C=C at 1645 cm^{-1} , N-H at 1540 cm^{-1} , C-H₂ at 1457 cm^{-1} , C-H₃ at 1373 cm^{-1} , and C-H at 1242 cm^{-1} . These findings suggest the potential existence of hemicellulose and lignin in the corn stem sample. Woźniak et al. (2021) also showed that the band's intensity at 1640 cm^{-1} is higher in lignin-rich samples due to the presence of the C=C functional group. Lignin is a complex aromatic polymer that contains several functional groups, including C-H, C=C, and C-O-C stretch.

Li et al. (2018) suggested that the presence of the C=C vibration band in the 1600-1510 cm^{-1} region is a better indicator of lignin than the peak at 1646 cm^{-1} , also present in hemicellulose. They also found that the broadbands from 1470 cm^{-1} to 1330 cm^{-1} are attributed to C-H vibration in the aromatic ring, not the 1242 cm^{-1} band in untreated corn stem.

Table 4. 4: Peak positions of the infrared spectra of corn stem

Assignment	Untreated Rice Husk (wavelength, cm^{-1})	Alkaline Treated Rice Husk (wavelength, cm^{-1}) 1)
Hydroxyl group and bonded OH stretching	3648	3329
C-H stretching, O-H stretch – Alkanes (CH; CH ₂ ; CH ₃), carboxylic acids	2915,1457,1373,1242	2890
C=O stretching (carboxylic acids and esters)	1716	1647
C-H bending – Alkanes (hemicellulose and pectin)	896	896
C-O stretching, C-O-C stretching – Alcohol (cellulose; hemicellulose; lignin), Carboxylic Acids, Esters, Ethers	1159,1031	1316, 1156, 1023
C=C stretching	1646	-
N-H bending	1540	-
Si-O-Si asymmetric	436	440

4.3.1(c) Corn Tassel

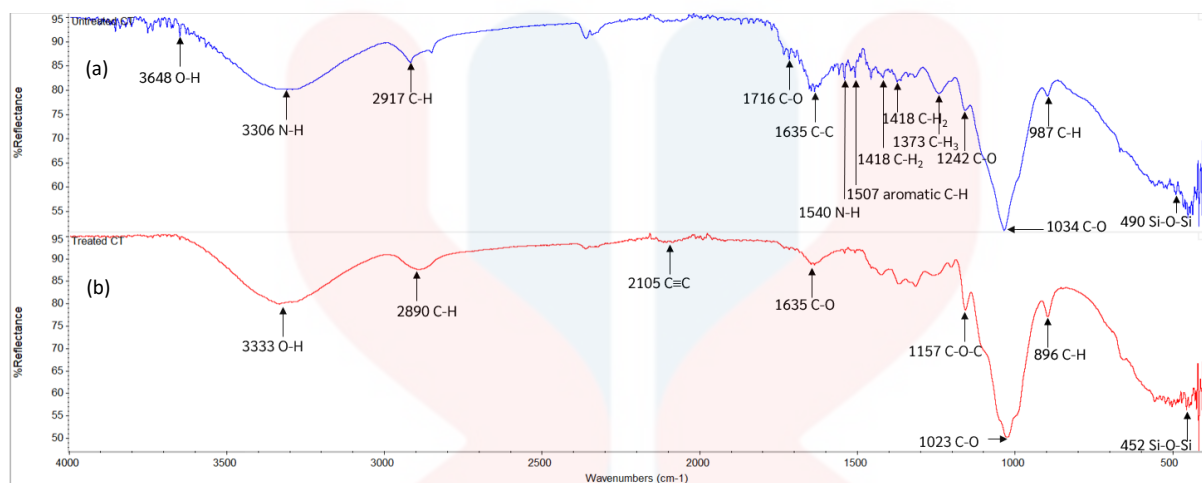


Figure 4. 11: FTIR spectra between (a) untreated and (b) treated corn tassel

According to the graph presented in Figure 4.11, the change in the O-H peak from 3648 cm^{-1} to 3333 cm^{-1} suggests a decrease in the intensity of hydrogen bonding in alkaline-treated corn tassels. The probable cause for this is the partial degradation of the hemicellulose and lignin molecules during the alkaline treatment, resulting in a decrease in the quantity of available hydrogen bonding sites. According to Maepa et al. (2015), their research shows that the peak of the maize tassel treated with 5% NaOH is ascribed to the stretching of α -cellulose (O-H). The observed shift in the C-H peak from 2917 cm^{-1} to 2890 cm^{-1} and from 987 cm^{-1} to 896 cm^{-1} suggests that the aliphatic hydrocarbons in the corn tassel treated with alkaline are more densely arranged compared to the untreated corn tassel. Jayaramudu et al. (2013) state that a peak at around 896 cm^{-1} can be attributed to the β -glycosidic linkage. This peak is a result of the stretching of the O-C-O bond and the deformation of the C-H bond in cellulose. This can be attributed to the crosslinking of the cellulose and hemicellulose chains during the alkaline treatment. The observed change in the C-O peak from 1716 cm^{-1} to 1635 cm^{-1} suggests that the carbonyl groups in the corn tassel treated with alkaline are more conjugated than the untreated corn tassel. The probable cause for this is the partial degradation of the hemicellulose and lignin molecules during the alkaline treatment, which exposes additional carbonyl groups. Furthermore, the change in the Si-O-Si peak from 490 cm^{-1} to 452 cm^{-1} suggests that the silicate bonds in the corn tassel treated with alkaline

have been reinforced. This is probably a result of eliminating contaminants from the outer layer of the corm tassel through an alkaline treatment.

Some specific peaks are only present in alkaline-treated corn tassels, such as $\text{C}\equiv\text{C}$ at 2105 cm^{-1} , ether C-O-C at 1157 cm^{-1} , and alcohol C-O at 1023 cm^{-1} . The presence of alkynes can be inferred from the $\text{C}\equiv\text{C}$ peak observed at 2105 cm^{-1} . Alkynes are hydrocarbons containing a minimum of one carbon-carbon triple bond. They are produced by removing water from alcohols and aldehydes (Zha et al., 2018). The alkynes present in corn tassels treated with alkaline substances can arise either from the removal of water molecules from sugars and other carbohydrates released during the alkaline treatment or from the removal of hydroxyl groups on the surface of the corn tassel.

Meanwhile, the C-O-C peak observed at 1157 cm^{-1} indicates the presence of ethers. Ethers are organic molecules characterized by two alkyl groups attached to an oxygen atom. They are produced through the interaction between alcohols and alkyl halides (Ouellette, 2015). Ethers may be produced in alkaline-treated corn tassel through the reaction between alcohols released during alkaline treatment and alkyl halides in the alkaline solution or through the reaction between hydroxyl groups on the corn tassel surface and alkyl halides in the alkaline solution. Furthermore, C-O peak at 1023 cm^{-1} indicates the formation of secondary alcohols by reducing ketones, aldehydes, or carbonyl groups on the surface of corn tassel.

Lastly, specific peaks are only found in untreated corn tassels, namely N-H at 3306 cm^{-1} and 1540 cm^{-1} , C-C at 1635 cm^{-1} , and C-H_2 and C-H_3 at 1418 cm^{-1} and 1373 cm^{-1} , respectively. The detection of the N-H peak signifies the existence of amides, functional groups frequently encountered in hemicellulose and lignin. The C-C peak indicates the presence of aromatic rings, characteristic of lignin. The C-H_2 and C-H_3 peaks indicate the presence of aliphatic hydrocarbons, which are found in both hemicellulose and lignin. The FTIR analysis reveals that the alkali treatment effectively eliminated the hemicelluloses and lignin from the maize tassel fibers.

Table 4. 5: Peak positions of the infrared spectra of corn tassel

Assignment	Untreated Rice Husk (wavelength, cm^{-1})	Alkaline Treated Rice Husk (wavelength, cm^{-1})
Hydroxyl group and bonded OH stretching	3648	3333
C-H stretching, O-H stretch – Alkanes (CH ; CH_2 ; CH_3), carboxylic acids	2917, 1418	2890
C-H bending – Alkanes (hemicellulose and pectin)	1507, 1459, 987	896
C-O stretching, C-O-C stretching – Alcohol (cellulose; hemicellulose; lignin), Carboxylic Acids, Esters, Ethers	1716, 1242, 1034	1635, 1157, 1023
C-C stretching	1635	-
$\text{C}\equiv\text{C}$ stretching	-	2105
N-H bending	3306, 1540	-
Si-O-Si asymmetric	490	452

4.3.1(d) Oil Palm Empty Fruit Bunch

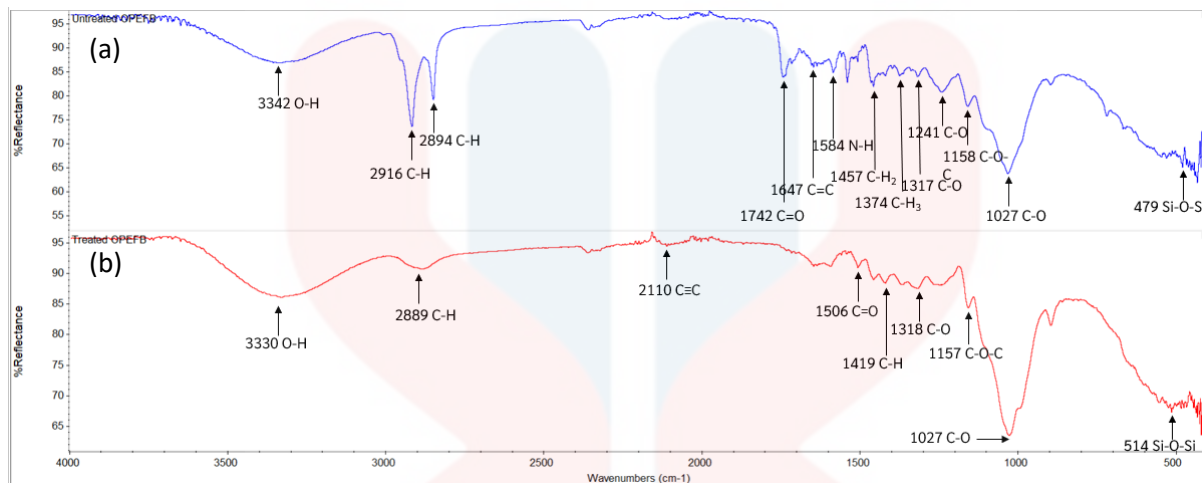


Figure 4. 12: Comparison between (a) untreated (b) treated oil palm empty fruit bunch

The analysis of Figure 4.12 reveals a noticeable change in the O-H peak, specifically from 3342 cm^{-1} to 3330 cm^{-1} . This shift may be attributed to removing hemicellulose and lignin from OPEFB, resulting in the exposure of a more significant number of hydroxyl groups on the surface of cellulose. The observed outcome may result in a reduction in the magnitude of the O-H peak, accompanied by a little displacement towards a lower wavenumber owing to an increase in hydrogen bonding. Additionally, the shift of the C-H peak from 2894 cm^{-1} to 2889 cm^{-1} might be attributed to the elimination of fatty acids and waxes in OPEFB. This removal process leads to a reduction in the strength of the C-H peak.

Moreover, the C-H peak can undergo a downward shift in wavenumber due to alterations in the intermolecular interactions between the alkane chains and other molecules. Subsequently, the observed shift of the C-O peak from 1317 cm^{-1} to 1318 cm^{-1} may be attributed to the cleavage of ether linkages in the hemicellulose and lignin components. This cleavage process results in the liberation of carboxylic acid groups, thus leading to the previously mentioned shift in the peak position. This phenomenon can potentially result in a rise in the strength of the C-O peak at 1318 cm^{-1} , correlated with the C-O stretching vibration seen in carboxylic acids. Additionally, the observed change in the C-O peak from 1317 cm^{-1} to 1027 cm^{-1} may be attributed to creation of new C-O bonds between the cellulose and the NaOH. The peak seen at 1027 cm^{-1} in the infrared spectrum indicates the C-O stretching vibration, specifically in primary alcohols. This implies that

the hydroxyl groups present on the surface of cellulose may have undergone a conversion to primary alcohol groups as a result of the NaOH treatment. The observed shift of the C-O-C peak from 1158 cm^{-1} to 1157 cm^{-1} may be attributed to the cleavage of ether linkages in hemicellulose and lignin. This cleavage event reduces the strength of the C-O-C peak at 1157 cm^{-1} , which is indicative of the C-O stretching vibration in ethers.

Furthermore, the untreated OPEFB exhibits the existence of certain peaks exclusively, which suggests the elimination of hemicellulose and lignin from the OPEFB sample. The observation of a peak at 1742 cm^{-1} , corresponding to C=O stretching, in the untreated OPEFB sample and its absence in the NaOH-treated OPEFB sample suggests that the NaOH treatment effectively removes hemicellulose and lignin components from the OPEFB material. According to Latip et al. (2019), the band's disappearance at 1729 cm^{-1} in NaOH-treated OPEFB fiber can be attributed to elimination of non-cellulose constituents, including hemicellulose, pectin, and lignin. This removal is likely due to the interaction between the functional groups of the carbonyl ester in coumaric lignin or the acetyl group of hemicellulose ester that potentially exists at this specific peak. In addition, the disappearance of the C=C stretching peak at 1647 cm^{-1} which is associated with the aromatic ring present in lignin, can be seen after the NaOH treatment, since it leads to the extraction of lignin from the OPEFB sample. The results of Kline et al. (2010) agree with the observation that the spectral region spanning from 1650 cm^{-1} to 1600 cm^{-1} exhibits distinctive features associated with lignin. The disappearance of the peak seen at 1574 cm^{-1} , which corresponds to the N-H bending vibration in proteins, may be attributed to the denaturation of proteins and the subsequent breaking of N-H bonds in OPEFB treated with NaOH. The use of alkaline treatment on oil palm empty fruit bunches (OPEFB) results in the elimination of the characteristic peaks shown at 1457 cm^{-1} (C-H₂) and 1374 cm^{-1} (C-H₃), which may be attributed to the removal of waxes and fatty acids. Furthermore, according to Hidayat et al. (2022), it has been proposed that the asymmetric deformation of the C-H bonds in lignin, namely the -CH₂ and -CH₃ groups, occurs within the spectral region of $1470\text{-}1450\text{ cm}^{-1}$.

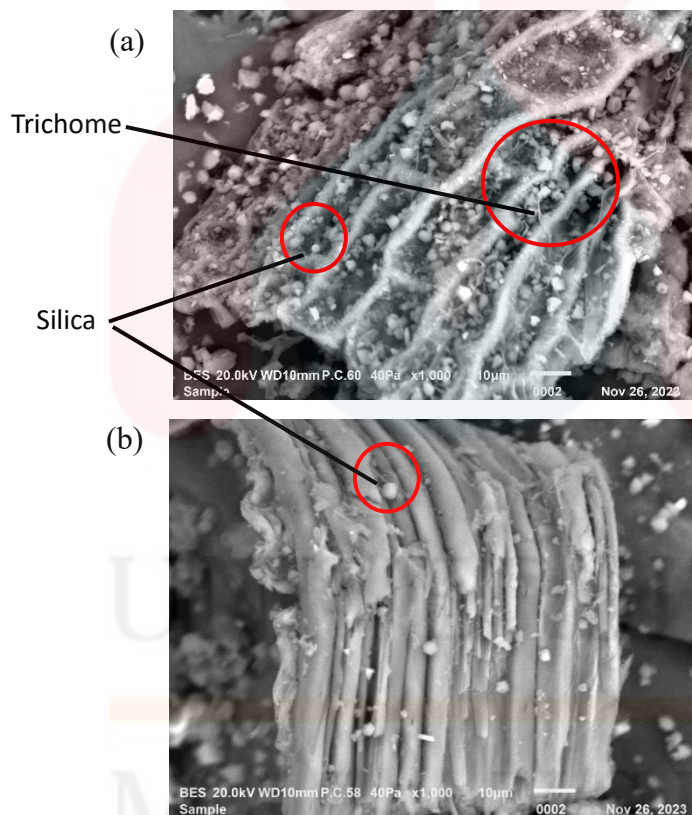
Table 4. 5: Peak positions of the infrared spectra of oil palm empty fruit bunch

Assignment	Untreated Rice Husk (wavelength, cm^{-1})	Alkaline Treated Rice Husk (wavelength, cm^{-1})
Hydroxyl group and bonded OH stretching	3342	3330
C-H stretching, O-H stretch – Alkanes (CH ; CH_2 ; CH_3), carboxylic acids	2916, 2894, 1457, 1374	2889
C=O stretching (carboxylic acids and esters)	1742	1506
C-H bending – Alkanes (hemicellulose and pectin)	-	1419
C-O stretching, C-O-C stretching – Alcohol (cellulose; hemicellulose; lignin), Carboxylic Acids, Esters, Ethers	1241, 1158, 1031	1318, 1157, 1027
C=C stretching	1647	-
C≡C stretching	-	2110
N-H bending	1584	-
Si-O-Si asymmetric	479	514

4.3.2 Morphology Study using Scanning Electron Microscopy (SEM)

4.3.2(a) Rice Husk

SEM is used to investigate the structure of the rice husk, corn stem, corn tassel, and oil palm empty fruit bunch before and after alkaline treatment. These visually suggest the removal of hemicellulose, lignin, wax, and some of the silica after being chemically treated. The results of the outer and inner surfaces of untreated rice husk are shown in Figure 4.13 (a), (b) and (c) treated rice husk.



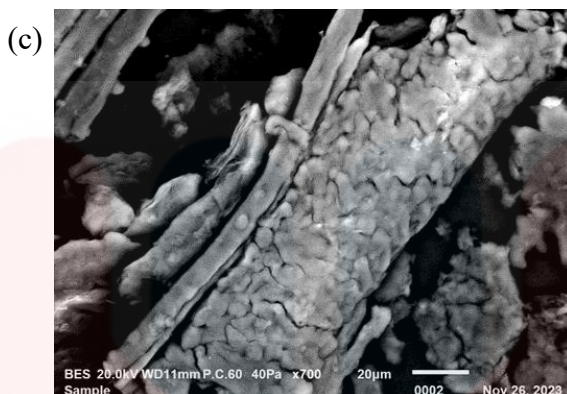


Figure 4. 13: SEM micrographs of untreated rice husk (a) outer, (b) inner surfaces and (c) treated rice husk

The scanning electron microscope (SEM) images show the outer and inner surfaces of untreated rice husks, which can be observed in Figures 4.13(a) and (b). The outer layer of the untreated rice husk exhibited a highly uneven texture, featuring linear ridges and a concentrated distribution of silica in bright, dome-like structures. This observation aligns with the research conducted by Das et al. in 2019, which noted that the external epidermal cells of untreated rice husks are arranged symmetrically and characterized by prominent domes. In contrast, the inner surface of the untreated rice husk appeared smooth. As stated by Johar et al. in 2012, rice husk primarily comprises outer epidermal cells with a corrugated structure, including a lemma, and an inner epidermis characterized by a smooth surface covered by a waxy layer containing hemicellulose and lignin. The silica content is primarily concentrated in the dome tips, with lower levels distributed in other areas of the rice husk.

Additionally, a study carried out by Park et al. (2003) employing energy dispersive X-ray micro-analysis (EDXA) and field-emission scanning electron microscopy (FE-SEM) to demonstrate the presence of silica across the entirety of the external surface of rice husk. This abundance of silica on the outer epidermis contributes to the husk's strength and rigidity while serving as a protective barrier for the rice grain against environmental factors and microbial threats, as highlighted by Fávaro et al. in 2010. Furthermore, untreated rice husks have trichomes, which are visible hair-like outgrowths on their surfaces. Trichomes have crucial roles in plant defense, providing both physical and chemical protection against pest assault and disease invasion (Huchelmann et al., 2017). Moreover, they play an important role in enhancing plant resilience to diverse biotic and abiotic stresses, such as dehydration, extreme temperatures, and ultraviolet radiation (Shang et al., 2020).

The Figure 4.13(b) above micrograph shows that the surface of the rice husk is rough and irregular, with many protrusions and indentations. The ridged structures are broken down, and the fiber's surface becomes rougher after the alkaline treatment. This indicates the particle removal such as silica, hemicellulose, and other impurities from the rice husk (Onoja et al., 2019). The protrusions may also be remnants of the vascular bundles that run through the rice husk. The rice husk is made up of a network of interconnected silica cells. These celluloses are roughly spherical or oval. The walls of the cells are thin and delicate, and they appear to be perforated in some places. Microscopically, the fracture exhibits a transgranular morphology, as evidenced by the jagged edges and fragmented cellulose structure visible in the SEM image. This indicates that the crack propagates through individual silica cells rather than preferentially following the intercellular boundaries. The network of silica cells creates a highly porous structure. This porosity can increase the surface area of cellulose, thus providing efficient binding of active ingredients onto the microbeads. Moreover, the interconnected network of pores acts as a reservoir for the encapsulated active ingredient. The size and distribution of the pores can be controlled, allowing for controlled release of the ingredient over time.

According to Monte et al. (2017), particular materials such as waxes, impurities, and other non-cellulosic materials have been removed from the outer epidermis surface of the rice husk after alkaline treatment. The surface morphology of the rice husk changed significantly with the appearance of the spaces due to the separation of fiber bundles due to the removal of lignin as a binder in lignocellulosic materials (Singh et al., 2014). The defibrillation process, induced by the alkaline treatment, involved the disruption of hydrogen bonds between the cellulose fibers, thereby promoting the separation of fibers into distinct individual forms (Hernández-Becerra et al., 2023). This phenomenon led to a notable increase in the surface area of the fibers, a critical factor in the subsequent stage of microbead production. This showed that the alkaline treatment took silica out of the rice husk and caused the undulated shape to become less organized. This could mean lignin and hemicellulose were also removed from the rice husk.

4.3.2(b) Corn Stem

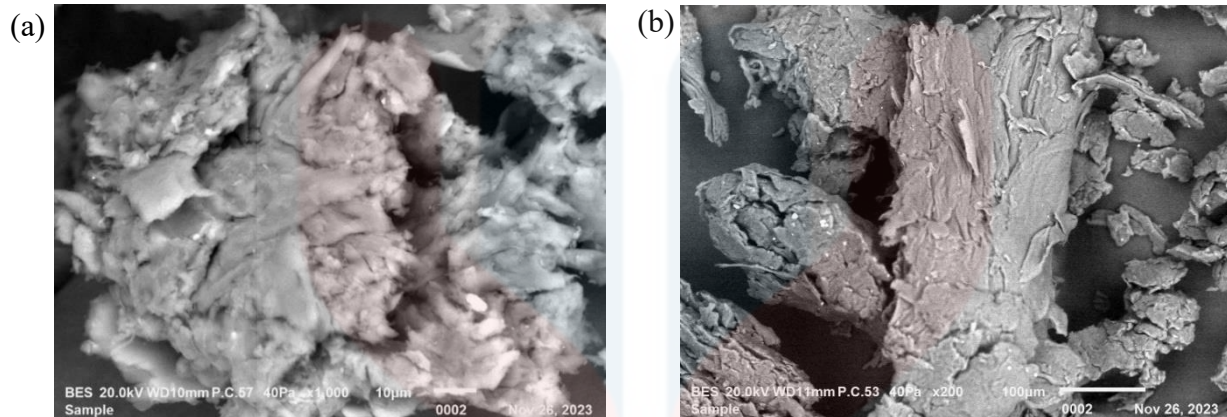


Figure 4.14: SEM micrograph of (a) untreated and (b) treated corn stem

Figure 4.14(a) shows the cross-section of an untreated corn stem when examined using a scanning electron microscope. The observation shows a circular shape with well-defined layers of tissue arranged in concentric layers. The smooth surfaces and orderly arrangements on the surface indicate a relatively uniform and organized structure of the plant material without large voids or gaps within the raw corn stalk. Han et al. (2019) further demonstrate that the surface of raw corn stalks is smooth and uniform. This indicates the raw corn stalk's surface lacks apparent irregularities or roughness. The surface of the raw corn stem is relatively flat and consistent, which suggests that the stalk may have a relatively dense and homogeneous structure. The intact and ordered appearance of the microfibrils in the cell wall structure suggested a well-preserved and organized arrangement of the structural components within the corn stalk. Nevertheless, Wang et al. (2020) discovered that untreated corn stems are arranged in distinct fiber bundles, which are elongated structures constituting the majority of the corn stalk. Fiber bundles of cellulose, hemicellulose, and lignin are distinctive attributes of natural plant materials, particularly in maize stems.

The Figure 4.14(b) above shows a significantly rough and irregular texture on the surface of the maize stem that has undergone treatment. This finding suggests a significant loss of the outer layer of cells, most likely due to the NaOH treatment's dissolving effects on cell wall components, particularly lignin and hemicellulose. These components play a crucial role in maintaining the rigidity and uniformity of the outer cell layer. Despite the treatment, the underlying cells maintain their distinctive spindle-shaped morphology. The elongated shape of the corn stem is adapted for

its function, which is to provide essential structural support and rigidity against bending and compression forces. Although the NaOH treatment may cause slight modifications to the thickness or surface characteristics of the cell wall, the general spindle shape remains largely unaffected.

The research by Trache et al. (2020) also shows that the cellulose extracted from maize stalks has a rod-like or fibrous structure that looks like long, thin rods with a constant or changing length and diameter. Similar to the finding of Bin et al. (2022), the alkaline treatment causes structural modifications due to its ability to remove hemicellulose and lignin from the cell walls of corn stalks. The removal of hemicellulose and lignin can create pores or voids within the structure of the corn stalk, affecting its overall porosity and permeability. However, Bin et al. (2022) have found that the surface roughness of corn stalk is potentially leading to a smoother or more uniform surface than the untreated corn stalk. It is worth mentioning that the formation of porous or vascular texture in the treated corn stalk can be attributed to the swelling and dissolution of the amorphous regions of the cellulose fibers. NaOH treatment can cause the fibers to swell and open up, exposing their internal structure and increasing their surface area (Kunusa et al., 2018).

In addition, the micrograph shows numerous fractures, most of which are longitudinally oriented along the corn stem's long axis. This preferred orientation indicates that the treatment decreased the cell wall's longitudinal stress tolerance. The alkaline treatment can induce morphological alterations in the fibers, including surface and structural changes. These alterations may affect the overall strength and stability of the cellulose and may result in fractures and irregular surfaces (Devi et al., 2022).

4.3.2(c) Corn Tassel

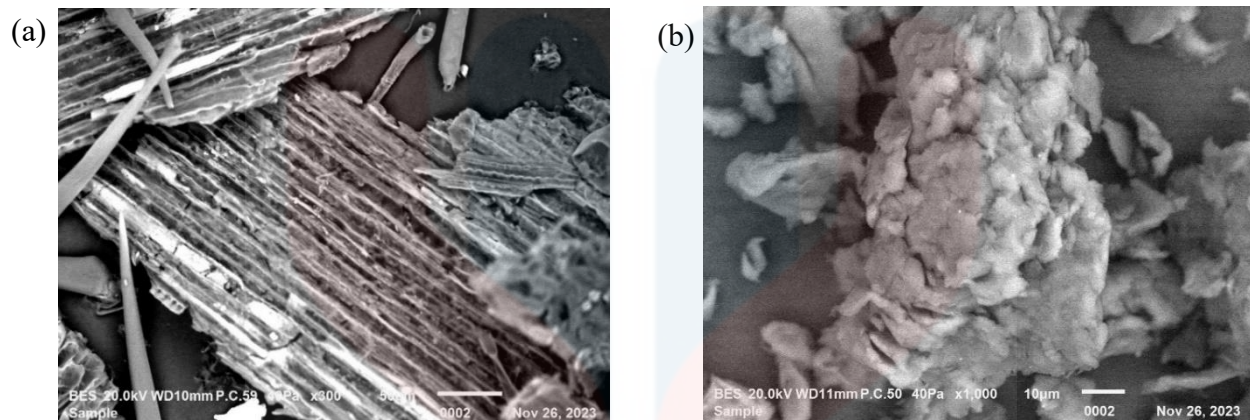


Figure 4. 15: SEM micrograph of (a) untreated and (b) treated corn tassel

The Figure 4.15 (a) above illustrates the morphology of untreated corn, revealing a surface characterized by rough and irregular features. This observation contrasts with the findings of Maepa et al. (2015), who reported that raw maize tassels typically exhibit a relatively smooth morphology. The rough surface characteristics observed in this study can likely be attributed to the presence of various surface structures, including cells and hairs.

Notably, the surface cells of the maize tassel appear elongated and rectangular, consistent with the findings of Moyo et al. (2014). These observations collectively suggest that the corn tassel possesses a rough and irregular surface, characterized by flattish rod-like structures that result from the fibrous nature of the maize tassel. The walls of these structures exhibit a dense composition and are coated with a layer of wax. Additionally, the micrograph reveals the presence of dark lines, corresponding to vascular bundles, which serve as conduits for water and nutrient transport within the plant.

Further examination of the untreated maize tassel's surface reveals the presence of linear ridges and furrows, formed by the arrangement of epidermal cells. The predominant components of the surface fibers include lignin, pectin, ash, and hemicellulose, which envelop the cellulose fibers. Lignin, as a complex organic polymer, provides structural integrity to plant cell walls, while pectin, a polysaccharide, serves as an adhesive substance between these walls. Hemicellulose, another complex carbohydrate, plays a critical role in binding cellulose fibers together.

Notably, the micrograph shows an absence of surface fractures, voids, and limited porosity in the untreated maize tassel, indicative of a compact structure with a reduced number of open spaces or pores. This reduced porosity suggests that the surface of the untreated maize tassel is denser and features fewer pores.

Figure 4.15(b) above reveals significant changes in the morphology of corn tassel cellulose after NaOH treatment. Compared to the cylindrical shape of untreated corn tassels, most treated cellulose exhibits flattened or irregular cross-sections. This phenomenon can be attributed to the partial dissolution and weakening of the cell wall by NaOH, causing the fibers to collapse and deform. Furthermore, the treated cellulose differs from the smooth surface of untreated corn tassels. They have a rough, textured surface with numerous minute cracks, wrinkles, and striations. These textural features, primarily induced by the dissolving effect of NaOH, significantly increase the surface area of the cellulose, potentially impacting its adsorption and reactivity. Additionally, the micrograph highlights a distinct void pattern in the fiber network. This pattern can be attributed to removing hemicellulose, a key component of the cell wall that acts as a binder between cellulose fibers. The NaOH treatment dissolves and removes hemicellulose, weakening the inter-fiber binding and forming visible gaps or spaces.

Another notable consequence of the NaOH treatment is the reduction in fiber size. This phenomenon can be explained by the partial removal of lignin, another cell wall component contributing to structural rigidity. The dissolution of lignin by NaOH weakens the fibers, making them susceptible to shrinkage and deformation, as evident in the reduced diameter observed in the SEM image. Finally, a marginal brightening is observed on the surface of the treated fibers. This effect can be attributed to removing waxy and cementing materials that naturally cover the cellulose surface (Maepa et al., 2015). By removing these substances, the NaOH treatment exposes the underlying rough cellulose, which might appear slightly brighter in the SEM image due to its increased light reflectance.

4.3.2(d) Oil Palm Empty Fruit Bunch

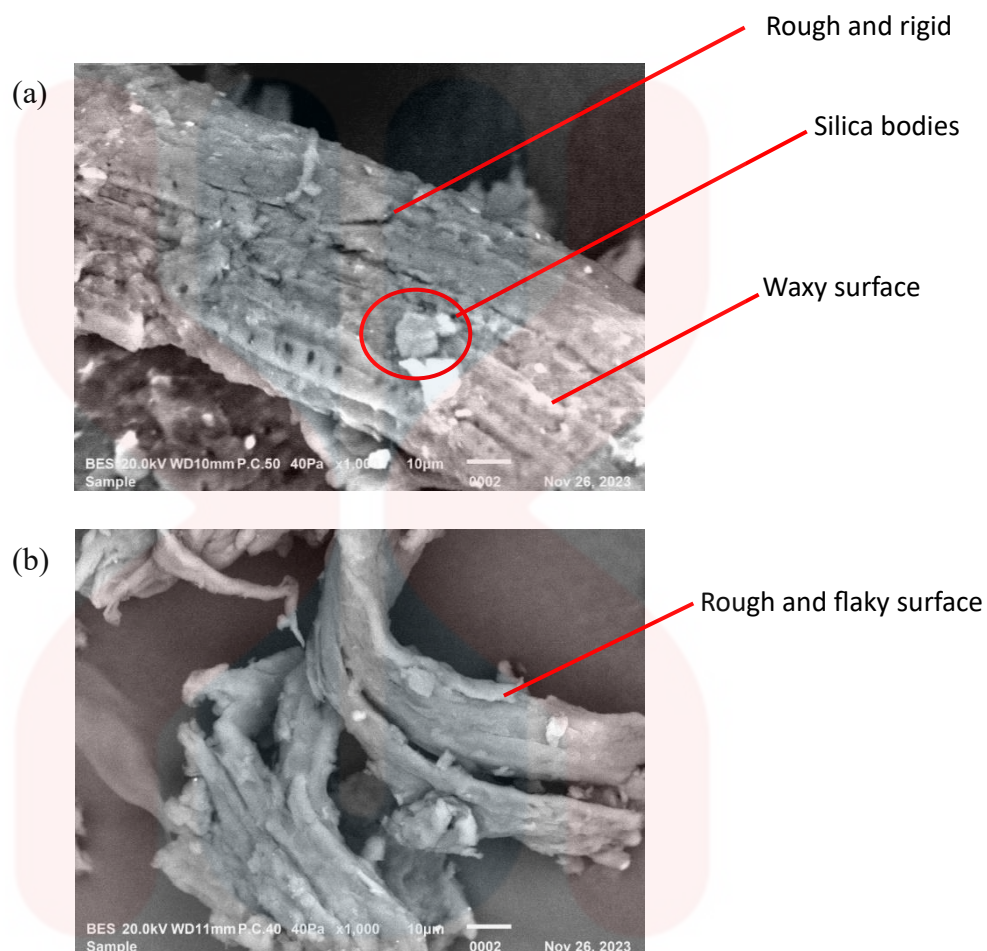


Figure 4. 16: SEM micrograph of (a) untreated and (b) treated oil palm empty fruit bunch

The Figure 4.16(a) above showing that untreated oil palm empty fruit bunch reveals its most prominent feature, which is the long, thin fibers running throughout the material. This micrograph also shows a rough surface covering the entire fiber area, indicating a rigid and highly ordered arrangement of fibrils within the untreated oil palm empty fruit bunch, as Rizal et al. (2018) observed. These fibers, primarily composed of cellulose, a strong and rigid polymer and a key component of plant cell walls, are bundled together in strands, providing strength and structural integrity to the empty fruit bunch. Notably, the fiber surfaces are marked by small pits resulting from cell removal during processing. These pits manifest as dark, circular holes in the fibers.

Moreover, the outer surface of the oil palm empty fruit bunch displays spherical structure embedded within its structure, possibly corresponding to the silica bodies detailed in the research by Isroi et al. in 2017. These spherical silica bodies, characterized by their spiky appearance, are attached to circular craters and are distributed across the strands of the oil palm empty fruit bunch, as highlighted by the findings of Mohammad et al. in 2020. These silica bodies on the fiber surface contribute to its hardness and resistance to degradation. This finding aligns with Arbaain et al. (2019) research, which also observed a rough surface with craters containing round-shaped silica bodies on the fiber's surface. Furthermore, the high hydrocarbon content of untreated oil palm empty fruit bunches, primarily composed of holocellulose, positions it as a potential source for various lignocellulosic-derived products, including microbeads.

The Figure 4.16(b) above also reveals the morphology of NaOH-treated oil palm empty fruit bunch (OPEFB) cellulose. The fibres appear predominantly elongated and roughly rectangular in cross-section, exhibiting relative straightness with some notable bending and kinking. Notably, the cellulose surfaces are characterized by a pronounced roughness and unevenness, showcasing a variety of distinct features. Among these are prominently observed linear features running parallel to the fibre axis, potentially attributable to the underlying cellulose microfibrils within the cell wall. Interestingly, some fibres exhibit cracks or fractures due to the consequence of the drying process following NaOH treatment, where rapid moisture loss can induce internal tension within the fibres, ultimately leading to transverse cracks.

Prior to the treatment, the raw OPEFB fibres are composed of bundled structures, where a matrix of lignin and hemicellulose tightly binds individual cells together. This arrangement often results in a visually uneven and tangled surface. Notably, the alkaline treatment significantly alters this morphology. The removal of impurities, primarily lignin and hemicellulose, leads to a smoother surface appearance on the treated fibres. Additionally, the fibre diameter decreases due to a process known as defibrillation, where the bundled structures open up and separate.

This observed various studies had aligned smooth surface morphology. Notably, Sisak et al. (2015) reported a distinct wrinkled surface morphology for extracted OPEFB cellulose, demonstrating a contrast to the irregular and unsmooth surface of the raw fibres. This wrinkled structure served as evidence of the successful removal of hemicellulose and lignin, revealing a

more refined and distinct cellulose morphology. Further, Alhijazi et al. (2020) emphasized the clearer and smoother morphology of alkaline-treated OPEFB fibres as an indicator of successful impurity and surface contaminant removal. This removal plays a crucial role in enhancing the surface properties of cellulose by creating a more uniform and pristine surface. This observation points towards an efficient extraction process that successfully eliminates non-cellulosic components, leading to a purer cellulose structure with potential applications in microbead production.

However, it is essential to acknowledge that not all studies report identical results. Latip et al. (2019) observed a contrast morphology, where the surface of OPEFB fibres became rough and cratered after NaOH treatment. This phenomenon can be attributed to the reorientation of densely packed crystalline cellulose regions into amorphous zones, allowing hydroxyl groups from the alkaline solution to interact with water molecules and ultimately leading to structural modifications within the fibres. The removal of certain binding and sizing elements also contributes to this increased surface area and porosity. Notably, Latip et al. (2019) observed the cratered surface morphology as a consequence of silica removal and partial lignin decomposition.

4.3.3 Determination of Crystallinity Structure using X-ray Diffraction (XRD)

4.3.3(a) Rice Husk

Cellulose possesses a crystalline structure, unlike hemicellulose and lignin, which are amorphous. This is due to the interaction of hydrogen bonds and Van der Waals forces between nearby molecules. The hydroxyl groups inside cellulose macromolecules form both intramolecular and intermolecular hydrogen bonds. This creates a variety of structured crystal patterns. The hydrogen bonds have a role in maintaining the integrity of the cellulose structure and its crystalline shape (Park et al., 2010). Etale et al. (2023) expand upon this, noting that cellulose's crystalline regions exhibit a remarkable degree of organization, characterized by linear chains of glucose molecules. These regions showcase a high level of structural order, imparting cellulose

with its exceptional strength and stability. In contrast, the amorphous regions within cellulose are less organized and possess a greater water content. These amorphous regions contribute to cellulose's overall flexibility and its capacity to interact with water and other molecules, making them a crucial component of plant cell walls.

The degree of crystallinity in extracted cellulose is a crucial factor in microbead production, as it directly impacts the mechanical properties and structure of the resulting microbeads. Higher crystallinity in the extracted cellulose leads to denser internal structures in the microbeads, resulting in increased stiffness, while lower crystallinity leads to less dense internal structures and decreased stiffness. Additionally, the crystallinity of the extracted cellulose affects the small molecule uptake and release kinetics of the microbeads, making it essential to control the degree of crystallinity for tailoring the properties of microbeads for specific applications.

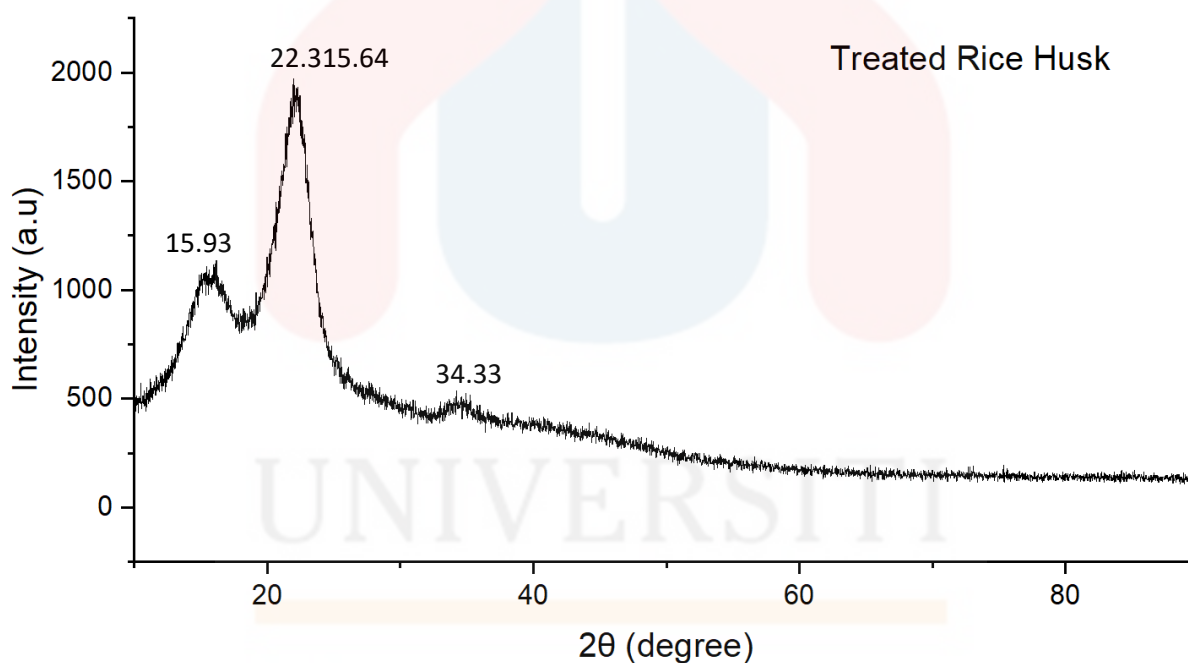


Figure 4. 17: XRD analysis for treated rice husk cellulose

The X-ray diffraction (XRD) pattern shown in Figure 4.17 has three clearly distinguishable diffraction peaks at 2θ angles of 15.93° , 22.31° , and 34.33° . These peaks are indicative of the typical crystalline structure of cellulose I, as obtained from rice husk. The peak with the highest intensity, positioned at an angle of $2\theta = 22.31^\circ$, had a crystallite size of 3.52 nm. Additionally, broad peaks were observed at angles of 15.93° and a small hump was observed at 34.33° , with

corresponding crystallite sizes of 2.73 nm and 8.66 nm. These findings provide further evidence of the existence of the cellulose I structure. The results are similar to those of a study done by Andalia et al. (2020), which showed that cellulose from rice husk has clear peaks at $2\theta = 16^\circ$, 21° , and 23° . Regarding the degree of crystallinity that the cellulose exhibits, the relative magnitudes of these crystalline peaks provide useful information. Higher peak intensities indicate increased crystallinity, which is a favourable characteristic for the production of microbeads. Crystalline cellulose provides structural integrity, whereas amorphous cellulose may not offer the same level of strength. Petroudy (2017) states that crystalline cellulose exhibits enhanced stiffness and a well-organized molecular structure, resulting in increased strength and rigidity. This attribute is crucial for preserving the structural integrity of microbeads, thereby preventing them from distorting or collapsing when subjected to pressure or external forces. The angular positions of the crystalline peaks, such as 22.31° and 34.33° , indicate the interplanar spacings inside the cellulose crystal lattice.

The obtained cellulose had a moderate degree of crystallinity, measuring 59.42%, and a proportion of amorphous material accounting for 40.58%. The study by Yunus (2019) revealed that the delignification and bleaching approach resulted in cellulose with a crystallinity of 58.73% and an amorphous content of 41.27%. The level of crystallinity achieved is significantly high. The fatigue of cellulose molecules occurs due to the removal of hemicellulose and lignin in the amorphous area. Eliminating the amorphous region results in an increased amount of crystalline cellulose, which exhibits a higher level of order and possesses a higher degree of cellulose (Hafid et al., 2021).

4.3.3(b) Corn Stem

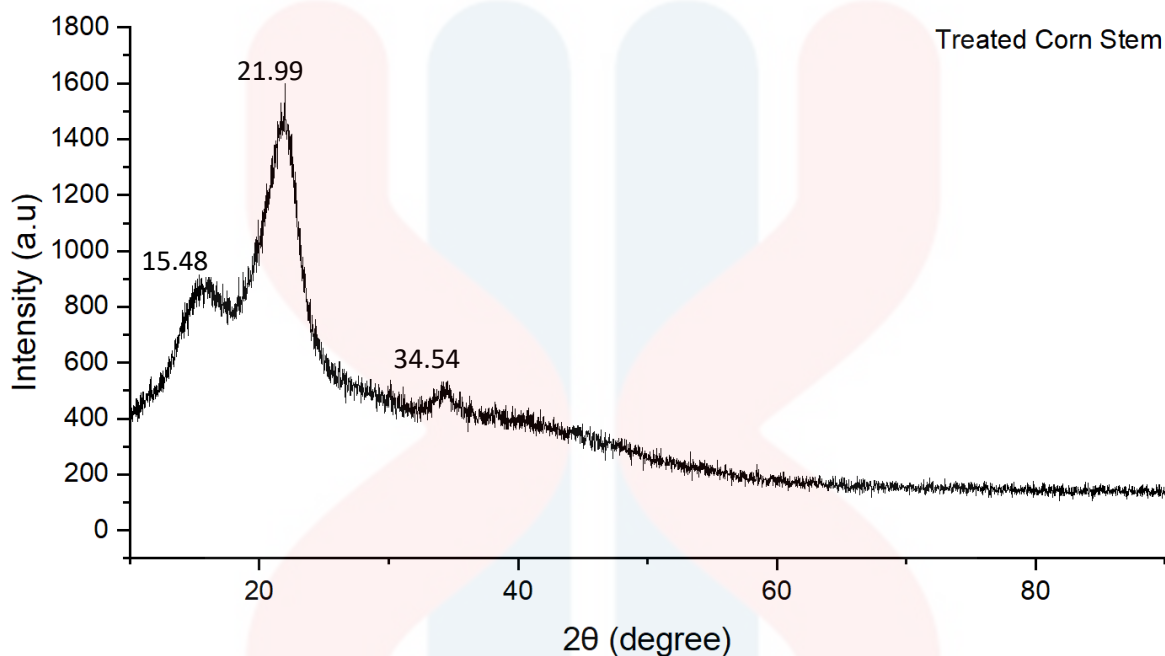


Figure 4. 18: XRD analysis for treated corn stem cellulose

The X-ray diffraction (XRD) pattern observed in Figure 4.18 has three distinct diffraction peaks at 2θ angles. The highest peak, located at an angle of $2\theta = 21.99^\circ$, corresponded to a crystallite size of 3.40 nm. In addition, wide peaks were detected at angles of 15.48° , and a slight bump was identified at 34.54° , indicating crystallite diameters of 2.65 nm and 10.2 nm, respectively. These findings offer additional proof of the presence of the cellulose I structure. The results align with the research conducted by Kampeerappun (2015), indicating that cellulose derived from corn stalk exhibits distinct peaks at $2\theta = 16^\circ$, 22° , and 35° .

The size of crystallites is significant in cellulose microbead production because lower crystallite size leads to a greater surface area per unit mass. The enhanced surface area can result in improved interactions, whether with polymers in composite formulations or solvents in solution-based processes, impacting cellulose microbeads characteristics and uses. Additionally, decreasing crystallite size might enhance mechanical characteristics, such as increased rigidity, due to a more homogeneous dispersion and alignment of the smaller crystallites inside the matrix material (Muralidharan et al., 2022). Bashir et al. (2021) state that microbeads typically range from 0.1

μm to 1 mm. Microbeads can be manufactured in various shapes and with a variety of polymers, including polypropylene (PP), polyethylene (PE), polymethyl methacrylate (PMMA), polyethylene terephthalate (PET), nylons (PA), polyurethanes, and polyester.

The cellulose obtained exhibited a moderate level of crystallinity, measured at 54.17%, along with a corresponding amount of amorphous material, comprising 45.83%. Liu et al. (2019) discovered that the corn stalk has a crystallinity degree of 65.2%, more significant than 54.17%. The alkaline treatment method makes this difference possible by reducing and eliminating amorphous non-cellulosic parts like hemicellulose and lignin. Crystallinity in cellulose refers to the degree to which the cellulose molecules are arranged in a regular, repeating pattern. In highly crystalline cellulose, the molecules are tightly packed together in a well-ordered structure, making the material stronger and more rigid. However, when cellulose is less crystalline, the molecular arrangement has more defects and irregularities, making the material weaker and more flexible (Bergensträhle-Wohlert et al., 2021). Therefore, it appeared that different plant species and the duration of the alkaline treatment process influenced the degree of crystallinity.

4.3.3(c) Corn Tassel

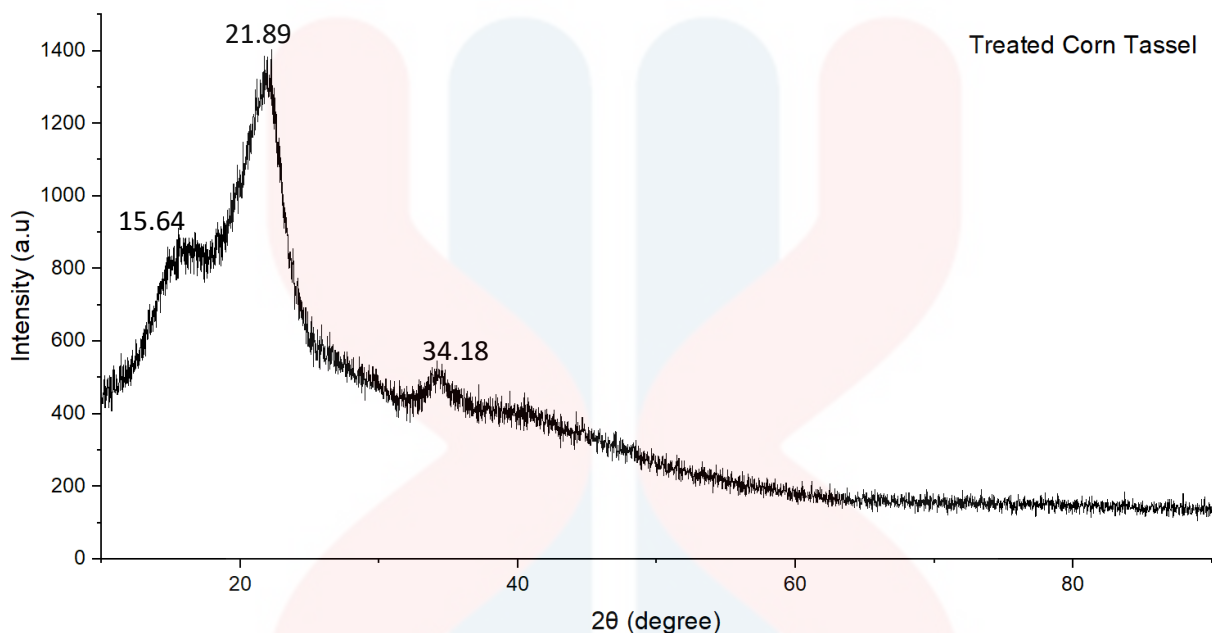


Figure 4. 19: XRD analysis for treated corn tassel cellulose

In Figure 4.19, the X-ray diffraction (XRD) pattern reveals three distinct diffraction peaks at specific 2θ angles. The highest peak, situated at $2\theta = 21.89^\circ$, corresponds to a crystallite size of 3.28 nm. Additionally, there are peaks detected at 15.64° and a subtle bump identified at 34.18° , indicating crystallite sizes of 4.15 nm and 14.42 nm, respectively. These findings provide further evidence of the presence of α -cellulose in the sample. Notably, these results align with prior research by Maepa et al. (2015), which reported distinct XRD peaks at $2\theta = 16.2^\circ$ and 22.5° for cellulose derived from corn tassel.

The presence of smaller crystallite sizes, measuring 3.28 nm and 4.15 nm, suggests that the cellulose material possesses relatively small crystalline domains. In the context of microbead production, these smaller crystallites contribute to the creation of a softer material. This softening effect arises from the fact that smaller crystallites exhibit a higher density of defects and dislocations, resulting in increased ductility. Consequently, such materials are less prone to fracturing under stress during the microbead production process. Furthermore, it is noteworthy that these small crystallites play a role in influencing the diffusion behavior of semicrystalline polymers commonly employed in microbead production. Their elevated surface area-to-volume ratio

significantly enhances the rate of diffusion, a characteristic with profound implications for both the microbead manufacturing process and the resulting properties of the microbeads.

In contrast, a crystallite size of 14.42 nm indicates the presence of substantially larger crystalline domains. These larger crystallites can have adverse effects, such as diminishing the material's mechanical flexibility and increasing its brittleness. Additionally, the sizable crystallites result in a reduced surface area available for interactions between the cellulose microbeads and other materials. Moreover, the extended degradation process associated with larger crystallites can compromise the biodegradability of the microbeads, potentially raising environmental concerns.

In terms of mechanical properties, larger crystallites can enhance a material's stiffness and strength. However, they also increase their vulnerability to fractures under stress. Furthermore, the size of these crystallites can impact the processing and manufacturing of the material. Larger crystallites pose challenges when it comes to shaping and processing compared to materials with smaller crystallites (Murthy, 2013). Nevertheless, cellulose with larger crystallite sizes exhibits higher thermal degradation temperatures or more excellent thermal stability. This is because the crystalline regions of cellulose possess a more ordered and stable structure, requiring more energy to break down during thermal degradation (Petroudy, 2017). Thermal stability plays a crucial role in cellulose microbead production, facilitating efficient processing while ensuring consistent and high-quality products.

The cellulose obtained in this study exhibited a moderate degree of crystallinity at 44.97%, with a significant portion (55.03%) being amorphous. This crystallinity index differs from the value reported by Maepa et al. (2015), which was 88.41% and can be attributed to differences in the XRD instrument's setup. Variances factors such as the type of X-ray source, optics, and detectors can lead to variations in peak positions and intensities.

4.3.3(d) Oil Palm Empty Fruit Bunch

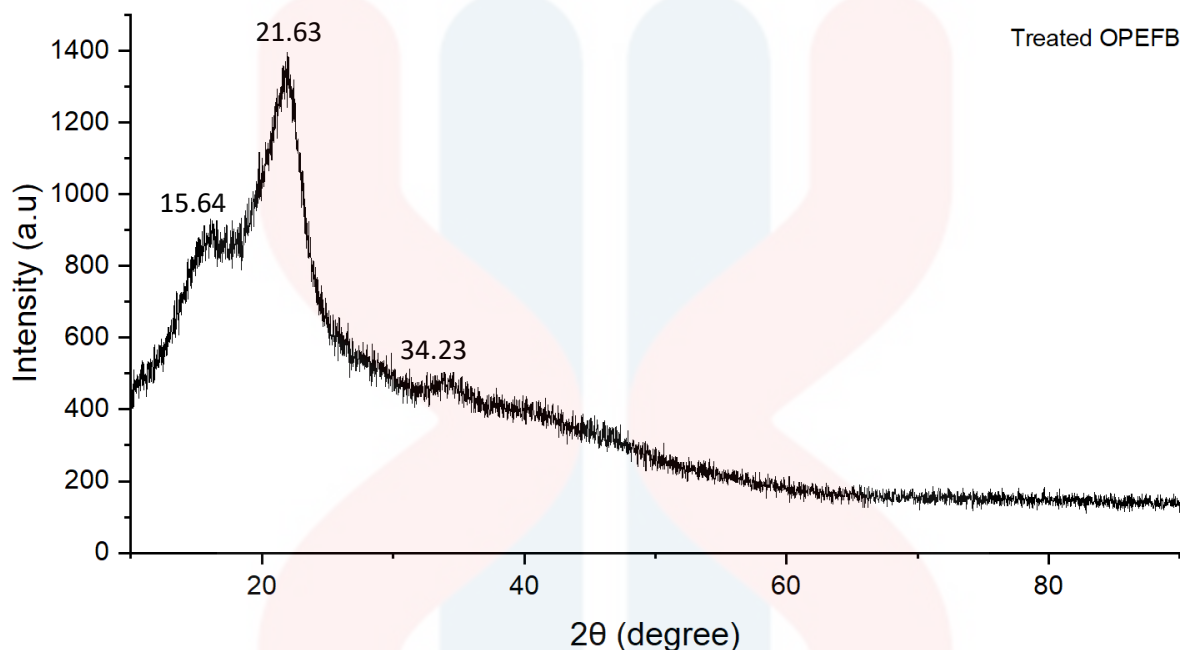


Figure 4. 20: XRD analysis for treated oil palm empty fruit bunch cellulose

In Figure 4.20, the X-ray diffraction (XRD) pattern reveals three distinct diffraction peaks at specific 2θ angles. The highest peak, situated at $2\theta = 15.64^\circ$, corresponds to a crystallite size of 4.47 nm. Additionally, there are peaks detected at 21.63° and a small hump identified at 34.23° , indicating crystallite sizes of 3.19 nm and 7.76 nm, respectively. These findings provide further evidence of the presence of type I cellulose in the sample when the cell-OPEFB occurs around 16° and 22° 2θ (Lu et al., 2020). Notably, these results align with prior research by Salleh and Salamun (2022), which reported distinct XRD peaks at $2\theta = 15$ to 16° and $2\theta = 21$ to 22° for cellulose derived from an empty oil palm fruit bunch. The intensity of the diffraction peak in Cell-OPEFB was higher within the range of 21-22, which might be attributed to the elimination of the non-crystalline portion of cellulose (Chen et al., 2020). The observed increase in the peak intensity at an angle of $2\theta = 22^\circ$ indicates a change in the cellulose structure from amorphous to crystalline. (Teow et al., 2020).

The crystallite size obtained has direct implications for cellulose microbead production, where a smaller crystallite size, such as 3.19 nm, indicates a more compact and ordered crystallite

structure, potentially leading to microbeads with enhanced density and porosity, which can be favorable for microbead applications. According to Daicho et al. (2018), nanocellulose with a high degree of crystallinity tends to be opaque, while nanocellulose with a lower degree of crystallinity can be more transparent. This is because the crystalline regions of cellulose scatter light while the amorphous regions do not. Thus, reducing the size of the crystallites can increase the transparency of the nanocellulose. Conversely, a larger crystallite size like 7.76 nm suggests a less dense and more loosely packed crystalline structure, impacting the strength and interactions of microbeads with other materials.

The cellulose obtained in this study exhibited a moderate degree of crystallinity at 42.78%, with a significant portion (57.21%) being amorphous. This crystallinity index differs from the value reported by Salleh and Salamun (2022), which was 75.51%, and the differences can be due to different sources of oil palm empty fruit bunches used due to the variations in the chemical composition and morphology of the cellulose. The processing parameters used to prepare the cellulose, such as the temperature and length of treatment, can also have an impact on the degree of crystallinity. Last but not least, the degree of purification can also affect the degree of crystallinity, as impurities can interfere with the formation of crystalline regions in cellulose (Emenike et al., 2023).

Table 4. 6: Crystallinity and amorphous percentage of different samples

Samples	Crystallinity, %	Amorphous, %
Rice husk	59.42	40.58
Corn stem	54.17	45.83
Corn tassel	44.97	55.03
Oil palm empty fruit bunch	42.78	57.21

The provided data in Table 4.6 summaries varying degrees of crystallinity and amorphousness in different samples. Notably, rice husk exhibits a notable degree of crystallinity, with approximately 59.42% of its structural composition displaying ordered and well-defined characteristics. This observation suggests that a substantial proportion of the cellulose and

hemicellulose components within rice husk are organized in a crystalline manner. Conversely, about 40.58% of rice husk's composition is found to be amorphous, indicating the presence of less structured and more disordered constituents, such as lignin and certain non-cellulosic polysaccharides.

Comparatively, corn stem manifests a moderately elevated degree of crystallinity, measuring at 54.17%. This value suggests that a significant portion of the cellulose and hemicellulose components within corn stem are arranged in an ordered and crystalline fashion. Additionally, corn stem displays a relatively high amorphous content of 45.83%, signifying the presence of disordered components like lignin and other non-cellulosic materials.

In the case of corn tassel, it exhibits a lower crystallinity percentage, standing at 44.97%, when compared to both rice husk and corn stem. This finding implies that a smaller fraction of cellulose and hemicellulose in corn tassel assumes a crystalline structure. Conversely, it displays a higher amorphous content of 55.03%, indicating a more pronounced presence of disordered materials, such as lignin and non-cellulosic polysaccharides.

Finally, the data reveals that oil palm empty fruit bunch displays the lowest degree of crystallinity among the examined samples, with a mere 42.78% of its structural makeup being crystalline. This outcome implies that a significant portion of the cellulosic and hemicellulosic components within oil palm empty fruit bunch remains disordered and lacks a crystalline arrangement. Conversely, it demonstrates the highest amorphous content, reaching 57.21%, suggesting a substantial presence of non-crystalline and less structured components, possibly attributed to a higher lignin content.

4.3.4 Thermal Stability Study using Thermogravimetric Analysis (TGA)

4.3.4(a) Rice Husk

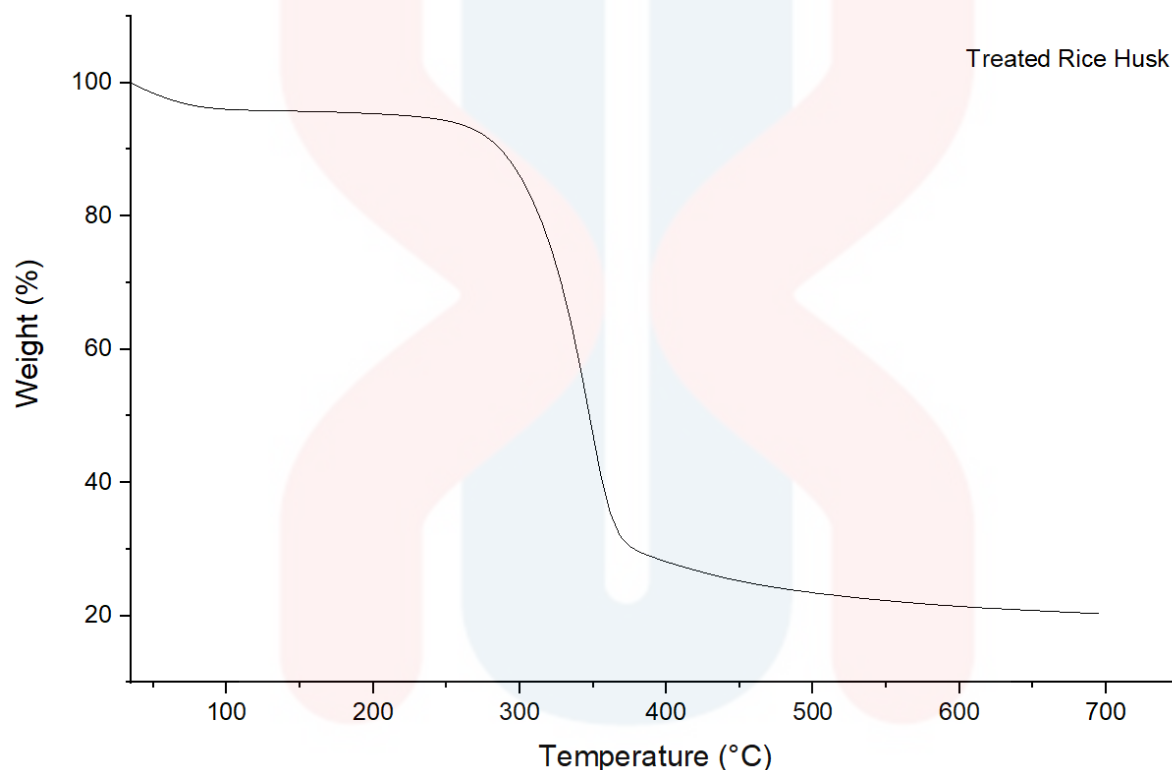


Figure 4. 21: TG analysis of alkaline-treated rice husk cellulose

Figure 4.21 shows a double-phase decomposition of alkali-treated rice husks, where alkali has eliminated waxy substances, natural lipids, hemicellulose, and aliphatic lignin chains. Analysis shows that the initial mass loss in rice husks occurs within the 42.6 to 110°C temperature range. Additionally, the material begins to decompose at 255°C. This observation aligns with the findings of Raza et al. (2022), who reported a mass loss in the 30-100°C range attributed to the evaporation of water within cellulose fibers. This stage primarily involves the removal of water and other volatile compounds, with the extent of this phenomenon influenced by the initial moisture content of the sample. Higher temperatures lead to a more significant decrease in mass (Johar et al., 2012). The degradation process initiates at 200°C, resulting in the breakdown of secondary volatile compounds encompassing various hemicellulose varieties. The decomposition of alkali-treated

rice husk occurs between 200 °C and approximately 371°C. Ciannamea et al. (2010) noted a peak at 360°C, corresponding to the thermal decomposition of α -cellulose (crystalline cellulose) and lignin degradation. He et al. (2022) also observed the decomposition of cellulose structure starting at temperatures exceeding 380°C, leading to a notable reduction in mass loss. These findings suggest cellulose breakdown occurs at higher temperatures than hemicellulose and lignin degradation (Samsalee et al., 2023). The residue produced at the ultimate decomposition temperature of 700°C is relatively small, approximately 20.46%, or 0.43 mg. This residue primarily arises from lignin decomposition and potentially a portion of silica during the alkali treatment. Consequently, processed rice husks yield only a limited residue at the desired temperature, chiefly composed of char originating from the condensed polycyclic aromatic structure of cellulose and silica (Ndazi et al., 2008).

4.3.4(b) Corn Stem

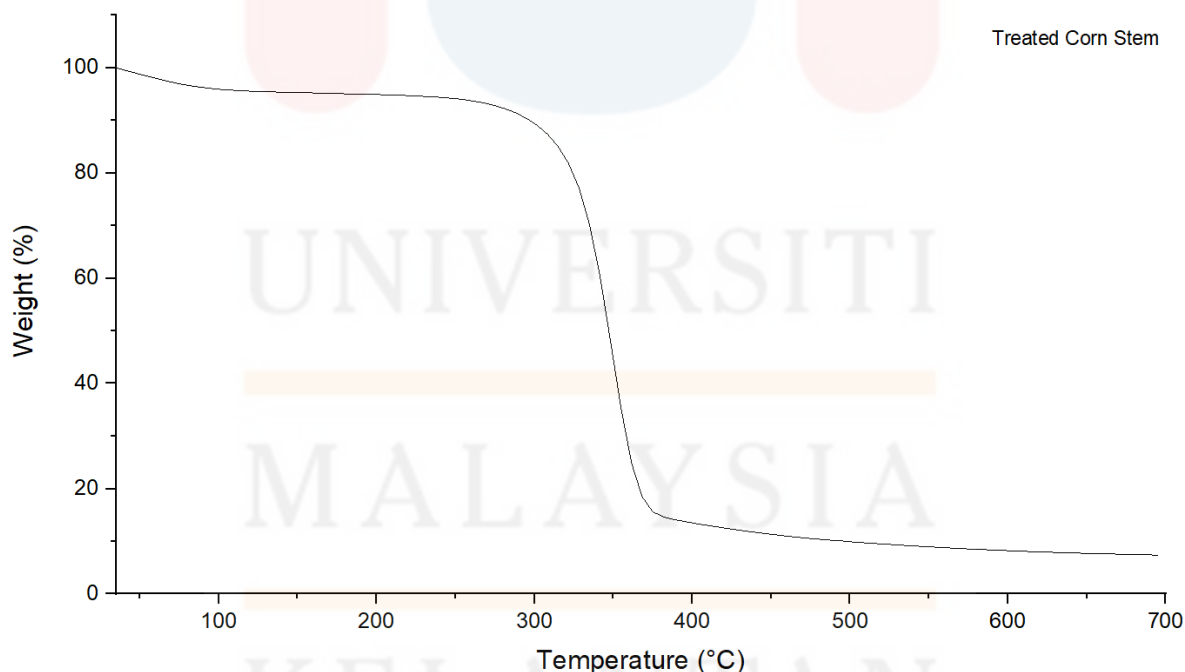


Figure 4. 22: TG analysis of alkaline treated corn stem cellulose

The thermal degradation of alkaline-treated maize stems is shown in Figure 4.30. The initial weight loss of 1.9094 mg or 86.79% in the temperature range of 40-110 °C can be attributed to eliminating moisture from the sample. Starting around 280°C, the material also begins to decompose. This observation is consistent with the results of Singh et al. (2020), who said that the decrease in mass throughout the temperature range of 30-125°C is mainly caused by eliminating moisture from the sample. The initial weight loss is due to the evaporation of physically adsorbed water and other volatile constituents in the maize stem. The primary degradation in the figure occurs between 240 and 400 °C, corresponding to a corresponding breakdown of the organic members in the sample due to heating. This indicates a critical stage of thermal degradation, in which the organic components undergo significant decomposition, resulting in the release of volatile substances and the alteration of the chemical composition of the samples. Jahan et al. (2010) observed that the sample undergoes thermal degradation at 250 and 400 °C temperatures. Costa et al. (2013) similarly found that the degradation onset temperature (T_o) of corn stover cellulose begins at around 261 °C, as the cellulose molecules undergo chemical and physical changes, breaking glycosidic bonds and releasing volatile products. The peak degradation temperature (T_{max}) of 349 °C is attributed to the cellulose molecules undergoing the most significant rate of bond cleavage, resulting in the generation of volatile compounds and char residues. The residue generated at the final decomposition temperature of 700°C is relatively small, amounting to approximately 7.57% or 0.17 mg. The residue at the end of the TGA analysis corresponds to the inorganic constituents or ash content of the samples that remain after the thermal breakdown of organic components in maize stem (Zhang et al., 2014). Cellulose can undergo charring during decomposition, resulting in the formation of a carbonaceous residue. This particular substance may prove challenging to break down further and will persist following the TGA analysis.

4.3.4(c) Corn Tassel

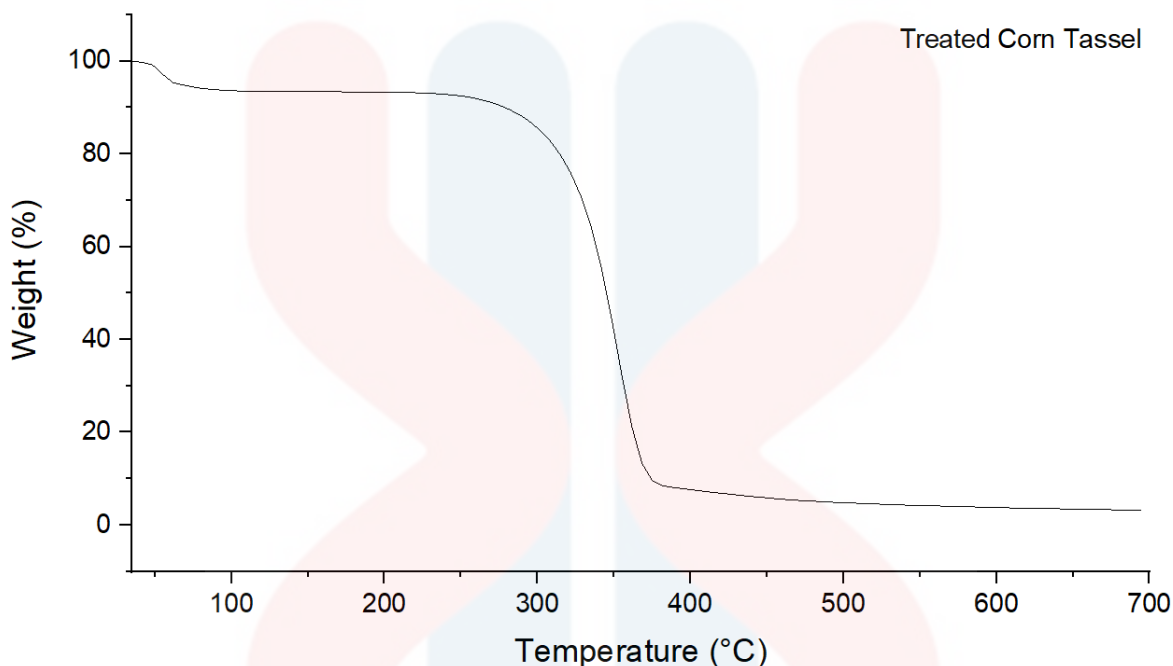


Figure 4. 23: TG analysis of alkaline treated corn tassel cellulose

Figure 4.23 illustrates the thermal stability and decomposition characteristics of cellulose extracted from maize tassels using an alkaline process. The thermogravimetric analysis (TGA) curve reveals a two-step decomposition behavior, signifying distinct thermal events. The primary decomposition stage is prominently evident within the temperature range of 46.75°C to 349.02°C, while the secondary decomposition phase occurs at higher temperatures, spanning from 396.82°C to 697.43°C. Notably, the onset of decomposition is observed at 250°C. The study by Maepa et al. (2015) reveals that the alkaline treatment of corn tassels significantly decreases weight. The primary cause of the weight reduction is the thermal depolymerization of the residual cellulose, hemicellulose, and lignin. The peak decomposition occurs within the temperature range of 278°C to 346°C. Another phase of weight loss is proposed, taking place between 346°C and 700°C. This weight loss results from the disruption of cellulose glycosidic chains and the breakdown of non-living components within the materials, as suggested by Liu et al. in 2006.

The figure above indicates that the initial weight loss detected below 100°C is likely due to the sample's evaporation of any remaining moisture. The degradation process began at approximately 100°C, marked by a reduction in mass and involving substantial depolymerization

and disintegration of the cellulose chains. This phase probably involved the emission of volatile compounds like furans, aligning with the usual cellulose pyrolysis mechanisms. The inflection point at 350.88°C suggests a transition within the central decomposition region, potentially signifying the depletion of readily cleavable cellulose components or the onset of slower decomposition pathways.

At 349.02°C, the main decomposition region stops while much of the cellulose has been turned into volatile products, and only a stable char residue is left. After the primary decomposition region plateau (349.02°C–396.8°C), a secondary weight loss stage was observed in the following decomposition region. This implies further degradation of the remaining char residue, likely caused by slower pyrolysis events and smaller, more stable volatile substances emission. The occurrence of an inflection point at 451.04°C in the second decomposition zone suggests a further change in the rate of weight loss. This change might be attributed to the depletion of particular components within the char or a shift towards even slower breakdown mechanisms. The second plateau occurred at a temperature of 697.43°C, suggesting that critical heat-related processes have finished and a stable residue is present.

The thermogravimetric analysis of cellulose extracted from corn tassels yielded a significant deposition of 3.15% of the biomass, or 72.52 mg. This residue, recognized as char, remained unburnt and non-volatile. Cellulose molecules contain tightly packed crystalline domains that act as tiny shields, blocking the heat impact of pyrolysis. The cohesive chemical connections between cellulose chains produce a densely woven structure demonstrating high thermal degradation resilience (Bregado et al., 2019). This intrinsic resistance enhances the development of char throughout the breakdown process. Combining cellulose's tightly woven fabric structure and the catalytic influence of naturally occurring inorganic ions can increase char production at relatively lower temperatures (Lee et al., 2008). When coupled with cellulose's structural characteristics, the presence of inorganic ions fosters char formation during thermal degradation. This char formation establishes a protective layer that retards the propagation of flames and enhances the mechanical properties of composites comprising cellulosic natural fibers. Moreover, the large surface area of cellulose chains allows for more char to be formed, further strengthening the material's resistance to thermal degradation (Nurazzi et al., 2021).

4.3.4(d) Oil Palm Empty Fruit Bunch

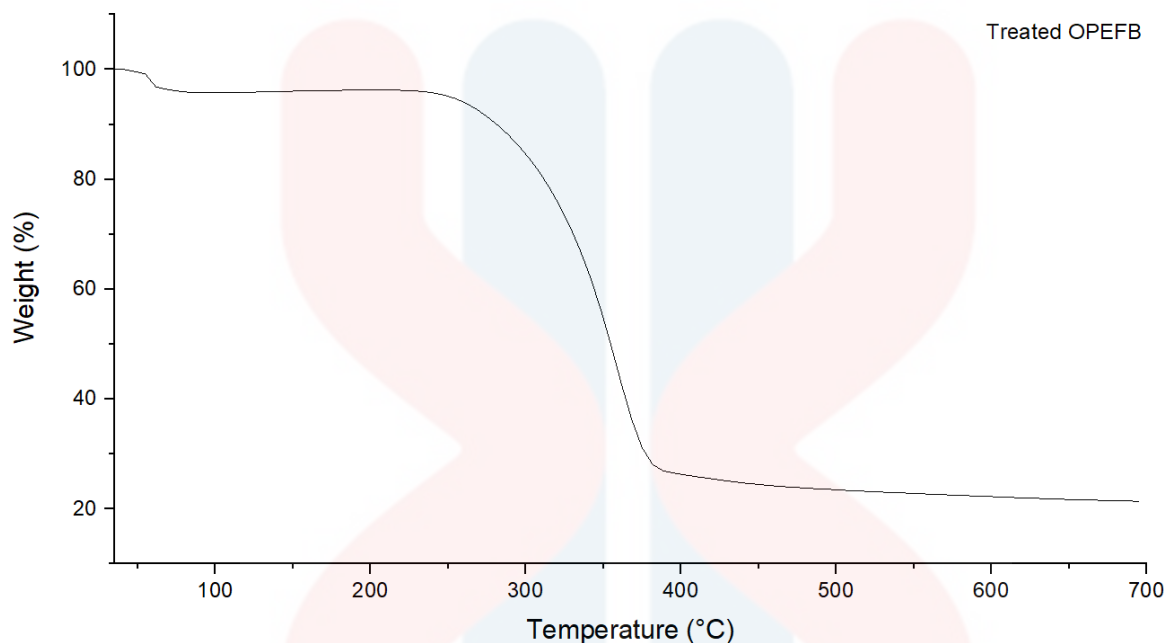


Figure 4. 24: TG analysis of alkaline treated oil palm empty fruit bunch cellulose

The Figure 4.24 above shows the TGA study of cellulose extracted from OPEFB after alkaline treatment demonstrates a degradation process in two distinct steps. The first phase of thermal degradation, starting to decompose at 260°C and occurring within the temperature range of 50°C to 398°C, results in a significant reduction in mass of 73.24%. According to Wahab's (2020) research, cellulose derived from oil palm empty fruit bunches has an initial reduction in weight at around 100 °C. The weight reduction is mainly due to eliminating moisture or water molecules physically or chemically attached to the cellulose structure (Ajayi et al., 2023). Lower temperatures cause the release of loosely attached water molecules and other easily evaporated contaminants found in the cellulose structure. Therefore, the early weight reduction contributes to the total decrease in mass observed throughout this phase. In addition, hemicellulose, a polysaccharide included in OPEFB along with cellulose, is thermally stable compared to crystalline cellulose. Patel and Parsania (2018) found that hemicellulose degrades more easily at lower temperatures (150–180 °C) compared to cellulose (200–230 °C). This is because hemicellulose has a significant amount of chain branching, which gives it a nanocrystalline structure.

In contrast, cellulose is a linear polymer with a higher degree of polymerization. The hemicellulose structure depolymerizes when the temperature rises because the glycosidic linkages weaken. This makes it break down into smaller molecules. Subsequently, these lesser-sized molecules undergo volatilization or further degradation, contributing to the significant mass loss observed. In addition, whereas crystalline cellulose has excellent thermal stability, amorphous cellulose is a less organized section within the cellulose structure and shows less heat resistance (Poletto et al., 2013). At this point, the amorphous cellulose starts to degrade by the heat cleavage of its glycosidic linkages. The depolymerization process results in the release of volatile fragments, leading to further mass loss. The inflection point occurring at a temperature of 59.97°C signifies the start of this coupled deterioration process. This threshold is the temperature at which the mass loss rate accelerates dramatically, suggesting the onset of fast degradation of the hemicellulose and amorphous cellulose chains.

The second degradation stage shows a reduction in weight of 4.81% and a decrease in mass of 0.12 mg. This occurs at temperatures ranging from 399.87°C to 674.11°C, while the heating rate remains constant at 10.00°C min⁻¹. An inflection point becomes apparent at a temperature of 401.22°C within this temperature range. A residue is produced during this specific analysis step, representing 21.52% of the initial sample weight, roughly equal to 0.53 mg. Ninduangdee et al. (2015) found that the temperature range of 160–400°C causes the breakdown of hemicellulose and cellulose, the main components of oil palm empty fruit bunches (OPEFB). Thermal degradation of hemicellulose and cellulose in OPEFB involves a sequence of chemical events that lead to the production of volatile gases and the creation of solid char. The volatile gases include water vapour, carbon dioxide, and other organic compounds, while the solid char comprises the residual carbonaceous material. Cellulose, a complex carbohydrate of glucose molecules bonded together, experiences heat degradation, which involves breaking its structure and releasing volatile substances, including alcohol, organic acids, and other small molecules (Chala et al., 2018). This residue in this analysis indicates that a fraction of the cellulose sample remains even after the heat treatment. The midpoint temperature of the second phase is approximately 473.94°C, representing the temperature at which the decomposition rate is at its peak.

CHAPTER 5

CONCLUSIONS AND RECOMMENDATIONS

5.1 Conclusions

In summary, cellulose extraction was successfully carried out from four distinct sources, namely rice husk (RH), corn stem (CS), corn tassel (CT), and oil palm empty fruit bunch (OPEFB) using alkaline delignification and bleaching methods. Notably, the highest cellulose yield percentage was achieved from OPEFB at 31.40%, with RH (29.28%), CS (14.30%), and CT (13.27%) following suit, indicating varying cellulose yields among the samples.

The presence of cellulose was characterized using FTIR, SEM, XRD, and TGA. In the FTIR analysis, a peak reduction signified the successful removal of non-cellulosic components such as hemicellulose, lignin, and silica. SEM micrographs revealed smoother surface morphologies and reduced impurities in the samples post-alkaline treatment. XRD analysis further revealed crystallinity differences, with RH exhibiting the highest crystallinity at 59.42%, followed by CS (54.17%), CT (44.97%), and OPEFB (42.78%).

Furthermore, the TGA analysis of cellulose extracted from RH, CS, CT, and OPEFB unveiled two-step decomposition behaviours. In each case, the primary decomposition stage occurred within temperature ranges of 200-250°C to 350-400°C, followed by a secondary decomposition phase at higher temperatures (350-500°C to 600-700°C). The observed weight loss during these phases was attributed to the thermal depolymerization of residual cellulose, hemicellulose, and lignin, as well as the disruption of cellulose glycosidic chains and the removal of moisture or water molecules linked to the cellulose structure. These findings offer valuable insights for potential applications, including microbead production with tailored properties such as controlled release characteristics and degradation rates, catering to diverse industrial and

biomedical needs. The cellulose extraction and characterization techniques provide a strong foundation for future research endeavours utilizing cellulose-derived materials.

5.2 Recommendations

Throughout the research, it is highly advised to replace the traditional bleaching process, which uses a mixture of sodium hydroxide (NaOH) and acetic acid (CH₃COOH), with more powerful bleaching agents such as hydrogen peroxide (H₂O₂) or sodium hypochlorite (NaOCl). This adjustment offers numerous appealing benefits. Firstly, H₂O₂ and NaOCl are well-known for their powerful bleaching properties, which result in substantially brighter and whiter cellulose. This function is beneficial when the extracted cellulose is used in applications with critical visual aesthetics and purity, such as manufacturing high-quality microbeads.

Furthermore, using H₂O₂ or NaOCl as a bleaching agent could speed up the bleaching process, lowering processing time and increasing overall experiment efficiency. These strong bleaching chemicals often provide faster results than conventional methods, which may need longer processing times. This efficiency boost contributes to streamlined production procedures, improving cost-effectiveness and the project's long-term competitiveness and sustainability.

In summary, using hydrogen peroxide (H₂O₂) or sodium hypochlorite (NaOCl) as bleaching agents in the cellulose extraction process has various benefits, including increased color brightness of the extracted cellulose and shorter bleaching times. These advantages considerably improve the project's ability to produce high-quality cellulose materials for various applications, including microbead production.

REFERENCES

- Abdel-Halim, E. (2014). Chemical modification of cellulose extracted from sugarcane bagasse: Preparation of hydroxyethyl cellulose. *Arabian Journal of Chemistry*, 7(3), 362–371. <https://doi.org/10.1016/j.arabjc.2013.05.006>
- Abral, H., Ariksha, J., Mahardika, M., Handayani, D., Aminah, I., Sandrawati, N., & Sapuan, S. (2020). Highly transparent and antimicrobial PVA based bionanocomposites reinforced by ginger nanofiber. *Polymer Testing*, 81, 106186. <https://doi.org/10.1016/j.polymertesting.2019.106186>
- Acharya, J., Kumar, U., & Rafi, P. M. (2018). Removal of Heavy Metal Ions from Wastewater by Chemically Modified Agricultural Waste Material as Potential Adsorbent-A Review. *International Journal of Current Engineering and Technology*, of. <https://doi.org/10.14741/ijcet/v.8.3.6>
- Ajayi, S. M., Olusanya, S. O., Sodeinde, K. O., Didunyemi, A. E., Atunde, M. O., Fapojuwo, D. P., Olumayede, E. G., & Lawal, O. S. (2023). Hydrophobic modification of cellulose from oil palm empty fruit bunch: Characterization and application in Pickering emulsions stabilization. *Carbohydrate Polymer Technologies and Applications*, 5, 100282. <https://doi.org/10.1016/j.carpta.2023.100282>
- Alhijazi, M., Zeeshan, Q., Safaei, B., Asmael, M., & Qin, Z. (2020). Recent Developments in Palm Fibers Composites: A review. *Journal of Polymers and the Environment*, 28(12), 3029–3054. <https://doi.org/10.1007/s10924-020-01842-4>
- Amidon, G. L., Meyer, P., & Mudie, D. M. (2009). Particle, Powder, and Compact Characterization. In *Elsevier eBooks* (pp. 271–293). <https://doi.org/10.1016/b978-0-12-802447-8.00010-8>
- Andalia, R., Rahmi, R., Julinawati, J., & Helwati, H. (2020). Isolation and characterization of cellulose from rice husk waste and sawdust with chemical method. *Jurnal Natural*, 20(1), 6–9. <https://doi.org/10.24815/jn.v20i1.12016>
- Arbaain, E. N. N., Bahrin, E. K., Ibrahim, M. F., Ando, Y., & Abd-Aziz, S. (2019). Biological Pretreatment of Oil Palm Empty Fruit Bunch by *Schizophyllum commune* ENN1 without Washing and Nutrient Addition. *Processes*, 7(7), 402. <https://doi.org/10.3390/pr7070402>

- Aridi, A. S., Chin, N. L., Ishak, N. A., Yusof, N. N. M., Kadota, K., Manaf, Y. N. A., & Yusof, Y. A. (2021). Effect of sodium hypochlorite concentration during pre-treatment on isolation of nanocrystalline cellulose from *Leucaena leucocephala* (Lam.) mature pods. *Bioresources*, 16(2), 3137–3158. <https://doi.org/10.15376/biores.16.2.3137-3158>
- Arya, A. C., Soeriaatmaja, R. a. D., Hetharia, D., Surjati, I., Nasution, B., Rubijono, R. D., & Priadi, Y. N. (2015). Environmental Friendly Lightweight Material from Natural Fibers of Oil Palm Empty Fruit Bunch. *Journal of Materials Science and Chemical Engineering*. <https://doi.org/10.4236/msce.2015.37025>
- Asadi, F., Shariatmadari, H., & Mirghaffari, N. (2008). Modification of rice hull and sawdust sorptive characteristics for remove heavy metals from synthetic solutions and wastewater. *Journal of Hazardous Materials*, 154(1–3), 451–458. <https://doi.org/10.1016/j.jhazmat.2007.10.046>
- Bajpai, P. (2016). Pretreatment of Lignocellulosic Biomass. In *Springer briefs in molecular science* (pp. 17–70). Springer Nature. https://doi.org/10.1007/978-981SS0-0687-6_4
- Balat, M., Balat, H., & Öz, C. (2008). Progress in bioethanol processing. *Progress in Energy and Combustion Science*, 34(5), 551–573. <https://doi.org/10.1016/j.peccs.2007.11.001>
- Bali, G., Meng, X., Deneff, J. I., Sun, Q., & Ragauskas, A. J. (2014). The effect of alkaline pretreatment methods on cellulose structure and accessibility. *ChemSusChem*, 8(2), 275–279. <https://doi.org/10.1002/cssc.201402752>
- Bashir, S. M., Kimiko, S., Mak, C. W., Fang, J., & Gonçalves, D. (2021). Personal care and cosmetic products as a potential source of environmental contamination by microplastics in a densely populated Asian city. *Frontiers in Marine Science*, 8. <https://doi.org/10.3389/fmars.2021.683482>
- Battegazzore, D., Bocchini, S., Alongi, J., & Frache, A. (2014). Rice husk as bio-source of silica: preparation and characterization of PLA–silica bio-composites. *RSC Advances*, 4(97), 54703–54712. <https://doi.org/10.1039/c4ra05991c>
- Behera, B. R., Sethi, B., Mishra, R. S., Dutta, S., & Thatoi, H. (2017). Microbial cellulases – Diversity & biotechnology with reference to mangrove environment: A review. *Journal of Genetic Engineering and Biotechnology*, 15(1), 197–210. <https://doi.org/10.1016/j.jgeb.2016.12.001>

- Bergenstråhle-Wohlert, M., Benselfelt, T., Wågberg, L., Furó, I., Berglund, L. A., & Wohlert, J. (2021). Cellulose and the role of hydrogen bonds: not in charge of everything. *Cellulose*, 29(1), 1–23. <https://doi.org/10.1007/s10570-021-04325-4>
- Bhattacharyya, D., Subasinghe, A., & Kim, N. (2015). Natural fibers. In *Elsevier eBooks* (pp. 102–143). <https://doi.org/10.1016/b978-0-323-26434-1.00004-0>
- Bian, H., Yang, Y., & Tu, P. (2021). Crystalline structure analysis of all-cellulose nanocomposite films based on corn and wheat straws. *Bioresources*, 16(4), 8353–8365. <https://doi.org/10.15376/biores.16.4.8353-8365>
- Bianchet, R. T., Cubas, A. L. V., Machado, M., & Moecke, E. H. S. (2020). Applicability of bacterial cellulose in cosmetics – bibliometric review. *Biotechnology Reports*, 27, e00502. <https://doi.org/10.1016/j.btre.2020.e00502>
- Bin, Y., Li, S., Jiao, F., Zhong, S., & Yuan, Y. (2022). Comparative effects of pretreatment on composition and structure of corn stalk for biocomposites. *Bioresources*, 17(3), 4395–4409. <https://doi.org/10.15376/biores.17.3.4395-4409>
- Bregado, J. L., Secchi, A. R., Tavares, F. W., De S Rodrigues, D., & Gambetta, R. (2019). Amorphous paracrystalline structures from native crystalline cellulose: A molecular dynamics protocol. *Fluid Phase Equilibria*, 491, 56–76. <https://doi.org/10.1016/j.fluid.2019.03.011>
- Chala, G. T., Lim, Y. P., Sulaiman, S. A., & Liew, C. L. (2018). Thermogravimetric analysis of empty fruit bunch. *MATEC Web of Conferences*, 225, 02002. <https://doi.org/10.1051/mateconf/201822502002>
- Chapman, H. N. (2019). X-Ray Free-Electron Lasers for the Structure and Dynamics of Macromolecules. *Annual Review of Biochemistry*, 88(1), 35–58. <https://doi.org/10.1146/annurev-biochem-013118-110744>
- Chen, Q., Shi, Y., Chen, G., & Min, C. (2020). Enhanced mechanical and hydrophobic properties of composite cassava starch films with stearic acid modified MCC (microcrystalline cellulose)/NCC (nanocellulose) as strength agent. *International Journal of Biological Macromolecules*, 142, 846–854. <https://doi.org/10.1016/j.ijbiomac.2019.10.024>
- Ciannamea, E. M., Stefani, P. M., & Ruseckaite, R. A. (2010). Medium-density particleboards from modified rice husks and soybean protein concentrate-based adhesives. *Bioresource Technology*, 101(2), 818–825. <https://doi.org/10.1016/j.biortech.2009.08.084>

- Costa, L. a. D. S., Fonsêca, A. F., Pereira, F., & Druzian, J. I. (2013). Extraction and Characterization of Cellulose Nanocrystals from Corn Stover. *Cellulose Chemistry and Technology*, 49(2), 127–133. [https://cellulosechemtechnol.ro/pdf/CCT2\(2015\)/p.127-133.pdf](https://cellulosechemtechnol.ro/pdf/CCT2(2015)/p.127-133.pdf)
- Da Silva Vallejo, M. C., Cordeiro, R., Dias, P. A., Moura, C., Henriques, M., Seabra, I. J., Malça, C., & Morouço, P. (2021). Recovery and evaluation of cellulose from agroindustrial residues of corn, grape, pomegranate, strawberry-tree fruit and fava. *Bioresources and Bioprocessing*, 8(1). <https://doi.org/10.1186/s40643-021-00377-3>
- Daffalla, S., Mukhtar, H., & Shaharun, M. S. (2020). Preparation and characterization of rice husk adsorbents for phenol removal from aqueous systems. *PLOS ONE*, 15(12), e0243540. <https://doi.org/10.1371/journal.pone.0243540>
- Dai, J., Patti, A. F., & Saito, K. (2016). Recent developments in chemical degradation of lignin: catalytic oxidation and ionic liquids. *Tetrahedron Letters*, 57(45), 4945–4951. <https://doi.org/10.1016/j.tetlet.2016.09.084>
- Daicho, K., Saito, T., Fujisawa, S., & Isogai, A. (2018). The crystallinity of nanocellulose: Dispersion-Induced disordering of the grain boundary in biologically structured cellulose. *ACS Applied Nano Materials*, 1(10), 5774–5785. <https://doi.org/10.1021/acsanm.8b01438>
- Das, O., Hedenqvist, M. S., Prakash, C., & Lin, R. (2019). Nanoindentation and flammability characterisation of five rice husk biomasses for biocomposites applications. *Composites Part A: Applied Science and Manufacturing*, 125, 105566. <https://doi.org/10.1016/j.compositesa.2019.105566>
- Devi, S., Poonia, P. K., Kumar, V., Tiwari, A., Meena, R. K., Kumar, U. S. U., Gulnaz, A., & Khalid, M. (2022). Characterization of Natural Fiber Extracted from Corn (*Zea mays* L.) Stalk Waste for Sustainable Development. *Sustainability*, 14(24), 16605. <https://doi.org/10.3390/su142416605>
- Duangpapeng, P., Ketthaisong, D., Lomthaisong, K., Lertrat, K., Scott, M. P., & Suriharn, B. (2018). Corn Tassel: A new source of phytochemicals and antioxidant Potential for Value-Added Product Development in the Agro-Industry. *Agronomy*, 8(11), 242. <https://doi.org/10.3390/agronomy8110242>
- Dullah, H. (2018). *Compatibility assessment for physical and mechanical properties of empty fruit bunch cement-bonded fibreboard*. <http://eprints.uthm.edu.my/id/eprint/154>

- Dwivedi, C., Pandey, I., Pandey, H., Ramteke, P. W., Pandey, A. C., Mishra, S. B., & Patil, S. (2017). Electrospun Nanofibrous Scaffold as a Potential Carrier of Antimicrobial Therapeutics for Diabetic Wound Healing and Tissue Regeneration. In *Elsevier eBooks* (pp. 147–164). <https://doi.org/10.1016/b978-0-323-52727-9.00009-1>
- learning-fields. (2020, April 1). *Corn - Living History Farms, Iowa | learning-fields*. Learning-fields. <https://www.lhf.org/learning-fields/crops/corn/>
- Ebnesajjad, S. (2006). Surface and Material Characterization Techniques. In *Elsevier eBooks* (pp. 43–75). <https://doi.org/10.1016/b978-081551523-4.50006-7>
- Emenike, E. C., Iwuozor, K. O., Saliu, O. D., Ramontja, J., & Adeniyi, A. G. (2023). Advances in the extraction, classification, modification, emerging and advanced applications of crystalline cellulose: A review. *Carbohydrate Polymer Technologies and Applications*, 6, 100337. <https://doi.org/10.1016/j.carpta.2023.100337>
- Etale, A., Onyianta, A. J., Turner, S. R., & Eichhorn, S. J. (2023). Cellulose: A review of water interactions, applications in composites, and water treatment. *Chemical Reviews*, 123(5), 2016–2048. <https://doi.org/10.1021/acs.chemrev.2c00477>
- Farhat, W., Venditti, R. A., Hubbe, M. A., Taha, C. E. D. M., Becquart, F., & Ayoub, A. (2016). A Review of Water-Resistant Hemicellulose-Based Materials: Processing and Applications. *Chemsuschem*, 10(2), 305–323. <https://doi.org/10.1002/cssc.201601047>
- Fatah, I. Y. A., Khalil, H. P. S. A., Hossain, M. S., Aziz, A. A., Davoudpour, Y., Dungani, R., & Bhat, A. H. (2014). Exploration of a Chemo-Mechanical Technique for the Isolation of Nanofibrillated Cellulosic Fiber from Oil Palm Empty Fruit Bunch as a Reinforcing Agent in Composites Materials. *Polymers*, 6(10), 2611–2624. <https://doi.org/10.3390/polym6102611>
- Fávaro, S. L., Lopes, M. S., De Carvalho Neto, A. G. V., De Santana, R. R., & Radovanovic, E. (2010). Chemical, morphological, and mechanical analysis of rice husk/post-consumer polyethylene composites. *Composites Part A: Applied Science and Manufacturing*, 41(1), 154–160. <https://doi.org/10.1016/j.compositesa.2009.09.021>
- FerroThinfilms Lab. (2018, August 14). *X-ray diffraction basics* [Video]. YouTube. https://www.youtube.com/watch?v=3Bj84zXA_Ag

- Festucci-Buselli, R. A., Otoni, W. C., & Joshi, C. P. (2007). Structure, organization, and functions of cellulose synthase complexes in higher plants. *Brazilian Journal of Plant Physiology*, 19(1), 1–13. <https://doi.org/10.1590/s1677-04202007000100001>
- Fook, L. T., & Yatim, J. M. (2015). AN EXPERIMENTAL STUDY ON THE EFFECT OF ALKALI TREATMENT ON PROPERTIES OF KENAF FIBER FOR REINFORCED CONCRETE ELEMENTS. *International Journal of Research in Engineering and Technology*, 04(08), 37–40. <https://doi.org/10.15623/ijret.2015.0408007>
- Frassoldati, A., & Ranzi, E. (2019). Modeling of Thermochemical Conversion of Biomasses. *Elsevier eBooks*. <https://doi.org/10.1016/b978-0-12-409547-2.11625-7>
- Friebel, C., Bischof, R. J., Schild, G., Fackler, K., & Gebauer, I. (2019). Effects of Caustic Extraction on Properties of Viscose Grade Dissolving Pulp. *Processes*, 7(3), 122. <https://doi.org/10.3390/pr7030122>
- Gabriel, T., Belete, A., Syrowatka, F., Neubert, R. H., & Gebre-Mariam, T. (2020). Extraction and characterization of celluloses from various plant byproducts. *International Journal of Biological Macromolecules*, 158, 1248–1258. <https://doi.org/10.1016/j.ijbiomac.2020.04.264>
- Gao, B., Sun, Y., & Sun, R. (2019). Fractional and structural characterization of lignin and its modification as biosorbents for efficient removal of chromium from wastewater: a review. *Journal of Leather Science and Engineering*, 1(1). <https://doi.org/10.1186/s42825-019-0003-y>
- Geng, W., Venditti, R. A., Pawlak, J. J., & Chang, H. (2018). Effect of delignification on hemicellulose extraction from switchgrass, poplar, and pine and its effect on enzymatic convertibility of cellulose-rich residues. *Bioresources*, 13(3), 4946–4963. <https://doi.org/10.15376/biores.13.3.4946-4963>
- Gerull, B., & Chou, P. M. (2020). Effectiveness of using different mechanical methods for extraction of nanocellulose from kapok husk. *Nucleation and Atmospheric Aerosols*. <https://doi.org/10.1063/5.0001967>
- Ginder-Vogel, M., & Sparks, D. L. (2010). The Impacts of X-Ray Absorption Spectroscopy on Understanding Soil Processes and Reaction Mechanisms. In *Developments in psychiatry* (pp. 1–26). Elsevier BV. [https://doi.org/10.1016/s0166-2481\(10\)34001-3](https://doi.org/10.1016/s0166-2481(10)34001-3)

- Gírio, F. M., Fonseca, C., Carvalheiro, F., Duarte, L. V., Marques, S., & Bogel-Lukasik, R. (2010). Hemicelluloses for fuel ethanol: A review. *Bioresource Technology*, 101(13), 4775–4800. <https://doi.org/10.1016/j.biortech.2010.01.088>
- Gomes, J., Batra, J., Chopda, V. R., Kathiresan, P., & Rathore, A. S. (2018). Monitoring and Control of Bioethanol Production From Lignocellulosic Biomass. In *Elsevier eBooks* (pp. 727–749). <https://doi.org/10.1016/b978-0-444-63992-9.00025-2>
- Goyal, S. K., Jogdand, S. V., & Agrawal, A. (2014). Energy use pattern in rice milling industries—a critical appraisal. *Journal of Food Science and Technology*, 51(11), 2907–2916. <https://doi.org/10.1007/s13197-012-0747-3>
- Gu, B., & Burgess, D. J. (2014). Polymeric Materials in Drug Delivery. In *Elsevier eBooks* (pp. 333–349). <https://doi.org/10.1016/b978-0-12-396983-5.00021-1>
- Hafid, H. S., Omar, F. N., Zhu, J., & Wakisaka, M. (2021). Enhanced crystallinity and thermal properties of cellulose from rice husk using acid hydrolysis treatment. *Carbohydrate Polymers*, 260, 117789. <https://doi.org/10.1016/j.carbpol.2021.117789>
- Han, J., Lee, J. H., & Roh, K. C. (2019). Herbaceous biomass Waste-Derived activated carbons for supercapacitors. *Journal of Electrochemical Science and Technology*, 9(2), 157–162. <https://doi.org/10.5229/jecst.2018.9.2.157>
- Hasanin, M. (2022). Cellulose-Based Biomaterials: Chemistry and Biomedical Applications. *Starch-starke*, 74(7–8), 2200060. <https://doi.org/10.1002/star.202200060>
- Hassan, M. M., Ward, A. A., & Eid, M. M. A. (2010). Mechanical, optical, and electrical properties of cellulosic semiconductor nanocomposites. *Journal of Applied Polymer Science*. <https://doi.org/10.1002/app.31352>
- He, Q., Bai, Y., Lu, Y., Cui, B., Huang, Z., Yang, Q., Jiang, D., & Shao, D. (2022). Isolation and characterization of cellulose nanocrystals from Chinese medicine residues. *Biomass Conversion and Biorefinery*. <https://doi.org/10.1007/s13399-022-03380-6>
- Hernandez, C., & Rosa, D.D. (2016). Extraction of cellulose nanowhiskers : natural fiber source , methodology and application.
- Hernández-Becerra, E., Osorio, M., Marín, D., Gañán, P., Pereira, M., Builes, D. H., & Castro, C. (2023). Isolation of cellulose microfibrils and nanofibrils by mechanical fibrillation in a water-free solvent. *Cellulose*, 30(8), 4905–4923. <https://doi.org/10.1007/s10570-023-05162-3>

- Hidayat, M. H., Aqilah, N. A. A., & Winata, A. W. (2022). Pretreatment of Oil Palm Empty Fruit Bunch using Caustic Soda Solution for Lignin Isolation. *Journal of Applied Science and Engineering*, 25(6), 1177–1182. <https://doi.org/10.32743/jase.202212-25-6-0013>
- Hospodarova, V., Singovszka, E., & Stevulova, N. (2018). Characterization of Cellulosic Fibers by FTIR Spectroscopy for Their Further Implementation to Building Materials. *American Journal of Analytical Chemistry*, 09(06), 303–310. <https://doi.org/10.4236/ajac.2018.96023>
- Huang, L., Ma, M., Ji, X., Choi, S., & Si, C. (2021). Recent Developments and Applications of Hemicellulose From Wheat Straw: A Review. *Frontiers in Bioengineering and Biotechnology*, 9. <https://doi.org/10.3389/fbioe.2021.690773>
- Huang, S., Zhou, L., Li, M., Wu, Q., & Zhou, D. (2017). Cellulose Nanocrystals (CNCs) from Corn Stalk: Activation Energy Analysis. *Materials*, 10(1), 80. <https://doi.org/10.3390/ma10010080>
- Huchelmann, A., Boutry, M., & Hachez, C. (2017). Plant glandular trichomes: natural cell factories of high biotechnological interest. *Plant Physiology*, 175(1), 6–22. <https://doi.org/10.1104/pp.17.00727>
- Ilham, Z. (2022). Biomass classification and characterization for conversion to biofuels. *Elsevier eBooks*, 69–87. <https://doi.org/10.1016/b978-0-12-824388-6.00014-2>
- International Journal of Pharmaceutical Research and Applications (IJPRA)*. (n.d.). <https://www.ijprajournal.com/past-issue-volume.php?issueid=32&title=Volume%206%20,%20Issue%203,%20May-June%202021>
- Isroi, Cifriadi, A., Panji, T., Wibowo, N. A., & Syamsu, K. (2017). Bioplastic production from cellulose of oil palm empty fruit bunch. *IOP Conference Series: Earth and Environmental Science*, 65, 012011. <https://doi.org/10.1088/1755-1315/65/1/012011>
- Jahan, M. S., Saeed, A., He, Z., & Ni, Y. (2010). Jute as raw material for the preparation of microcrystalline cellulose. *Cellulose*, 18(2), 451–459. <https://doi.org/10.1007/s10570-010-9481-z>
- Jakob, M., Mahendran, A. R., Gindl-Altmutter, W., Bliem, P., Konnerth, J., Müller, U., & Veigel, S. (2021). The strength and stiffness of oriented wood and cellulose-fibre materials: A

- review. *Progress in Materials Science*, 125, 100916.
<https://doi.org/10.1016/j.pmatsci.2021.100916>
- Javier-Astete, R., Dávalos, J. J., & Zolla, G. (2021). Determination of hemicellulose, cellulose, holocellulose and lignin content using FTIR in *Calycophyllum spruceanum* (Benth.) K. Schum. and *Guazuma crinita* Lam. *PLOS ONE*, 16(10), e0256559.
<https://doi.org/10.1371/journal.pone.0256559>
- Jayaramudu, J., Reddy, G. S. M., Varaprasad, K., Sadiku, R., Ray, S. S., & Rajulu, A. V. (2013). Effect of Alkali Treatment on the Morphology and Tensile Properties of *Cordia Dichotoma* Fabric/Polycarbonate Composites. *Advances in Polymer Technology*, 32(3).
<https://doi.org/10.1002/adv.21349>
- Johar, N., Ahmad, I., & Dufresne, A. (2012). Extraction, preparation and characterization of cellulose fibres and nanocrystals from rice husk. *Industrial Crops and Products*, 37(1), 93–99. <https://doi.org/10.1016/j.indcrop.2011.12.016>
- Jordan, B. M., & Dumais, J. (2010). Biomechanics of Plant Cell Growth. *eLS*.
<https://doi.org/10.1002/9780470015902.a0022336>
- Jørgensen, H., Kristensen, J., & Felby, C. (2007). Enzymatic conversion of lignocellulose into fermentable sugars: challenges and opportunities. *Biofuels, Bioproducts and Biorefining*, 1(2), 119–134. <https://doi.org/10.1002/bbb.4>
- Kampeerapappun, P. (2015). Extraction and Characterization of Cellulose Nanocrystals Produced by Acid Hydrolysis from Corn Husk. *Journal of Metals, Materials and Minerals*, 25(1), 19–26. <https://doi.org/10.14456/jmmm.2015.3>
- Kangas, H., Liitiä, T., Rovio, S., Ohra-Aho, T., Heikkinen, H., Tamminen, T., & Poppius-Levlin, K. (2014). Characterization of dissolved lignins from acetic acid Lignofibre (LGF) organosolv pulping and discussion of its delignification mechanisms. *Holzforschung*, 69(3), 247–256. <https://doi.org/10.1515/hf-2014-0070>
- Khazraji, A. C., & Robert, S. (2013). Self-Assembly and Intermolecular Forces When Cellulose and Water Interact Using Molecular Modeling. *Journal of Nanomaterials*, 2013, 1–12.
<https://doi.org/10.1155/2013/745979>
- Kline, L. M., Hayes, D. G., Womac, A. R., & Labbé, N. (2010). Simplified determination of lignin content in hard and soft woods via UV-spectrophotometric analysis of biomass dissolved

- in ionic liquids. *Bioresources*, 5(3), 1366–1383. <https://doi.org/10.15376/biores.5.3.1366-1383>
- Kucharska, K., Rybarczyk, P., Hołowacz, I., Łukajtis, R., Glinka, M., & Kamiński, M. (2018). Pretreatment of Lignocellulosic Materials as Substrates for Fermentation Processes. *Molecules*, 23(11), 2937. <https://doi.org/10.3390/molecules23112937>
- Kunusa, W. R., Isa, I., Laliyo, L. a. R., & Iyabu, H. (2018). FTIR, XRD and SEM Analysis of Microcrystalline Cellulose (MCC) Fibers from Corncorbs in Alkaline Treatment. *Journal of Physics*, 1028, 012199. <https://doi.org/10.1088/1742-6596/1028/1/012199>
- Latip, N. A., Sofian, A. H., Ali, M. F., Ismail, S. N., & Idris, D. M. N. D. (2019). Structural and morphological studies on alkaline pre-treatment of oil palm empty fruit bunch (OPEFB) fiber for composite production. *Materials Today: Proceedings*, 17, 1105–1111. <https://doi.org/10.1016/j.matpr.2019.06.529>
- Lee, H., Hamid, S., & Zain, S. K. (2014). Conversion of Lignocellulosic Biomass to Nanocellulose: Structure and Chemical Process. *The Scientific World Journal*, 2014, 1–20. <https://doi.org/10.1155/2014/631013>
- Lee, J. G., Shin, E. J., Pavelka, R. A., Kirchner, M. S., Dounas-Frazer, D. R., McCloskey, B. D., Petrick, D. E., McKinnon, J. T., & Herring, A. M. (2008). Effect of metal doping on the initial pyrolysis chemistry of cellulose chars. *Energy & Fuels*, 22(4), 2816–2825. <https://doi.org/10.1021/ef700637s>
- Li, J., Hu, H., Li, H., Huang, L., Chen, L. Q., & Ni, Y. (2017). Kinetics and mechanism of hemicelluloses removal from cellulosic fibers during the cold caustic extraction process. *Bioresource Technology*, 234, 61–66. <https://doi.org/10.1016/j.biortech.2017.03.026>
- Li, W., Zhang, Y., Das, L., Wang, Y., Li, M., Wanninayake, N., Pu, Y., Kim, D. Y., Cheng, Y., Ragauskas, A. J., & Shi, J. (2018). Linking lignin source with structural and electrochemical properties of lignin-derived carbon materials. *RSC Advances*, 8(68), 38721–38732. <https://doi.org/10.1039/c8ra08539k>
- Li, X., Xu, R., Yang, J., Nie, S., Liu, D., Liu, Y., & Si, C. (2019). Production of 5-hydroxymethylfurfural and levulinic acid from lignocellulosic biomass and catalytic upgradation. *Industrial Crops and Products*, 130, 184–197. <https://doi.org/10.1016/j.indcrop.2018.12.082>

- Liu, C., Xu, F., Sun, J., Ren, J., Curling, S., Sun, R., Fowler, P. A., & Baird, M. S. (2006). Physicochemical characterization of cellulose from perennial ryegrass leaves (*Lolium perenne*). *Carbohydrate Research*, 341(16), 2677–2687. <https://doi.org/10.1016/j.carres.2006.07.008>
- Liu, Q., Luo, L., & Zheng, L. (2018). Lignins: Biosynthesis and Biological Functions in Plants. *International Journal of Molecular Sciences*, 19(2), 335. <https://doi.org/10.3390/ijms19020335>
- Liu, X., Chen, X., Yang, L., Chen, H., Tian, Y., & Wang, Z. (2015). A review on recent advances in the comprehensive application of rice husk ash. *Research on Chemical Intermediates*, 42(2), 893–913. <https://doi.org/10.1007/s11164-015-2061-y>
- Lu, J., Lang, J., Lan, P., Yang, H., Yang, J., Wu, X., & Zhang, H. (2020). Evaluation of surface activity of hydrophobic modified nanocrystalline cellulose. *Cellulose*, 27(16), 9299–9309. <https://doi.org/10.1007/s10570-020-03415-z>
- Maepa, C., Jayaramudu, J., Okonkwo, J. O., Ray, S. S., Sadiku, R., & Ramontja, J. (2015). Extraction and Characterization of Natural Cellulose Fibers from Maize Tassel. *International Journal of Polymer Analysis and Characterization*, 20(2), 99–109. <https://doi.org/10.1080/1023666x.2014.961118>
- Mahmood, N., Gupta, A., Beg, M. D. H., Chua, G. K., & Asim, M. (2014). Laccase application in medium density fibreboard to prepare a bio-composite. *RSC Advances*, 4(22), 11520–11527. <https://doi.org/10.1039/c3ra40593a>
- Malaysian Palm Oil Board. (2022). Overview 2022. Retrieved from <https://bepi.mpob.gov.my/images/overview/Overview2022.pdf>.
- Mariana, M., Alfatah, T., Khalil, H. P. S. A., Yahya, E. B., Farayibi, P. K., Nuryawan, A., Mistar, E. M., Abdullah, C. K., Abdulmadjid, S. N., & Ismail, H. (2021). A current advancement on the role of lignin as sustainable reinforcement material in biopolymeric blends. *Journal of Materials Research and Technology*, 15, 2287–2316. <https://doi.org/10.1016/j.jmrt.2021.08.139>
- Marzoug, I. B., Sakli, F., & Roudesli, S. (2010). Separation of ultimate and technical esparto grass fibres: comparison between extraction methods. *Journal of the Textile Institute*, 101(12), 1050–1056. <https://doi.org/10.1080/00405000903230267>

- Mauer, L. J., & Bradley, R. H. (2017). Moisture and Total Solids Analysis. In *Food science text series* (pp. 257–286). Springer Nature. https://doi.org/10.1007/978-3-319-45776-5_15
- Megashah, L. N., Ariffin, H., Zakaria, M. N., & Hassan, M. K. (2018). Properties of Cellulose Extract from Different Types of Oil Palm Biomass. *IOP Conference Series: Materials Science and Engineering*, 368, 012049. <https://doi.org/10.1088/1757-899x/368/1/012049>
- Menczel, J. D., & Prime, R. B. (2009). *Thermal Analysis of Polymers: Fundamentals and Applications*. John Wiley & Sons.
- Misson, M., Haron, R., Kamaroddin, M. F. A., & Amin, N. a. S. (2009). Pretreatment of empty palm fruit bunch for production of chemicals via catalytic pyrolysis. *Bioresource Technology*, 100(11), 2867–2873. <https://doi.org/10.1016/j.biortech.2008.12.060>
- Mohammad, I. N., Ongkudon, C. M., & Misson, M. (2020). Physicochemical properties and lignin degradation of Thermal-Pretreated oil palm Empty fruit bunch. *Energies*, 13(22), 5966. <https://doi.org/10.3390/en13225966>
- Monte, L. S., Escócio, V. A., De Sousa, A. A., Furtado, C. R. G., Leite, M. C. a. M., Visconte, L. L. Y., & Pacheco, E. B. a. V. (2017). Study of time reaction on alkaline pretreatment applied to rice husk on biomass component extraction. *Biomass Conversion and Biorefinery*, 8(1), 189–197. <https://doi.org/10.1007/s13399-017-0271-9>
- Moyo, M., Okonkwo, J. O., & Agyei, N. M. (2014). Maize tassel-modified carbon paste electrode for voltammetric determination of Cu(II). *Environmental Monitoring and Assessment*, 186(8), 4807–4817. <https://doi.org/10.1007/s10661-014-3739-0>
- Muffler, K., Poth, S., Sieker, T., Tippkötter, N., & Ulber, R. (2011). Bio-Feedstocks. In *Encyclopedia of Analytical Science, Second Edition*. <https://doi.org/10.1016/b978-0-08-088504-9.00088-x>
- Muralidharan, V., Gochhayat, S., Palanivel, S., & Madhan, B. (2022). Influence of preparation techniques of cellulose II nanocrystals as reinforcement for tannery solid waste–based gelatin composite films. *Environmental Science and Pollution Research*, 30(6), 14284–14303. <https://doi.org/10.1007/s11356-022-23058-w>
- Murthy, N. S. (2013). Scattering techniques for structural analysis of biomaterials. In *Elsevier eBooks* (pp. 34–72). <https://doi.org/10.1533/9780857093684.34>

- Nasrazadani, S., & Hassani, S. (2016). Modern analytical techniques in failure analysis of aerospace, chemical, and oil and gas industries. In *Elsevier eBooks* (pp. 39–54). <https://doi.org/10.1016/b978-0-08-100117-2.00010-8>
- Nazli, M. H., Halim, R. A., Abdullah, A., Hussin, G., & Samsudin, A. A. (2018). Potential of feeding beef cattle with whole corn crop silage and rice straw in Malaysia. *Tropical Animal Health and Production*, 50(5), 1119–1124. <https://doi.org/10.1007/s11250-018-1538-2>
- Ndazi, B. S., Nyahumwa, C., & Tesha, J. V. (2008). Chemical and thermal stability of rice husks against alkali treatment. *Bioresources*, 3(4), 1267–1277. <https://doi.org/10.15376/biores.3.4.1267-1277>
- Ndazi, B., Nyahumwa, C., & Tesha, J. V. (2008). Chemical and thermal stability of rice husks against alkali treatment. *ResearchGate*. https://www.researchgate.net/publication/26543503_Chemical_and_thermal_stability_of_rice_husks_against_alkali_treatment
- Ng, H. M., Sin, L. T., Tee, T. T., Bee, S. T., Hui, D., Low, C. Y., & Rahmat, A. R. (2015). Extraction of cellulose nanocrystals from plant sources for application as reinforcing agent in polymers. *Composites Part B: Engineering*, 75, 176–200. <https://doi.org/10.1016/j.compositesb.2015.01.008>
- Ninduangdee, P., Kuprianov, V. I., Young, E., Kaewrath, R., Youngyuen, P., & Atthawethworawuth, W. (2015). Thermogravimetric studies of oil palm empty fruit bunch and palm kernel shell: TG/DTG analysis and modeling. *Energy Procedia*, 79, 453–458. <https://doi.org/10.1016/j.egypro.2015.11.518>
- Ningtyas, K. L., Agassi, T. N., & Putri, P. G. (2022). Utilization of Waste Cellulose Raw Material for Making Paper Pulp. *IOP Conference Series*, 1012(1), 012091. <https://doi.org/10.1088/1755-1315/1012/1/012091>
- Noah, A. S. (2022). Oil Palm Empty Fruit Bunches (OPEFB) – Alternative Fibre Source for Papermaking. In *IntechOpen eBooks*. <https://doi.org/10.5772/intechopen.98256>
- Nurazzi, N. M., Asyraf, M. R. M., Rayung, M., Norrrahim, M. N. F., Shazleen, S. S., Rani, M. M. S., Rafiqah, S. A., Aisyah, H. A., Radzi, M. H. M., Sabaruddin, F. A., Sapuan, S., Zainudin, E. S., & Abdan, K. (2021). Thermogravimetric Analysis Properties of Cellulosic Natural Fiber Polymer Composites: A Review on Influence of Chemical Treatments. *Polymers*, 13(16), 2710. <https://doi.org/10.3390/polym13162710>

- O'Brien, J. J., Torrente-Murciano, L., Mattia, D., & Scott, J. L. (2017a). Continuous Production of Cellulose Microbeads via Membrane Emulsification. *ACS Sustainable Chemistry & Engineering*, 5(7), 5931–5939. <https://doi.org/10.1021/acssuschemeng.7b00662>
- Ogbuefi, P. S., Nwaokafor, P., Njoku, I. J., & Uzuegbunam, O. J. (2020). Elemental Characterization of Rice Husk Ash from Local Rice Species in South Eastern Nigeria. *Chemistry Africa*. <https://doi.org/10.1007/s42250-020-00188-7>
- Omran, A. a. B., Mohammed, A., Sapuan, S., Sapuan, S., Asyraf, M. R. M., Koloor, S. S. R., & Petru, M. (2021). Micro- and Nanocellulose in Polymer Composite Materials: A Review. *Polymers*, 13(2), 231. <https://doi.org/10.3390/polym13020231>
- Onoja, D. A., Ahemen, I., & Iorfa, T. F. (2019). Synthesis and Characterization of Cellulose Based Nanofibres from Rice Husk. *IOSR Journal of Applied Physics (IOSR-JAP)*, Volume 11(Issue 2 Ser. III), Pages 80-87. <https://doi.org/10.9790/4861-1102038087>
- Ouarhim, W., Zari, N., Bouhfid, R., & Qaiss, A. E. K. (2019). Mechanical performance of natural fibers-based thermosetting composites. In *Elsevier eBooks* (pp. 43–60). <https://doi.org/10.1016/b978-0-08-102292-4.00003-5>
- Ouellette, R. J. (2015). Ethers and epoxides. In *Elsevier eBooks* (pp. 277–297). <https://doi.org/10.1016/b978-0-12-801889-7.00016-9>
- Pallares-Rusiñol, A., Bernuz, M., Moura, S. L., Fernández-Senac, C., Rossi, R., Martí, M., & Pividori, M. I. (2023). Advances in exosome analysis. In *Elsevier eBooks* (pp. 69–117). <https://doi.org/10.1016/bs.acc.2022.09.002>
- Park, B., Wi, S. G., Lee, K. H., Singh, A. P., Yoon, T., & Kim, Y. S. (2003). Characterization of anatomical features and silica distribution in rice husk using microscopic and micro-analytical techniques. *Biomass and Bioenergy*, 25(3), 319–327. [https://doi.org/10.1016/s0961-9534\(03\)00014-x](https://doi.org/10.1016/s0961-9534(03)00014-x)
- Park, S., Baker, J. O., Himmel, M. E., Parilla, P. A., & Johnson, D. K. (2010). Cellulose crystallinity index: measurement techniques and their impact on interpreting cellulase performance. *Biotechnology for Biofuels*, 3(1). <https://doi.org/10.1186/1754-6834-3-10>
- Patel, J. P., & Parsania, P. H. (2018). Characterization, testing, and reinforcing materials of biodegradable composites. In *Elsevier eBooks* (pp. 55–79). <https://doi.org/10.1016/b978-0-08-100970-3.00003-1>

- Peanparkdee, M., & Iwamoto, S. (2019). Bioactive compounds from by-products of rice cultivation and rice processing: Extraction and application in the food and pharmaceutical industries. *Trends in Food Science and Technology*, 86, 109–117. <https://doi.org/10.1016/j.tifs.2019.02.041>
- Pednekar, P. P., Godiyal, S., Jadhav, K. R., & Kadam, V. J. (2017). Mesoporous silica nanoparticles: a promising multifunctional drug delivery system. In *Elsevier eBooks* (pp. 593–621). <https://doi.org/10.1016/b978-0-323-46144-3.00023-4>
- Peng, D., Ouyang, F., Deng, M., Nie, L., & Kong, S. (2021). A comprehensive characterization of different fractions of corn stover and their relationships to multipollutant sorption characteristics. *Adsorption Science & Technology*, 2021, 1–19. <https://doi.org/10.1155/2021/9988938>
- Petroudy, S. R. D. (2017). Physical and mechanical properties of natural fibers. In *Elsevier eBooks* (pp. 59–83). <https://doi.org/10.1016/b978-0-08-100411-1.00003-0>
- Pevelen, D. D. L. (2010). Small Molecule X-Ray Crystallography, Theory and Workflow. In *Elsevier eBooks* (pp. 2559–2576). <https://doi.org/10.1016/b978-0-12-374413-5.00359-6>
- Pham, C. D., Le, T. M., Nguyen, C. T. X., Vo, N., Do, N. H. N., Le, K. A., Mai, T. P., & Le, P. T. K. (2022). Review of The Role of Pretreatment Step in Nanocellulose Production from Rice Straw. *CHEMICAL ENGINEERING TRANSACTIONS*, VOL.97, 67–72. <https://doi.org/10.3303/CET2297012>
- Pinto, E., Aggrey, W. N., Boakye, P., Amenuvor, G., Sokama-Neuyam, Y. A., Fokuo, M. O., Karimaie, H., Sarkodie, K., Adenutsi, C. D., Erzuah, S., & Rockson, M. a. D. (2022). Cellulose processing from biomass and its derivatization into carboxymethylcellulose: A review. *Scientific African*, 15, e01078. <https://doi.org/10.1016/j.sciaf.2021.e01078>
- Poletto, M., Pistor, V., & Zattera, A. J. (2013). Structural characteristics and thermal properties of native cellulose. In *InTech eBooks*. <https://doi.org/10.5772/50452>
- Raja, P. B., Munusamy, K. R., Perumal, V., & Ibrahim, M. N. M. (2022). Characterization of nanomaterial used in nanobioremediation. In *Elsevier eBooks* (pp. 57–83). <https://doi.org/10.1016/b978-0-12-823962-9.00037-4>
- Rani, N. L., Chakravarthy, M. P., Mohana, K. N., Lokanath, N. K., & Sridhar, M. A. (2015). Synthesis, Characterization and Hirshfeld Surface Analysis of a 2-thiophene Acetic Acid

- Derivative. *Molecular Crystals and Liquid Crystals*, 607(1), 223–231. <https://doi.org/10.1080/15421406.2014.928978>
- Raval, N., Jain, S., Kalyane, D., Youngren-Ortiz, S. R., Chougule, M. B., & Tekade, R. K. (2019). Importance of Physicochemical Characterization of Nanoparticles in Pharmaceutical Product Development. In *Elsevier eBooks* (pp. 369–400). <https://doi.org/10.1016/b978-0-12-817909-3.00010-8>
- Raza, M., Abu-Jdayil, B., Banat, F., & Al-Marzouqi, A. H. (2022). Isolation and Characterization of Cellulose Nanocrystals from Date Palm Waste. *ACS Omega*, 7(29), 25366–25379. <https://doi.org/10.1021/acsomega.2c02333>
- Rizal, N. F. a. A., Ibrahim, M. F., Zakaria, M. R., Bahrin, E. K., Abd-Aziz, S., & Hassan, M. A. (2018). Combination of Superheated Steam with Laccase Pretreatment Together with Size Reduction to Enhance Enzymatic Hydrolysis of Oil Palm Biomass. *Molecules*, 23(4), 811. <https://doi.org/10.3390/molecules23040811>
- Rongpipi, S., Ye, D., Gomez, E. D., & Gomez, E. W. (2019). Progress and Opportunities in the Characterization of Cellulose – An Important Regulator of Cell Wall Growth and Mechanics. *Frontiers in Plant Science*, 9. <https://doi.org/10.3389/fpls.2018.01894>
- Royan, N. R. R., Sulong, A. B., Yuhana, N. Y., Chen, R. S., Ghani, M. H. A., & Ahmad, S. (2018). UV/O₃ treatment as a surface modification of rice husk towards preparation of novel biocomposites. *PLOS ONE*, 13(5), e0197345. <https://doi.org/10.1371/journal.pone.0197345>
- Ruan, Z., Wang, X., Liu, Y., & Liao, W. (2019). Corn. In *Elsevier eBooks* (pp. 59–72). <https://doi.org/10.1016/b978-0-12-814138-0.00003-4>
- Saadatkhah, N., García, A. C., Ackermann, S. L. G., Leclerc, P., Latifi, M., Samih, S., Patience, G. S., & Chaouki, J. (2019). Experimental methods in chemical engineering: Thermogravimetric analysis—TGA. *The Canadian Journal of Chemical Engineering*, 98(1), 34–43. <https://doi.org/10.1002/cjce.23673>
- Salleh, N., & Salamun, N. (2022). Characterization of Cellulose Derived from Oil Palm Empty Fruit Bunch. *Proceedings of Science and Mathematics, Vol. 14, 2022*, 7373. <https://docplayer.net/235113542-Extraction-and-characterization-of-cellulose-derived-from-oil-palm-empty-fruit-bunch.html>

- Samsalee, N., Meerasri, J., & Sothornvit, R. (2023). Rice husk nanocellulose: Extraction by high-pressure homogenization, chemical treatments and characterization. *Carbohydrate Polymer Technologies and Applications*, 6, 100353. <https://doi.org/10.1016/j.carpta.2023.100353>
- Satbaev, B. N., Yefremova, S. V., Zharmenov, A. A., Kablanbekov, A., Yermishin, S., Shalabaev, N. T., Satbaev, A. B., & Vr, K. (2021). Rice Husk Research: From Environmental Pollutant to a Promising Source of Organo-Mineral Raw Materials. *Materials*, 14(15), 4119. <https://doi.org/10.3390/ma14154119>
- Sato, H., Uraki, Y., Kishimoto, T., & Sano, Y. (2003). New process for producing cellulose acetate from wood in concentrated acetic acid. *Cellulose*, 10(4), 397–404. <https://doi.org/10.1023/a:1027359708581>
- Sayakulu, N. F., & Soloi, S. (2022). The Effect of Sodium Hydroxide (NaOH) Concentration on Oil Palm Empty Fruit Bunch (OPEFB) Cellulose Yield. *Journal of Physics*, 2314(1), 012017. <https://doi.org/10.1088/1742-6596/2314/1/012017>
- Selvakumar, K., & Meenakshisundaram, O. (2022). Effect of alkali treated and untreated cellulose fibers and human hair on FTIR and tensile properties for composite material applications. *SN Applied Sciences*, 4(3). <https://doi.org/10.1007/s42452-022-04946-9>
- Shang, F., Wenbin, M., Wu, H., Xu, F., Chen, X., & Wang, J. (2020). Paper New Allele of HL6 regulates trichome elongation in rice. *Rice Science*, 27(6), 480–492. <https://doi.org/10.1016/j.rsci.2020.09.005>
- Siemens, M. E. (2018). Tutorial on Multidimensional Coherent Spectroscopy. In *Elsevier eBooks* (pp. 150–163). <https://doi.org/10.1016/b978-0-12-803581-8.09526-6>
- Singh, A. K. (2016). Experimental Methodologies for the Characterization of Nanoparticles. In *Elsevier eBooks* (pp. 125–170). <https://doi.org/10.1016/b978-0-12-801406-6.00004-2>
- Singh, A., Kushwaha, A., Sen, S., Goswami, S., Katiyar, S., Kumar, A., Borah, S. N., Goswami, L. N., & Hussain, C. M. (2022). Recent advancement in microwave-assisted pyrolysis for biooil production. In *Elsevier eBooks* (pp. 197–219). <https://doi.org/10.1016/b978-0-323-85387-3.00014-8>
- Singh, B. (2018). Rice husk ash. *Elsevier eBooks*, 417–460. <https://doi.org/10.1016/b978-0-08-102156-9.00013-4>

- Singh, H., Patil, T. V., Vineeth, S. K., Das, S., Pramanik, A., & Mhaske, S. T. (2020). Isolation of microcrystalline cellulose from corn stover with emphasis on its constituents: Corn cover and corn cob. *Materials Today: Proceedings*, 27, 589–594. <https://doi.org/10.1016/j.matpr.2019.12.065>
- Singh, R., Shukla, A., Tiwari, S., & Srivastava, M. (2014). A review on delignification of lignocellulosic biomass for enhancement of ethanol production potential. *Renewable & Sustainable Energy Reviews*, 32, 713–728. <https://doi.org/10.1016/j.rser.2014.01.051>
- Sisak, M. a. A., Daik, R., & Ramli, S. (2015). Characterization of cellulose extracted from oil palm empty fruit bunch. *AIP Conference Proceedings*. <https://doi.org/10.1063/1.4931295>
- Sudiyani, Y., Styarini, D., Triwahyuni, E., Sudiarmanto, Sembiring, K. C., Aristiawan, Y., Abimanyu, H., & Han, M. (2013). Utilization of Biomass Waste Empty Fruit Bunch Fiber of Palm Oil for Bioethanol Production Using Pilot–Scale Unit. *Energy Procedia*, 32, 31–38. <https://doi.org/10.1016/j.egypro.2013.05.005>
- Tarchoun, A. F., Trache, D., & Klapötke, T. M. (2019). Microcrystalline cellulose from *Posidonia oceanica* brown algae: Extraction and characterization. *International Journal of Biological Macromolecules*, 138, 837–845. <https://doi.org/10.1016/j.ijbiomac.2019.07.176>
- Teow, Y. H., Amirudin, S. N., & Ho, K. C. (2020). Sustainable approach to the synthesis of cellulose membrane from oil palm empty fruit bunch for dye wastewater treatment. *Journal of Water Process Engineering*, 34, 101182. <https://doi.org/10.1016/j.jwpe.2020.101182>
- Terrett, O. M., & Dupree, P. (2019). Covalent interactions between lignin and hemicelluloses in plant secondary cell walls. *Current Opinion in Biotechnology*, 56, 97–104. <https://doi.org/10.1016/j.copbio.2018.10.010>
- Torres-Rivero, K., Bastos-Arrieta, J., Fiol, N., & Florido, A. (2021). Metal and metal oxide nanoparticles: An integrated perspective of the green synthesis methods by natural products and waste valorization: applications and challenges. In *Comprehensive Analytical Chemistry* (pp. 433–469). Elsevier BV. <https://doi.org/10.1016/bs.coac.2020.12.001>
- Trache, D., Tarchoun, A. F., Derradji, M., Hamidon, T. S., Masruchin, N., Brosse, N., & Hussin, M. H. (2020). Nanocellulose: From fundamentals to advanced applications. *Frontiers in Chemistry*, 8. <https://doi.org/10.3389/fchem.2020.00392>
- Trilokesh, C., & Uppuluri, K. B. (2019). Isolation and characterization of cellulose nanocrystals from jackfruit peel. *Scientific Reports*, 9(1). <https://doi.org/10.1038/s41598-019-53412-x>

- Trilokesh, C., & Uppuluri, K. B. (2021). Biobutanol from lignocellulosic biomass and microalgae: scope, technology, and economics. In *Elsevier eBooks* (pp. 163–223). <https://doi.org/10.1016/b978-0-12-820297-5.00008-6>
- Unapumnuk, K., Keener, T. C., Lu, M., & Khang, S. (2006). Pyrolysis Behavior of Tire-Derived Fuels at Different Temperatures and Heating Rates. *Journal of the Air & Waste Management Association*, 56(5), 618–627. <https://doi.org/10.1080/10473289.2006.10464481>
- Undavalli, V. K., Ling, C., & Kumar, S. (2021). Impact of alternative fuels and properties on elastomer compatibility. In *Elsevier eBooks* (pp. 113–132). <https://doi.org/10.1016/b978-0-12-818314-4.00001-7>
- Vac Coat. (2023, June 8). The Best Introduction To Scanning Electron Microscope (SEM) - VacCoat. *VacCoat*. <https://vaccoat.com/blog/scanning-electron-microscope-sem/>
- Varma, R. S. (2019). Biomass-Derived Renewable Carbonaceous Materials for Sustainable Chemical and Environmental Applications. *ACS Sustainable Chemistry & Engineering*, 7(7), 6458–6470. <https://doi.org/10.1021/acssuschemeng.8b06550>
- Wahab, N. A. (2020). EXTRACTION AND CHARACTERISATION OF CELLULOSE FROM THE RESIDUE OF OIL PALM EMPTY FRUIT BUNCH-XYLAN EXTRACTION. *Journal of Oil Palm Research*. <https://doi.org/10.21894/jopr.2020.0052>
- Wang, T., & Zhao, Y. (2021). Optimization of bleaching process for cellulose extraction from apple and kale pomace and evaluation of their potentials as film forming materials. *Carbohydrate Polymers*, 253, 117225. <https://doi.org/10.1016/j.carbpol.2020.117225>
- Wang, Y., Li, S., Ma, L., Dong, S., & Liu, L. (2020). Corn stalk as starting material to prepare a novel adsorbent via SET-LRP and its adsorption performance for Pb(II) and Cu(II). *Royal Society Open Science*, 7(3), 191811. <https://doi.org/10.1098/rsos.191811>
- Wen, S., Liu, J., & Deng, J. (2021). Methods for the detection and composition study of fluid inclusions. In *Elsevier eBooks* (pp. 27–68). <https://doi.org/10.1016/b978-0-12-819845-2.00003-x>
- Wirawan, W. A., Choiron, M. A., Siswanto, E., & Widodo, T. D. (2022). Morphology, Structure, and Mechanical Properties of New Natural Cellulose Fiber Reinforcement from Waru (*Hibiscus Tiliaceus*) Bark. *Journal of Natural Fibers*, 19(15), 12385–12397. <https://doi.org/10.1080/15440478.2022.2060402>

- Woźniak, M., Ratajczak, I., Wojcieszak, D., Waśkiewicz, A., Szentner, K., Przybył, J., Borysiak, S., & Goliński, P. (2021). Chemical and structural characterization of maize stover fractions in aspect of its possible applications. *Materials*, 14(6), 1527. <https://doi.org/10.3390/ma14061527>
- Xie, H., Du, H., & Yang, X. (2018). Recent Strategies in Preparation of Cellulose Nanocrystals and Cellulose Nanofibrils Derived from Raw Cellulose Materials. *International Journal of Polymer Science*, 2018, 1–25. <https://doi.org/10.1155/2018/7923068>
- Yang, X., Wu, Y., Zhang, Y., Yang, E., Qu, Y., Xu, H., Chen, Y., Irbis, C., & Yan, J. (2020). A Thermo-Active Laccase Isoenzyme From *Trametes trogii* and Its Potential for Dye Decolorization at High Temperature. *Frontiers in Microbiology*, 11. <https://doi.org/10.3389/fmicb.2020.00241>
- Youssefian, S., Jakes, J. E., & Rahbar, N. (2017). Variation of Nanostructures, Molecular Interactions, and Anisotropic Elastic Moduli of Lignocellulosic Cell Walls with Moisture. *Scientific Reports*, 7(1). <https://doi.org/10.1038/s41598-017-02288-w>
- Yunus, M. A. (2019). Extraction cellulose from rice husk. *Jurnal Akta Kimia Indonesia*, 12(2), 79. <https://doi.org/10.20956/ica.v12i2.6559>
- Zaid, O., Ahmad, J., Siddique, M., & Aslam, F. (2021). Effect of incorporation of rice husk ash instead of cement on the performance of steel fibers reinforced concrete. *Frontiers in Materials*, 8. <https://doi.org/10.3389/fmats.2021.665625>
- Zha, G., Fang, W., Li, Y., Leng, J., Chen, X., & Qin, H. (2018). SO₂F₂-Mediated Oxidative Dehydrogenation and Dehydration of Alcohols to Alkynes. *Journal of the American Chemical Society*, 140(50), 17666–17673. <https://doi.org/10.1021/jacs.8b10069>
- Zhang, J., Feng, L., Wang, D., Zhang, R., Liu, G., & Cheng, G. (2014). Thermogravimetric analysis of lignocellulosic biomass with ionic liquid pretreatment. *Bioresource Technology*, 153, 379–382. <https://doi.org/10.1016/j.biortech.2013.12.004>
- Zhang, Q., Lin, L., & Ye, W. (2018). Techniques for extraction and isolation of natural products: a comprehensive review. *Chinese Medicine*, 13(1). <https://doi.org/10.1186/s13020-018-0177-x>
- Zhao, X., Chen, J., Chen, F., Wang, X., Zhu, Q., & Ao, Q. (2013). Surface characterization of corn stalk superfine powder studied by FTIR and XRD. *Colloids and Surfaces B: Biointerfaces*, 104, 207–212. <https://doi.org/10.1016/j.colsurfb.2012.12.003>

Короткова, Т. Г., Ksandopulo, S. J., Donenko, A. P., Bushumov, S. A., & Данильченко, А. (2016).

Physical properties and chemical composition of the rice husk and dust. *Oriental Journal of Chemistry*, 32(6), 3213–3219. <https://doi.org/10.13005/ojc/320644>

Сатбаев, Б. Н., Yefremova, S., Zharmenov, A. A., Kablanbekov, A., Yermishin, S., Шалабаев,

Н. Т., Сатбаев, А. Б., & Khen, V. (2021). Rice Husk Research: From environmental pollutant to a Promising Source of Organo-Mineral Raw materials. *Materials*, 14(15), 4119. <https://doi.org/10.3390/ma14154119>

UNIVERSITI
MALAYSIA
KELANTAN

APPENDIX A

CALCULATION

A1 Yield percentage of each samples

$$\text{Yield (\%)} = \frac{\text{final weight of extracted cellulose (g)}}{\text{initial weeight of sample (g)}} \times 100\%$$

a) Rice husk cellulose

Initial weight = 10 g

Final weight of extracted cellulose = 2.928 g

$$\begin{aligned} \text{Yield (\%)} &= \frac{2.928 \text{ g}}{10 \text{ g}} \times 100\% \\ &= 29.2 \% \end{aligned}$$

b) Corn stem cellulose

Initial weight = 10 g

Final weight of extracted cellulose = 1.43 g

$$\begin{aligned} \text{Yield (\%)} &= \frac{1.43 \text{ g}}{10 \text{ g}} \times 100\% \\ &= 14.30\% \end{aligned}$$

c) Corn tassel cellulose

Initial weight = 10 g

Final weight of extracted cellulose = 1.327 g

$$\begin{aligned} \text{Yield (\%)} &= \frac{1.327 \text{ g}}{10 \text{ g}} \times 100\% \\ &= 13.27\% \end{aligned}$$

b) Oil palm empty fruit bunch cellulose

Initial weight = 10 g

Final weight of extracted cellulose = 3.14 g

$$\begin{aligned} \text{Yield (\%)} &= \frac{3.14 \text{ g}}{10 \text{ g}} \times 100\% \\ &= 31.40\% \end{aligned}$$

A2 Crystallinity Index

$$\text{CrI (\%)} = \frac{(I_{002} - I_{\text{am}})}{I_{002}} \times 100\%$$

The symbol I_{002} represents the highest intensity observed in the diffraction peak corresponding to the (002) lattice plane, while I_{am} represents the intensity of the scattering caused by the amorphous portion of the samples. The diffraction peak associated with the (002) plane is situated at an angle of approximately $2\theta = 22^\circ$, while the intensity resulting from the scattering by the amorphous section is found around $2\theta = 18^\circ$.

a) Rice husk cellulose

$$I_{002} = 1971.86$$

$$I_{\text{am}} = 800.18$$

$$\text{CrI (\%)} = \frac{(1971.86 - 800.18)}{1971.86} \times 100\%$$

$$= \frac{1171.68}{1971.86} \times 100\%$$

$$= 59.42\%$$

b) Corn stem cellulose

$$I_{002} = 1594.19$$

$$I_{\text{am}} = 730.62$$

$$\text{CrI (\%)} = \frac{(1594.19 - 730.62)}{1594.19} \times 100\%$$

$$= \frac{863.57}{1594.19} \times 100\%$$

$$= 54.17\%$$

c) Corn tassel cellulose

$$I_{002} = 1377.86$$

$$I_{\text{am}} = 758.10$$

b) Oil palm empty fruit bunch cellulose

$$I_{002} = 1378.80$$

$$I_{\text{am}} = 788.85$$

$$\text{CrI (\%)} = \frac{(1377.89 - 758.10)}{1377.89} \times 100\%$$

$$= \frac{619.79}{1377.89} \times 100\%$$

$$= 44.97\%$$

$$\text{CrI (\%)} = \frac{(1378.80 - 788.85)}{1378.80} \times 100\%$$

$$= \frac{589.95}{1378.80} \times 100\%$$

$$= 42.78\%$$